

September 8, 2017

Dear Associate Editor Dr. Pope,

Re: Revisions of amt-2017-170 by Savage et al.

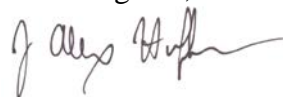
Here you will find a summary of revisions for our recently reviewed manuscript. Both referees recommended publication after relatively minor changes and comments. We have responded point-by-point to these comments and are confident that the manuscript is improved and ready for acceptance. The only substantive change to the manuscript is the addition of a few additional paragraphs of discussion adding context to the results, as requested by Referee #2.

Attached within this document you will find documents in the following order:

- Point-by-point responses to Referees #1 and 2 (copied directly from documents uploaded to AMT)
- Revised manuscript (with all changes tracked and highlighted in yellow for changes requested by referees and in green for all other minor edits)
- Manuscript supplement

With these changes we hope you will find the revised manuscript soon acceptable for publication.

Best Regards,



J. Alex Huffman, Ph.D.
Associate Professor

1 **Response to referee comment on amt-2017-170 by Savage et al.**

2
3 **Anonymous Referee #1**

4 Received and published: 22 July 2017

5
6 **Note regarding document formatting:** black text shows original referee comment, blue text shows
7 author response, and red text shows quoted manuscript text. Changes to manuscript text are
8 shown as *italicized and underlined*. Bracketed comment numbers (e.g. [R1.1]) were added for
9 clarity. All line numbers refer to discussion/review manuscript.

10
11
12 **General Comments:** The manuscript is very well written and I believe of great relevance to the
13 bioaerosol scientific community. The authors present very interesting and novel work testing a
14 Light induced fluorescence (LIF) instrument (WIBS-4A) whilst attempting to display the data in
15 new ways. Thus I believe the paper should be published upon the correction of some minor
16 technical/specific issues discussed below.

17 Author response: We thank the referee for his/her positive assessment and summary.

18 Specific/technical comments:

19
20 [R1.1] L196 I believe that this line is misleading, while a value of 0 does indicate a particle is a
21 perfect sphere values just above this do not indicate that they are rod-like as directed by the
22 sentence “Whereas larger AF values greater than 0 and less than 100, indicate rod-like particles”
23 What is the average/median AF value seen for PSL for instance? I doubt they are seen to be 0.
24 Values increasing towards 100 do indicate an increasing rod-like morphology however Indeed
25 placement of the AF values of the PSL sphere in table one would be useful.

26 [A1.1] As requested, we added median values (\pm standard deviation) of AF to Table 1 for
27 PSLs.

28 To clarify the statement we added text in this paragraph at L198 (italicized text added):
29 “A perfectly spherical particle would theoretically exhibit an AF value of 0, whereas
30 larger AF values greater than 0 and less than 100 indicate rod-like particles (Kaye et al.,
31 1991; Gabey et al., 2010; Kaye et al., 2005). *In practice, spherical PSL particles exhibit a*
32 *median AF value of ~ 5 (Table 1).* It is important to note that *the AF* parameter is not
33 rigorously a shape factor like used in other aerosol calculations (DeCarlo et al.,
34 2004; Zelenyuk et al., 2006) and only very roughly relates a measure of particle
35 sphericity.”

36
37 [R1.2] L 302 What is a blade of air? Blast perhaps?

38 [A1.2] We added text at L302 to clarify the description of the experiment.

39 “For each experiment, an agar plate with a mature fungal colony was sealed inside the
40 chamber. *A thin, wide* nozzle was positioned so that *the delivered air stream*
41 *approximated* a blade of air *that* *approached* the top of the spore colony at a shallow
42 angle in order to eject spores into a *roughly* horizontal trajectory.”

43
44 [R1.3] L 337 What was considered sufficiently fine?

45 [A1.3] We added clarifying text at L337:
46 “The setup was modified (method P2) for a small subset of samples whose solid powder
47 was sufficiently fine to produce high number concentrations of particles (e.g. >200 cm⁻³)
48 and that contained enough submicron aerosol material to risk coating the internal flow
49 path and damaging optical components of the instrument.”

50
51 [R1.4] Table 2 Pyrdoxine particle 7 in Biofluorophores has no number in the saturated column

52 [A1.4] We added missing values for Pyrdoxine in Table 2.

53 [R1.5] Were there any issues with contamination whilst using a NAD?

54 [A1.5] There were no contamination issues while running NAD, but the fear of
55 contamination was one reason we employed aerosolization method P2. Between each
56 sample, the instrument ran pumping for about 10 min to prevent contamination. If the
57 baseline of that ambient data collected in those 10 min was higher, other measures were
58 taken to ensure the optical cavity was not coated.

59 [R1.6] L555 Are intact pollen not counted? Or do they saturate the sizing detector and are thus
60 mis-sized?

61 [A1.6] Intact pollen that make it into the instrument are counted. Most pollen grains are
62 much larger than the upper size limit of the instrument (~20 μm), however. Thus, species
63 of pollen with large grain sizes exhibit a size mode in the WBS near this upper size limit.
64 (e.g. Pollen 1, 2, 5, etc.). Any particles larger than this are integrated into the largest
65 sizing bin, which saturates the sizing detector. A clarifying sentence was added:

66 L557: “... upper size limit of particle collection (~20 μm as operated). Particles larger
67 than this limit saturate the sizing detector and are binned together into the ~20 μm bin.”

68 [R1.7] L560-3 Given that the pollen are disrupted, they now have the intine of the pollen
69 exposed. Thus is it this rather than the fraction of the pollen that is radiated the most important?

70 [A1.7] The intact pollen and fragmented pollen indeed present different types of material
71 to the excitation pulses and may, therefore, present different emission properties as a
72 result. We believe the following, existing text clarifies this point:

73 L557: “It is important to note that excitation pulses from the Xe flash lamps are not likely
74 to penetrate the entirety of large pollen particles, and so emission information is likely
75 limited to outer layers of each pollen grain. Excitation pulses can penetrate a relatively
76 larger fraction of the smaller pollen fragments, however, meaning that the differences in
77 observed fluorescence may arise from differences the layers of material interrogated.”

78 [R1.8] L609 should the line say “adds either A and C” rather than “adds either B and C”

79 [A1.8] This was a typo. The text was modified to correct this error:

80 L 609: “The “pathway” of change, for Pollen 9, starts as A-type at small particle size and
81 adds B and eventually ABC (A→AB→ABC), whereas Pollen 8 starts primarily with B-
82 type at small particle size and separately adds either B and C en route to ABC (B→AB
83 or BC→ABC).”

84 [R1.9] L647 tryptophan does not appear to follow $A \rightarrow BC \rightarrow ABC$ pathway from visual
85 inspection of the associated graph.

86 [A1.9] This was also a typo. The pathway listed for tryptophan was correct, as follows:

87 “For example Biofluorophore 1 (riboflavin) follows the pathway $B \rightarrow C \rightarrow BC$ while
88 Biofluorophore 11 (tryptophan) follows the pathway $A \rightarrow BC \rightarrow \underline{AB} \rightarrow ABC$.”

89 [R1.10] Similarly in the discussion of the pathways for riboflavin the particles appear to have
90 either B or C character to start with before gaining the required character to become BC. The
91 pathway you describe does not suggest this. It suggests that particles pass from B to C to BC

92 [A1.10] The referee brings up a good point here. The concept of “pathway” here does not
93 make sense to move from B to C to BC. Instead, there is a population of B particles and a
94 separate population of C particles, each of which can separately move to become BC
95 particles as particle size increases. To clarify this, the text has been changed as follows:

96 L646: “For example Biofluorophore 1 (riboflavin) follows the pathway $B \text{ or } C \rightarrow BC \dots$ ”

1 **Response to referee comment on amt-2017-170 by Savage et al.**

2
3 **Referee #2: Anne Perring**

4 Received and published: 10 August 2017

5
6 **Note regarding document formatting:** black text shows original referee comment, blue text shows
7 author response, and red text shows quoted manuscript text. Changes to manuscript text are 7
8 shown as *italicized and underlined*. All line numbers refer to discussion/review manuscript.
9

10
11 General Comments: This manuscript presents a very large set of laboratory observations of
12 different kinds of fluorescent aerosol (both biological and non-biological) using a WIBS 4A,
13 presented in the context of a recent analysis framework. The authors use this dataset to evaluate
14 the ability of the WIBS to detect a variety of biological aerosol, to characterize the observed
15 response in a particular instrument and to make recommendations for excluding common
16 interferents. They have also extended the utility of the analysis framework by systematically
17 investigating the effect of size on the fluorescence response for a given bioaerosol population
18 and have additionally evaluated the performance of the asymmetry factor parameter, an output
19 which is often used but which is of unknown value in distinguishing different types of particles.
20 The paper is well written and the community is sorely in need of this kind of characterization and
21 critical analysis of performance if we are to make robust measurements of atmospheric
22 abundances of bioaerosol. Questions of potential interferences are one of the largest hurdles in
23 the use of UV-LIF technologies and this paper is a valuable piece of that puzzle. I have a few
24 comments and suggestions as outlined below for the authors to consider but I certainly
25 recommend publication in ACP with only minor modifications.
26

27 Author response: We thank the referee for her positive assessment and summary.

28
29 Specific/technical comments:

30
31 [R2.1] On p5, I'm not totally sure how you guys are doing the calibration but I think you should
32 probably include a bit more detail. Did you just run a few sizes of PSL and then fit with a 2nd
33 order polynomial? Was there any consideration of the expected instrumental response given Mie
34 theory? I have run some calculations of expected response and compared that to PSLs and
35 usually get reasonable correspondence but I'm not sure than a 2nd degree polynomial is
36 sufficient to capture the expected shape of the response. Admittedly any differences are likely at
37 the larger sizes and probably don't impact the results much but size is one of the parameters that
38 is used heavily and there seems to be wide variability in how it is treated. Most critically the size
39 you are reporting is not simply the size the WIBS reports based on its internal calibration but is
40 instead based on the observed peak heights and calibrated by you using multiple
41 PSL sizes. I think this point could be made clearer as many WIBS users seem to still use the
42 WIBS internal calibration, simply checked periodically with one size of PSLs. 2nd order
43 polynomial extrapolation to larger sizes than are represented by PSLs are an additional
44 uncertainty.
45

46 [A2.1] The referee introduces an important point that we didn't explicitly discuss in the
47 manuscript. In particular, we agree that particle sizing reported by the WIBS instrument
48 is critically erroneous if not properly calibrated. To clearly introduce this concept and the
49 method by which we calibrated particle size, the following text was added to Section 2.2:

50 “The particle size reported by the internal WIBS calibration introduces significant
51 sizing errors and critically needs to be calibrated before analyzing or reporting particle
52 size. Particle size calibration was achieved here by using a one-time 27-point calibration
53 curve generated using non-fluorescent PSLs ranging in size from 0.36 to 15 μm . This
54 calibration involved several steps. For each physical sample, approximately 1,000 to
55 10,000 individual particles were analyzed using the WIBS (several minutes of collection).
56 Data collected for each samples was analyzed by plotting a histogram of the side scatter
57 response reported in the raw data files (FL2_sctpk). A Gaussian curve was fitted to the
58 most prominent mode in the distribution. The median value of the fitted peak for observed
59 side scatter was then plotted against the physical diameter (as reported on the bottle) for
60 each PSL sample. A 2nd degree polynomial function was fitted to this curve to create the
61 calibration equation that was used on all laboratory data used here. The calibration
62 between observed particle size and physical diameter may be affected by wiggles in the
63 optical scattering relationship suggested by Mie theory. These theoretical considerations
64 were not used for the calibrations reported here, and so uncertainties in reported size are
65 expected to increase at larger diameters.

66 Following the one-time 27-point calibration, the particle sizing response was checked
67 periodically using a 5-point calibration. The responses of these calibration checks were
68 within one standard deviation unit of each other and so the more comprehensive
69 calibration was always used. These quicker checks were performed using non-fluorescent
70 PSLs (Polysciences, Inc., Pennsylvania), including 0.51 μm (part number 07307), 0.99
71 μm . (07310), 1.93 μm (19814), 3.0 μm (17134), and 4.52 μm (17135).”

72
73 [R2.2] Can you include a statement and/or reference for how representative these chemically-
74 produced “brown carbon” compounds are of atmospheric brown carbon? This may be addressed
75 in the Powelson reference and you do discuss it a bit later in the paper, however it would be
76 useful to have some discussion of this in the methods section when brown carbon is introduced.
77 I.e., we know it's a surrogate but it's the best option we have. We expect the absorption spectrum
78 is similar but the cross section is different by...

79
80 [A2.2] Indeed, there are many different pathways to brown carbon formation in the
81 atmosphere. We chose to utilize methods published by Powelson et al. (2014) primarily
82 because the experiments were more easily achievable due to their bulk-phase nature and
83 because we did not need to find access to a reaction flow-tube. Small, water soluble
84 carbonyl compounds such as methylglyoxal, glycolaldehyde and glyoxal can undergo
85 Maillard-type browning reactions or aldol condensation reactions in the presence of
86 ammonium salts, amino acids (glycine) or primary amines (methylamine), like those
87 reagents used in this study. Table 1 in the Powelson et al. (2014) reference reports
88 atmospheric concentrations (in both cloud and aerosol) for each reagent used here. In the
89 last paragraph of their paper the authors also present a short analysis of global emissions

90 of these compounds, concluding in the last line of the paper that “because of lower MAC
91 [mass absorption coefficients] values for products of aldehyde-amine-AS browning
92 reactions, they are likely responsible for <10% of light absorption by atmospheric brown
93 carbon.” We felt these details were beyond the scope of relevance for our manuscript,
94 but have added a few sentences of context to the methods (Section 3.1.2) as requested.
95

96 L271: “These reactions were chosen, because the reaction products were achievable
97 using bulk-phase aqueous chemistry and did not require more complex laboratory
98 infrastructure. They represent three examples of reactions possible in cloud-water using
99 small, water-soluble carbonyl compounds mixed with either ammonium sulfate or a
100 primary amine (Powelson et al., 2014). A large number of reaction pathways exist to
101 produce atmospheric brown carbon, however, and the products analyzed here are
102 intended primarily to introduce the possible importance of brown carbon droplets and
103 coatings to fluorescence-based aerosol detection (Huffman et al., 2012).”
104

105 Reference: Powelson, M. H., Espelien, B. M., Hawkins, L. N., Galloway, M. M., and De
106 Haan, D. O.: Brown Carbon Formation by Aqueous-Phase Carbonyl Compound
107 Reactions with Amines and Ammonium Sulfate, Environmental Science & Technology,
108 48, 985-993, 10.1021/es4038325, 2014.
109

110 [R2.3] Initially it took me a while to figure out what you meant in the text and figures by
111 “miscellaneous particles”. Although the samples are delineated in the table, it might be better to
112 relabel “miscellaneous particles” as “common household fibers” or something more descriptive
113 for ease of reading.
114

115 [A2.3] This is a good idea and we have changed “miscellaneous particles” to “common
116 household fibers” in all places that it occurred in the manuscript text, figures, and
117 supplement.
118

119 [R2.4] I think it is worth explicitly noting somewhere in this manuscript that all of the
120 populations sampled are fresh samples and we do not know how atmospheric aging would
121 impact our ability to detect ambient bioaerosols. It is a necessary benchmark to understand what
122 the fresh emissions would look like however we do not know how the fraction of particles
123 detected would change over time so this may not perfectly reflect (would be a best case scenario
124 of?) our ability to detect ambient particles.
125

126 [A2.4] We have added the following text after L267:

127 “It is important to note that all particle types analyzed here essentially represent “fresh”
128 emissions. It is unclear how atmospheric aging might impact their surface chemical
129 properties or how their observed fluorescence properties might evolve over time.”
130

131 [R2.5] I think the nuances of what you are seeing with the dust is critically useful and I would
132 like to see a bit more context for these numbers and more detailed discussion of the different
133 samples rather than lumping them all into a “dust” category. The expectation is that dust, by
134 number, is much more abundant than bioaerosols such that, even if only 1% of a certain
135 population of dust is misidentified, it could be a huge number relative to the abundance of

136 bioaerosol. I suggest expanding the discussion of the dust to include where these dusts are from
137 and whether you have any idea about how abundant these different kinds of dust are in the
138 atmosphere. Is it possible at this stage to put bounds on how much dust may impact WIBS
139 measurements in different environments?

140

141 [A2.5] All dust samples were generously loaned from a collection in the Department of
142 Geology and Earth Science in the School of Earth and Environmental Sciences at the
143 University of Manchester, and we were not able to investigate details regarding
144 atmospheric concentrations and geographic trends associated with each.

145

146 The referee's question about constraining the importance of weakly fluorescent non-
147 biological material is an important point of discussion, but also very complicated.
148 Prompted by the important comment we included a simple analysis along with a
149 relatively detailed additional paragraph suggesting the general scenarios that could
150 increase quantitative uncertainties and the impact these may have on conclusions drawn
151 about an ambient air mass. The following text was inserted at L795:

152

153 *"It is important here to provide brief atmospheric context to these measurements.
154 Whether 3σ or 9σ thresholds are used, no UV-LIF technology can unambiguously
155 distinguish between all biological and non-biological aerosol types, and so a minority of
156 misidentified particles will always remain. The key aim is not to remove these completely,
157 but to group particles of interest as cleanly as possible with an estimate of the relative
158 magnitude of misidentification. As a simple exercise to estimate this process, consider
159 two scenarios where each sampled air mass contains a total of 10,000 particles, each 3
160 μm in diameter.*

161

162 • *Assume as Scenario 1 that the particle mode is comprised of 10% Dust 10
163 (taken as a representative, weakly fluorescent dust), 5% Fungi 1 (taken as a
164 representative fungal spore type), and 85% other non-fluorescent material
165 (i.e. sea salt, silicates, non-absorbing organic aerosol). In this scenario, 6.9%
166 of the 485 particles exhibiting some type of fluorescence (FL any) using the
167 3σ threshold would be misidentified from fluorescing dust and separately
168 4.4% of the 427 particles using the 9σ threshold.*

169

170 • *Assume as Scenario 2 that a strong dust event is comprised of 90% Dust 10
169 mixed 10% Fungi 1. Here, 25% of the 1139 fluorescent particles would be
170 misidentified from dust using the 3σ threshold and 17.2% of 985 fluorescent
171 particles using 9σ .*

172

173 *These simple calculations using only dust and fungal spores suggests that a minimum
174 of a few percent of fluorescing particles are expected to arise from non-biological
175 materials, and so the uncertainty in the fraction of fluorescence by these types of analyses
176 are probably limited to no lower than $\pm 5\%$. The uncertainty in assigning the absolute
177 number of fluorescent particles to biological material is somewhat more uncertain,
178 however. For example, if 10,000 dust particles of which only 1% were fluorescent were
179 to be mixed with a small population of 100 biological particles of which 100% were
180 fluorescent, then the number concentration of fluorescent particles would over-count the
biological particles by a factor of two. In this way, the number concentration of*

181 fluorescent particles is much more susceptible to uncertainties from non-biological
182 particles. The overall uncertainty in discerning between particles will also be strongly
183 dependent on air mass composition. For example, in Scenario 2 hypothesized to simulate
184 a dust storm, the fraction of particle misidentification can be significantly higher when
185 the relative fraction of a weakly fluorescing material is especially high. Air masses that
186 contain non-biological materials that have anomalously high fluorescent fractions would
187 increase the rate of particle misidentification even more dramatically. These scenarios
188 only consider the total fraction of particles to be fluorescent, not taking into account the
189 differing break-down of fluorescent particle type as a function of the 3 different
190 fluorescent channels. Taking these details into account will reduce the fraction of particle
191 misidentification as a function of the similarity between observed biological and non-
192 biological material. As a result, UV-LIF results should be considered uniquely in all
193 situations with appreciation of possible influences from differing aerosol composition on
194 fluorescence results. Additionally, individuals utilizing WIBS instrumentation are
195 cautioned to use the assignment of “biological aerosols” from UV-LIF measurements
196 with great care and are rather encouraged to use “fluorescent aerosol” or some
197 variation more liberally. Ultimately, further analysis methods, including clustering
198 techniques (e.g. Crawford et al., 2015; Crawford et al., 2016; Ruske et al., 2017) will
199 likely need to be employed to further improve discrimination between ambient particles and
200 to reduce the relative rate of misidentification. It should also be noted, however, that a
201 number of ambient studies have compared results of UV-LIF instruments with
202 complementary techniques for bioaerosol detection and have reported favorable
203 comparisons (Healy et al., 2014; Gosselin et al., 2016; Huffman et al., 2012). So while
204 uncertainties remain, increasing anecdotal evidence supports the careful use of UV-LIF
205 technology for bioaerosol detection.”

206
207 [R2.6] The suite of particles investigated is impressive and I can appreciate that it is not
208 reasonable to discuss each individual particle type in detail. However, similar to the above
209 comment, I think the current discussion is a little bit too case-study oriented and would benefit
210 from a bit more distillation/bigger picture. I found myself wondering how representative HULIS 5
211 and the 15% fluorescent dust particles are of those populations. This is already addressed
212 somewhat but I recommend expanding the discussion or possibly adding a section specifically
213 about implications of known interferences on ambient measurements.

214
215 [A2.6] Textual context was added to the manuscript as a part of response [R2.5].
216 Additionally, we investigated the properties of HULIS 5, which was presented within the
217 manuscript as an outlier in terms of high fluorescence, as suggested by the referee. This
218 material is indeed not expected to be a common type of material one would expect to see
219 in the atmosphere, as discussed in the text added below (after L522):

220
221 “HULIS 5 is a fulvic acid collected from a eutrophic, saline coastal pond in Antarctica.
222 The collection site lacks the presence of terrestrial vegetation, and therefore all dissolved
223 organic material present originates from microbes. HULIS 5, therefore, is not expected
224 to be representative of soil-derived HULIS present in atmospheric samples in most areas
225 of the world. We present the properties of this material as an example of relatively highly

226 fluorescing, non-biological aerosol types that could theoretically occur, but without
227 comment about its relative importance or abundance.”

228
229 The following text was modified at L685:

230 “As a ‘worst case’ scenario, HULIS 5 shows ca. 60% of particles to be fluorescent using
231 the 3σ threshold, but this material is unlikely to be representative of commonly observed
232 soil HULIS, as discussed above.”

233
234 The following text was modified at L785:

235 “It is important to note that HULIS 5 was one of a large number of analyzed particle
236 types and in the minority of HULIS types, however, and it is unlikely that this microbe-
237 derived material clear how likely these highly fluorescent materials would be observed
238 are to occur in any given ambient air mass at most locations. More studies may be
239 required to sample dusts, HULIS types, soot and smoke, brown organic carbon materials,
240 and various coatings in different real-world settings and at various stages of aging to
241 better understand how specific aerosol types may contribute to UV-LIF interpretation at a
242 given study location.”

243
244 [R2.7] It seems that these results are fairly consistent with the Hernandez et al findings except
245 for a couple of things. First, there are a lot of non-fluorescent particles in several of the pollen
246 samples if I’m reading the supplemental graphs correctly. This is surprising as we have always
247 found nearly all pollen particles in a sample to be fluorescent in previous analyses (i.e. the
248 Hernandez paper). It’s a little hard to see it in the Hernandez paper but, if you add up each row in
249 Table A1 (which shows the percentage of a given sample that showed up as a particular type),
250 they don’t quite sum to 100% and, for at least those pollen samples, we had >95% of all particles
251 detected as fluorescent. So I am surprised to see so many pollens with a large non-fluorescent
252 contribution here. Second, in Hernandez, the type B presentation was at most a minor (<10%)
253 fraction of particles for a given population and even that only appeared in a handful of biological
254 samples (for two different instruments). Here it seems that many of the pollen samples have a
255 substantial fraction of particles manifesting as type B. This is unfortunate as it seems that type B
256 is often also found in possible non-biological interferences. Have the authors thought about what
257 might drive this kind of variability? I suppose it could be specific to certain pollen species, it
258 could be instrument variability or it could be something to do with the samples or nebulization
259 but this probably deserves a little discussion.

260
261 [A2.7] It is an interesting comment that the fraction of pollen grains exhibiting
262 fluorescence as reported by the Hernandez et al. paper was e.g. >95%, whereas more
263 pollen species are shown here with higher non-fluorescent fractions. Most pollen species
264 were used only in either the Hernandez et al. paper or our work, but not both. *Phleum*
265 *pratense* is the only exception, used in both studies, and it interestingly shows similar
266 non-fluorescent fractions of ~2% or less in both manuscripts. Similarly, the fraction of
267 *Phleum pratense* shown in Figure 2 of Hernandez et al. (visually) shows approximately
268 95% of particles to have B-type properties. This fraction is similar to the fraction we
269 report (i.e. Figure 3a). This could indicate a higher degree of instrumental agreement than
270 initially obvious and that observed differences in fluorescent properties are influenced
271 heavily by the choice of pollen grains analyzed in both studies.

272
273
274
275
276
277
278
279
280
281
282
283
284
285
286
287
288
289
290
291
292
293
294
295
296
297
298
299
300
301
302
303
304
305
306
307
308
309
310
311
312
313
314
315
316

That said, there are clear reasons one would expect instrument to show different patterns to separately aerosolized pollen. For example:

(1) The conditions for pollen growth and biological state may be different, given that the pollen came from different distributors. The storage conditions, age, and aerosolization processes were also different and could impact the chemical and physical states of the material as well as the fraction of pollen grains that fractured before analysis.

(2) The observed differences in fluorescent properties can also be heavily influenced by instrument properties. For example, instrument gains can be set differently in each instrument. It may be that our FL2 detector has higher sensitivity, resulting in more B fraction particles.

It is unclear how all these factors might combine to quantitatively compare the minor differences between observations. The most reliable answer to improve differences in results would be to perform similar laboratory measurements with collocated instruments, which we suggest could be important to the community. Beyond this, it is becoming increasingly clear that calibrating different WIBS instruments based on an absolute fluorescence standard is critically important. Work like the referee's recent paper (Robinson et al., 2016) will help solve similar conundrums in the future.

[R2.8] The discussion of the size dependence of fluorescence is nice. I think it would be worth double checking that there is not a size-dependence in the FL2 detector for non-fluorescent particles. I think there was a batch of bad notch filters at some point in WIBS production that led to some bleed through of flash lamp light to that detector. This may be somewhat hard to assess given that some PSLs have a fluorescent surfactant (and thus "normal" non-fluorescent-doped PSLs will sometimes fluoresce) but it can be done with dioctyl sebacate or AmSO₄ or any other non-fluorescent material (which need not be mono disperse).

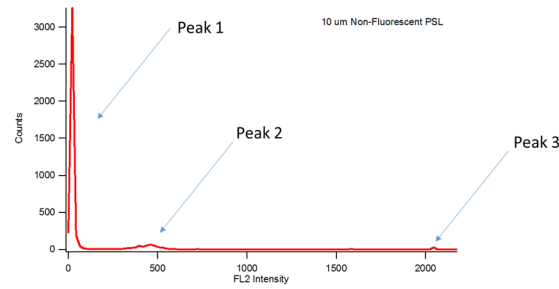
[A2.8] Based on the referee's suggestion, we looked into the size-dependence of the FL2 detector, as shown below. Histogram plots of fluorescence intensity in each fluorescence channel were created for each PSL sample, and Gaussians fits were applied to each mode present (3 peaks in Figure R.1). To determine whether there was a particle size dependence on the FL2 detector, four pieces of information were extracted from each histogram and plotted as a function of PSL particle diameter (Fig. R.2). Figures R.2A and B show the relationship of the median intensity of the two non-saturating modes from the histogram. Figure R.3-C shows the percent of particles that saturated the FL2 detector, and Figure R.3-D shows the median fluorescence intensity of all the data. Non-fluorescent PSLs ranging in size from 0.3 – 15 μm in size were plotted in Figure R.2, the two colors representing size calibrations from two separate occasions.

The two data sets show no obvious size correlation for peak 1 or peak 2 present in the FL2 channel, seen as essentially a flat relationship in Figure R.2A and R.2B. If there was a size dependence on the FL2 detector one would expect an increase in FL2 intensity as a function of particle size increases. There is an increase in percent FL2 saturation values for PSLs between ~1 and 4 μm, but only to a total of approximately 1.5% (Fig. R.2C).

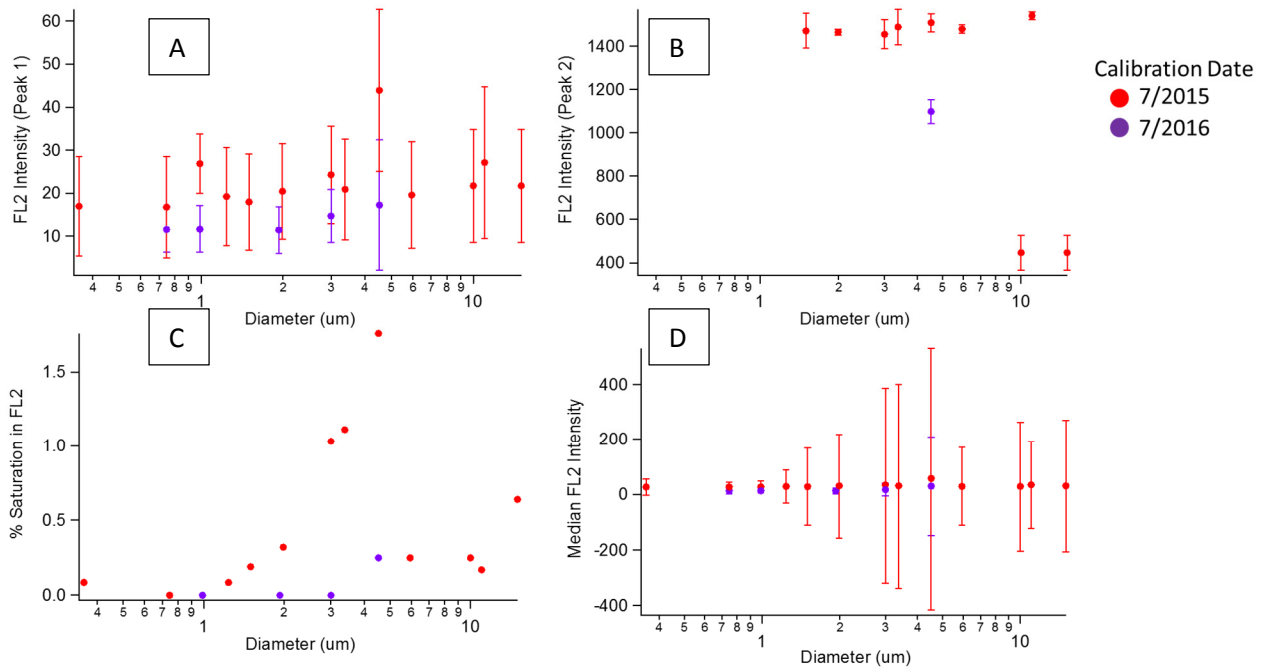
317 Finally, overall median values for the FL2 intensity also do not show a size dependence
318 correlation.

319
320 Based on this follow-up analysis we conclude that there was no obvious trend between
321 the measurements at the FL2 detector and particle size. This suggests that bleed through
322 from the flash lamp was not present in this case, and so it is unlikely that the instrument
323 is affected by any possible bad notch filters. This suggestion was an excellent one to
324 consider, however, and we suggest that other WIBS users be aware of this possible
325 problem and check their instrument(s) in a similar fashion.

326
327



328
329
330 Figure R.1: Histogram of FL2 responses shows multiple fluorescent modes for these 10 um
331 PSLs.
332



333
334 Figure R.2: (A) FL2 intensity vs. diameter for peak 1, (B) FL2 intensity vs. diameter for
335 peak 2, percent saturation in FL2 channel vs. diameter and (C) median fluorescence
336 intensity vs. diameter.
337

338 [R2.9] I appreciate your discussion of the asymmetry factor and the potential problems with it.
339 On lines 726-727 I believe you meant to say that the forward-scattering detector may not be able
340 to reliably estimate either size or AF? I also think you could give at least a hint at your ultimate
341 conclusion about the AF measurement in your initial discussion of this measurement and,
342 possibly, in the abstract. On my first read-through, after seeing the AF calculation in the text and
343 the AF values included in the table, I thought you might not examine that parameter critically.
344 Just something along the lines of “The performance of the asymmetry factor is assessed across
345 populations as a function of particle size.”

346

347 [A2.9] We changed L728:

348 “For this reason we postulate that the ~~side~~ forward-scattering detector may not be able to
349 reliably estimate ~~either particle size or~~ AF when particles are near the sizing limits.”

350

351 We added text after L38 in the abstract:

352 “The performance of the particle asymmetry factor (AF) reported by the instrument was
353 assessed across particle types as a function of particle size, and comments on the reliability
354 of this parameter are given.”

355

356 We added text after L759 in the conclusion:

357 “Lastly, we looked at the reliability of using the forward scattering to estimate particle
358 shape. Results showed a strong correlation between AF and size for various biological
359 and non-biological particles, indicating the AF parameter may not be reliable for
360 discriminating between different particle types.”

361

1 Systematic Characterization and Fluorescence Threshold Strategies for the Wideband Integrated
2 Bioaerosol Sensor (WIBS) Using Size-Resolved Biological and Interfering Particles

3 NICOLE SAVAGE¹, Christine Krentz¹, Tobias Könemann², Taewon T. Han³, Gediminas
4 Mainelis³, Christopher Pöhlker², John A. Huffman¹

5 ¹ *University of Denver, Department of Chemistry and Biochemistry, Denver, USA*

6 ² *Max Planck Institute for Chemistry, Multiphase Chemistry and Biogeochemistry Departments,*
7 *Mainz, Germany*

8 ³ *Rutgers, The State University of New Jersey, Department of Environmental Science, New*
9 *Jersey, USA*

10

11 **Abstract**

12 Atmospheric particles of biological origin, also referred to as bioaerosols or primary biological
13 aerosol particles (PBAP), are important to various human health and environmental systems.
14 There has been a recent steep increase in the frequency of published studies utilizing commercial
15 instrumentation based on ultraviolet laser/light-induced fluorescence (UV-LIF), such as the
16 WIBS (wideband integrated bioaerosol sensor) or UV-APS (ultraviolet aerodynamic particle
17 sizer), for bioaerosol detection both outdoors and in the built environment. Significant work over
18 several decades supported the development of the general technologies, but efforts to
19 systematically characterize the operation of new commercial sensors has remained lacking.
20 Specifically, there have been gaps in the understanding of how different classes of biological and
21 non-biological particles can influence the detection ability of LIF-instrumentation. Here we
22 present a systematic characterization of the WIBS-4A instrument using 69 types of aerosol
23 materials, including a representative list of pollen, fungal spores, and bacteria as well as the most
24 important groups of non-biological materials reported to exhibit interfering fluorescent
25 properties. Broad separation can be seen between the biological and non-biological particles
26 directly using the five WIBS output parameters and by taking advantage of the particle
27 classification analysis introduced by Perring et al. (2015). We highlight the importance that
28 particle size plays on observed fluorescence properties and thus in the Perring-style particle
29 classification. We also discuss several particle analysis strategies, including the commonly used
30 fluorescence threshold defined as the mean instrument background (forced trigger; FT) plus 3
31 standard deviations (σ) of the measurement. Changing the particle fluorescence threshold was
32 shown to have a significant impact on fluorescence fraction and particle type classification. We
33 conclude that raising the fluorescence threshold from FT + 3 σ to FT + 9 σ does little to reduce the
34 relative fraction of biological material considered fluorescent, but can significantly reduce the
35 interference from mineral dust and other non-biological aerosols. We discuss examples of highly
36 fluorescent interfering particles, such as brown carbon, diesel soot, and cotton fibers, and how
37 these may impact WIBS analysis and data interpretation in various indoor and outdoor
38 environments. The performance of the particle asymmetry factor (AF) reported by the instrument
39 was assessed across particle types as a function of particle size, and comments on the reliability
40 of this parameter are given. A comprehensive online supplement is provided, which includes size
41 distributions broken down by fluorescent particle type for all 69 aerosol materials and comparing
42 two threshold strategies. Lastly, the study was designed to propose analysis strategies that may

43 be useful to the broader community of UV-LIF instrumentation users in order to promote deeper
44 discussions about how best to continue improving UV-LIF instrumentation and analysis
45 strategies.

46 **1. Introduction**

47 Biological material emitted into the atmosphere from biogenic sources on terrestrial and
48 marine surfaces can play important roles in the health of many living systems and may influence
49 diverse environmental processes (Cox and Wathes, 1995;Pöschl, 2005;Després et al.,
50 2012;Fröhlich -Nowoisky et al., 2016). Bioaerosol exposure has been an increasingly important
51 component of recent interest, motivated by studies linking airborne biological agents and adverse
52 health effects in both indoor and occupational environments (Douwes et al., 2003). Bioaerosols
53 may also impact the environment by acting as giant cloud condensation nuclei (GCCN) or ice
54 nuclei (IN), having an effect on cloud formation and precipitation (Ariya et al., 2009;Delort et
55 al., 2010;Möhler et al., 2007;Morris et al., 2004). Biological material emitted into the
56 atmosphere is commonly referred to as Primary Biological Aerosol Particles (PBAP) or
57 bioaerosols. PBAP can include whole microorganisms, such as bacteria and viruses, reproductive
58 entities (fungal spores and pollen) and small fragments of any larger biological material, such as
59 leaves, vegetative detritus, fungal hyphae, or biopolymers, and can represent living, dead,
60 dormant, pathogenic, allergenic, or biologically inert material (Després et al., 2012). PBAP often
61 represent a large fraction of supermicron aerosol, for example up to 65% by mass in pristine
62 tropical forests, and may also be present in high enough concentrations at submicron sizes to
63 influence aerosol properties (Jaenicke, 2005;Penner, 1994;Pöschl et al., 2010).

64 Until recently the understanding of physical and chemical processes involving bioaerosols
65 has been limited due to a lack of instrumentation capable of characterizing particles with
66 sufficient time and size resolution (Huffman and Santarpia, 2017). The majority of bioaerosol
67 analysis historically utilized microscopy or cultivation-based techniques. Both are time-
68 consuming, relatively costly and cannot be utilized for real-time analysis (Griffiths and
69 Decosemo, 1994;Agranovski et al., 2004). Cultivation techniques can provide information about
70 properties of the culturable fraction of the aerosol (e.g. bacterial and fungal spores), but can
71 greatly underestimate the diversity and abundance of bioaerosols because the vast majority of
72 microorganism species are not culturable (Amann et al., 1995;Chi and Li, 2007;Heidelberg et al.,
73 1997). Further, because culture-based methods cannot detect non-viable bioaerosols, information
74 about their chemical properties and allergenicity has been poorly understood.

75 In recent years, advancements in the chemical and physical detection of bioaerosols have
76 enabled the development of rapid and cost-effective techniques for the real-time characterization
77 and quantification of airborne biological particles (Ho, 2002;Hairston et al., 1997;Huffman and
78 Santarpia, 2017;Sodeau and O'Connor, 2016). One important technique is based on ultraviolet
79 laser/light-induced fluorescence (UV-LIF), originally developed by military research
80 communities for the rapid detection of bio-warfare agents (BWA) (e.g. Hill et al., 2001;Hill et
81 al., 1999a;Pinnick et al., 1995). More recently, UV-LIF instrumentation has been
82 commercialized for application toward civilian research in fields related to atmospheric and
83 exposure science. The two most commonly applied commercial UV-LIF bioaerosol sensors are
84 the wideband integrated bioaerosol sensor (WIBS; University of Hertfordshire, Hertfordshire,
85 UK, now licensed to Droplet Measurement Technologies, Longmont, CO, USA), and the

86 ultraviolet aerodynamic particle sizer (UV-APS; licensed to TSI, Shoreview, MN, USA). Both
87 sensors utilize pulsed ultraviolet light to excite fluorescence from individual particles in a real-
88 time system. The wavelengths of excitation and emission were originally chosen to detect
89 biological fluorophores assumed to be widely present in airborne microorganisms (e.g.
90 tryptophan-containing proteins, NAD(P)H co-enzymes, or riboflavin) (Pöhlker et al., 2012).
91 Significant work was done by military groups to optimize pre-commercial sensor performance
92 toward the goal of alerting for the presence of biological warfare agents such as anthrax spores.
93 The primary objective from this perspective is to positively identify BWAs without being
94 distracted by false-positive signals from fluorescent particles in the surrounding natural
95 environment (Primmerman, 2000). From the perspective of basic atmospheric science, however,
96 the measurement goal is often to quantify bioaerosol concentrations in a given environment. So,
97 to a coarse level of discrimination, BWA-detection communities aim to ignore most of what the
98 atmospheric science community seeks to detect. Researchers on such military-funded teams also
99 have often not been able to publish their work in formats openly accessible to civilian
100 researchers, so scientific literature is lean on information that can help UV-LIF users operate and
101 interpret their results effectively. Early UV-LIF bioaerosol instruments have been in use for two
102 decades and commercial instruments built on similar concepts are emerging and becoming
103 widely used by scientists in many disciplines. In some cases, however, papers are published with
104 minimal consideration of complexities of the UV-LIF data. This study presents a detailed
105 discussion of several important variables specific to WIBS data interpretation, but that can apply
106 broadly to operation and analysis of many similar UV-LIF instruments.

107 The commercially available WIBS instrument has become one of the most commonly
108 applied instrument toward the detection and characterization of bioaerosol particles in both
109 outdoor and indoor environments. As will be discussed in more detail, the instrument utilizes two
110 wavelengths of excitation (280 nm and 370 nm), the second of which is close to the one
111 wavelength utilized by the UV-APS (355 nm). Both the WIBS and UV-APS, in various version
112 updates, have been applied to many types of studies regarding outdoor aerosol characterization.
113 For example they have been important instruments: in the study of ice nuclei (Huffman et al.,
114 2013;Mason et al., 2015;Twohy et al., 2016), toward the understanding of outdoor fungal spore
115 concentrations (Gosselin et al., 2016;Saari et al., 2015a;O'Connor et al., 2015b), to investigate
116 the concentration and properties of bioaerosols from long-range transport (Hallar et al., 2011), in
117 tropical aerosol (Gabey et al., 2010;Whitehead et al., 2010;Huffman et al., 2012;Valsan et al.,
118 2016;Whitehead et al., 2016), in urban aerosol (Huffman et al., 2010;Saari et al., 2015b;Yu et al.,
119 2016), from composting centers (O'Connor et al., 2015), at high altitude (Crawford et al.,
120 2016;Gabey et al., 2013;Perring et al., 2015;Ziemba et al., 2016), and in many other
121 environments (Healy et al., 2014;Li et al., 2016;O'Connor et al., 2015a). The same
122 instrumentation has been utilized for a number of studies involving the built, or indoor,
123 environment as well (Wu et al., 2016). As a limited set of examples, these instruments have been
124 critical components in the study of bioaerosols in the hospital environment (Lavoie et al.,
125 2015;Handorean et al., 2015) and to study the emission rates of biological particles directly from
126 humans (Bhangar et al., 2016) in school classrooms (Bhangar et al., 2014), and in offices (Xie et
127 al., 2017).

128 Despite the numerous and continually growing list of studies that utilize commercial UV-LIF
129 instrumentation, only a handful of studies have published results from laboratory work
130 characterizing the operation or analysis of the instruments in detail. For example, Kanaani et al.

131 (2007;2008;2009) and Agranovski et al. (2003, 2004, 2005) presented several examples of UV-
132 APS operation with respect to bio-fluorophores and biological particles. Healy et al. (2012)
133 provided an overview of fifteen spore and pollen species analyzed by the WIBS, and Toprak and
134 Schnaiter (2013) discussed the separation of dust from ambient fluorescent aerosol by applying a
135 simple screen of any particles that exhibited fluorescence in one specific fluorescent channel.
136 Hernandez et al. (2016) presented a summary of more than 50 pure cultures of bacteria, fungal
137 spores, and pollen species analyzed by the WIBS and with respect to fluorescent particle type.
138 Fluorescent particles observed in the atmosphere have frequently been used as a lower-limit
139 proxy for biological particles (e.g. Huffman et al. 2010), however it is well known that a number
140 of key particle types of non-biological origin can fluoresce. For example, certain examples of
141 soot, humic and fulvic acids, mineral dusts, and aged organic aerosols can exhibit fluorescent
142 properties, and the effects that these play in the interpretation of WIBS data is unclear (Bones et
143 al., 2010; Gabey et al., 2011; Lee et al., 2013; Pöhlker et al., 2012; Sivaprakasam et al., 2004).

144 The simplest level of analysis of WIBS data is to provide the number of particles that exceed
145 the minimum detectable threshold in each of the three fluorescence categories. Many papers on
146 ambient particle observations have been written using this data analysis strategy with both the
147 WIBS and UV-APS data. Such analyses are useful and can provide an important first layer of
148 discrimination by fluorescence. To provide more complicated discrimination as a function of
149 observed fluorescence intensity, however, brings associated analysis and computing challenges,
150 i.e. users often must write data analysis code themselves, and processing large data sets can push
151 the limits of standard laboratory computers. Discriminating based on fluorescence intensity also
152 requires more detailed investigations into the strategy by which fluorescent thresholds can be
153 applied to define whether a particle is considered fluorescent. Additionally, relatively little
154 attention has been given to the optical properties of non-biological particles interrogated by the
155 WIBS and to optimize how best to systematically discriminate between biological aerosol of
156 interest and materials interfering with those measurements.

157 Here we present a comprehensive and systematic laboratory study of WIBS data in order to
158 aid the operation and data interpretation of commercially available UV-LIF instrumentation. This
159 work presents 69 types of aerosol materials, including key biological and non-biological
160 particles, interrogated by the WIBS-4A and shows the relationship of fluorescent intensity and
161 resultant particle type as a function of particle size and asymmetry. A discussion of thresholding
162 strategy is given, with emphasis on how varying strategies can influence characterization of
163 fluorescent properties and either under- or over-prediction of fluorescent biological particle
164 concentration.

165 **2. WIBS Instrumentation**

166 **2.1 Instrument Design and Operation**

167 The WIBS (Droplet Measurement Technologies; Longmont, Colorado) uses light scattering
168 and fluorescence spectroscopy to detect, size, and characterize the properties of interrogated
169 aerosols on a single particle basis (instrument model 4A utilized here). Air is drawn into the
170 instrument at a flow rate of 0.3 L/min and surrounded by a filtered sheath flow of 2.2 L/min. The
171 aerosol sample flow is then directed through an intersecting a 635 nm, continuous wave (cw)
172 diode laser, which produces elastic scattering measured in both the forward and side directions.

173 Particle sizing in the range of approximately 0.5 μm to 20 μm is detected by the magnitude of
174 the electrical pulse detected by a photomultiplier tube (PMT) located at 90 degrees from the laser
175 beam. Particles whose measured cw laser-scattering intensity (particle size) exceed user-
176 determined trigger thresholds will trigger two xenon flash lamps (Xe1 and Xe2) to fire in
177 sequence, approximately 10 microseconds apart. The two pulses are optically filtered to emit at
178 280 nm and 370 nm, respectively. Fluorescence emitted by a given particle after each excitation
179 pulse is detected simultaneously using two PMT detectors. -The first PMT is optically filtered to
180 detect the total intensity of fluorescence in the range 310-400 nm and the second PMT in the
181 range 420-650 nm. So for every particle that triggers xenon lamp flashes, Xe1 produces a signal
182 in the FL1 (310-400 nm) and FL2 (420-650 nm) channels, whereas the Xe2 produces only a
183 signal in the FL3 (420-650 nm) channel because elastic scatter from the Xe2 flash saturates the
184 first PMT. The WIBS-4A has two user defined trigger thresholds, T1 and T2 that define which
185 data will be recorded. Particles producing a scattering pulse from the cw laser that is below the
186 T1 threshold will not be recorded. This enables the user to reduce data collection during
187 experiments with high concentrations of small particles. Particles whose scattering pulse exceeds
188 the T2 threshold will trigger xenon flash lamp pulses for interrogation of fluorescence. Note that
189 the triggering thresholds mentioned here are fundamentally different from the analysis thresholds
that will be discussed in detail later.

191 Forward-scattered light is detected using a quadrant PMT. The detected light intensity in
192 each quadrant are combined using Equation 1 into an asymmetry factor (AF), where k is an
193 instrument defined constant, E is the mean intensity measured over the entire PMT, and E_i is the
194 intensity measured at the i^{th} quadrant (Gabey et al., 2010).

$$195 \quad AF = \frac{k(\sum_{i=1}^n (E - E_i)^2)^{1/2}}{E} \quad (1)$$

196 This parameter relates to a rough estimate of the sphericity of an individual particle by
197 measuring the difference of light intensity scattered into each of the four quadrants. A perfectly
198 spherical particle would theoretically exhibit an AF value of 0, whereas larger AF values greater
199 than 0 and less than 100, indicate rod-like particles (Kaye et al., 1991; Gabey et al., 2010; Kaye et
200 al., 2005). **In practice, spherical PSL particles (polystyrene latex spheres) exhibit a median AF**
201 **value of approximately 5 (Table 1).** It is important to note that the AF is parameter is not
202 rigorously a shape factor like used in other aerosol calculations (DeCarlo et al., 2004; Zelenyuk et
203 al., 2006) and only very roughly relates a measure of particle sphericity.

204 2.2 WIBS Calibration

205 **The particle size reported by the internal WIBS calibration introduces significant sizing**
206 **errors and critically needs to be calibrated before analyzing or reporting particle size. Particle**
207 **size calibration was achieved here by using a one-time 27-point calibration curve generated**
208 **using non-fluorescent PSLs ranging in size from 0.36 to 15 μm . This calibration involved several**
209 **steps. For each physical sample, approximately 1,000 to 10,000 individual particles were**
210 **analyzed using the WIBS (several minutes of collection). Data collected for each sample was**
211 **analyzed by plotting a histogram of the side-scatter response reported in the raw data files**
212 **(FL2_sctpk). A Gaussian curve was fitted to the most prominent mode in the distribution. The**
213 **median value of the fitted peak for observed side scatter was then plotted against the physical**

214 diameter (as reported on the bottle) for each PSL sample. A 2nd degree polynomial function was
215 fitted to this curve to create the calibration equation that was used on all laboratory data
216 presented here. The calibration between observed particle size and physical diameter may be
217 affected by wiggles in the optical scattering relationship suggested by Mie theory. These
218 theoretical considerations were not used for the calibrations reported here, and so uncertainties in
219 reported size are expected to increase marginally at larger diameters.

220 Following the one-time 27-point calibration, the particle sizing response was checked
221 periodically using a 5-point calibration. The responses of these calibration checks were within
222 one standard deviation unit of each other and so the more comprehensive calibration equation
223 was used in all cases. These quicker checks were performed using ing within the instrument was
224 calibrated periodically by aerosolizing several sizes of non-fluorescent PSLs polystyrene latex
225 spheres (PSLs; (Polysciences, Inc., Pennsylvania), including 0.51 μm (part number 07307), 0.99
226 μm . (07310), 1.93 μm (19814), 3.0 μm (17134), and 4.52 μm (17135). A histogram of signal
227 intensity was plotted separately for each PSL, and the peak of a Gaussian fit to those data was
228 then plotted versus the physical diameter of the PSL. A second degree polynomial fit was used to
229 generate an equation in order to calibrate side scatter values into size.

230 Fluorescence intensity in each WIBS channel was calibrated using 2.0 μm Green (G0200),
231 2.1 μm Blue (B0200), and 2.0 μm Red (R0200) fluorescent PSLs (Thermo-Scientific,
232 Sunnyvale, California). For each particle type, a histogram of the fluorescence intensity signal in
233 each channel was fitted with a Gaussian function, and the median intensity was recorded.
234 Periodic checks were performed using the same stock bottles of the PSLs in order to verify that
235 mean fluorescence intensity of each had not shifted more than one standard deviation between
236 particle sample types (Table 1). The particle fluorescence standards used present limitations due
237 to variations in fluorescence intensity between stocks of particles and due to fluorophore
238 degradation over time. To improve reliability between instruments, stable fluorescence standards
239 and calibration procedures (e.g. Robinson et al., 2017) will be important.

240 Voltage gain settings for the three PMTs that produce sizing, fluorescence, and AF values,
241 respectively, significantly impact measured intensity values and are recorded here for rough
242 comparison of calibrations and analyses to other instruments. The voltage settings used for all
243 data presented here were set according to manufacturer specifications and are as follows: PMT₁
244 (AF) 400 V, PMT₂ (particle sizing and FL1 emission) 450 mV, and PMT₃ (FL2, FL3 emission)
245 732 mV.

246 2.3 WIBS Data Analysis

247 An individual particle is considered to be fluorescent in any one of the three fluorescence
248 channels (FL1, FL2, or FL3) when its fluorescence emission intensity exceeds a given baseline
249 threshold. The baseline fluorescence can be determined by a number of strategies, but commonly
250 has been determined by measuring the observed fluorescence in each channel when the xenon
251 lamps are fired into the optical chamber when devoid of particles. This is referred to as the
252 “forced trigger” (FT) process, because the xenon lamp firing is not triggered by the presence of a
253 particle. The instrument background is also dependent on the intensity and orientation of Xe
254 lamps, voltage gains of PMTs, quality of PMTs based on production batch, orientation of optical
255 components i.e. mirrors in the optical chamber, etc. As a result of these factors, the background

256 or baseline of a given instrument is unique and cannot be used as a universal threshold. All
257 threshold values used in this study can be listed in supplementary Table S1. Fluorescence
258 intensity in each channel is recorded at an approximate FT rate of one value per second for a
259 user-defined time period, typically 30-120 seconds. The baseline threshold in each channel has
260 typically been determined as the average plus 3x the standard deviation (σ) of forced trigger
261 fluorescence intensity measurement (Gabey et al., 2010), however alternative applications of the
262 fluorescence threshold will be discussed. Particles exhibiting fluorescence intensity lower than
263 the threshold value in each of the three channels are considered to be non-fluorescent. The
264 emission of fluorescence from any one channel is essentially independent of the emission in the
265 other two channels. The pattern of fluorescence measured allows particles to be categorized into
266 7 fluorescent particle types (A, B, C, AB, AC, BC, or ABC) as depicted in Figure 1, or as
267 completely non-fluorescent (Perring et al., 2015).

268 Other threshold strategies have also been proposed and will be discussed. For example,
269 Wright et al. (2014) used set fluorescence intensity value boundaries rather than using the
270 standard Gabey et al. (2010) definition that applies a threshold as a function of observed
271 background fluorescence. The Wright et al. (2014) study proposed five separate categories of
272 fluorescent particles (FP1 through FP5). Each definition was determined by selecting criteria for
273 excitation-emission boundaries and observing the empirical distribution of particles in a 3-
274 dimensional space (FL1 vs. FL2 vs. FL3). For the study reported here, only the FP3 definition
275 was used for comparison, because Wright et al. (2014) postulated the category as being enriched
276 with fungal spores during their ambient study and because they observed that these particles
277 scaled more tightly with observed ice nucleating particles. The authors classified a particle in the
278 FP3 category if the fluorescence intensity in FL1 > 1900 arbitrary units (a.u) and between 0-500
279 a.u for each FL2 and FL3.

280 **3. Materials and methods**

281 **3.1 Aerosol Materials**

282 *3.1.1 Table of materials*

283 All materials utilized, including the vendors and sources from where they were acquired,
284 have been listed in supplemental Table S1, organized into broad particle type groups: biological
285 material (fungal spores, pollen, bacteria, and biofluorophores) and non-biological material (dust,
286 humic-like substances or HULIS, polycyclic aromatic hydrocarbons or PAHs, combustion soot
287 and smoke, and **common household fibersmiscellaneous non-biological materials**). Combustion
288 soot and smoke are grouped into one set of particles analyzed and are hereafter referred to as
289 “soot” samples. **It is important to note that all particle types analyzed here essentially represent**
290 **“fresh” emissions. It is unclear how atmospheric aging might impact their surface chemical**
291 **properties or how their observed fluorescence properties might evolve over time.**

292 *3.1.2 Brown carbon synthesis*

293 Three different brown carbon solutions were synthesized using procedures described by
294 Powelson et al. (2014): (Rxn 1) methylglyoxal + glycine, (Rxn 2) glycolaldehyde +
295 methylamine, and (Rxn 3) glyoxal + ammonium sulfate. **These reactions were chosen, because**
296 **the reaction products were achievable using bulk-phase aqueous chemistry and did not require**

297 more complex laboratory infrastructure. They represent three examples of reactions possible in
298 cloud-water using small, water-soluble carbonyl compounds mixed with either ammonium
299 sulfate or a primary amine (Powelson et al., 2014). A large number of reaction pathways exist to
300 produce atmospheric brown carbon, however, and the products analyzed here are intended
301 primarily to introduce the possible importance of brown carbon droplets and coatings to
302 fluorescence-based aerosol detection (Huffman et al., 2012).

303 Reactions conditions were reported previously, so only specific concentration and volumes
304 used here are described. All solutions described are aqueous and were dissolved into 18.2 MΩ
305 water (Millipore Sigma; Denver, CO). For reaction 1, 25.0 mL of 0.5 M methylglyoxal solution
306 was mixed with 25 mL of 0.5 M glycine solution. For reaction 2, 5.0 mL of 0.5 M glyoxal trimer
307 dihydrate solution was mixed with 5.0 mL of 0.5 M ammonium sulfate solution. For reaction 3,
308 10.0 mL of 0.5 M glycolaldehyde solution was mixed with 10.0 mL of 0.5 M methylamine
309 solution. The pH of the solutions was adjusted to approximately pH 4 by adding 1 M oxalic acid
310 in order for the reaction to follow the appropriate chemical mechanism (Powelson et al., 2014).
311 The solutions were covered with aluminum foil and stirred at room temperature for 8 days, 4
312 days, and 4 days; for reactions 1, 2, and 3, respectively. Solutions were aerosolized via the liquid
313 aerosolization method described in Section 3.2.4.

314 **3.2 Aerosolization Methods**

315 *3.2.1 Fungal spore growth and aerosolization*

316 Fungal cultures were inoculated onto sterile, disposable polystyrene plates (Carolina,
317 Charlotte, NC) filled with agar growth media consisting of malt extract medium mixed with
318 0.04 M of streptomycin sulfate salt (S6501, Sigma-Aldrich) to suppress bacterial colony growth.
319 Inoculated plates were allowed to mature and were kept in a sealed Plexiglas box for 3-5 weeks
320 until aerosolized. Air conditions in the box were monitored periodically and were consistently
321 25-27 °C and 70% relative humidity.

322 Fungal cultures were aerosolized inside an environmental chamber constructed from a re-
323 purposed home fish tank (Aqueon Glass Aquarium, 5237965). The chamber has glass panels
324 with dimensions 20.5 L x 10.25 H x 12.5 W inch (supplemental Fig. S1). Soft rubber beading
325 seals the top panel to the walls, allowing isolation of air and particles within the chamber. Two
326 tubes are connected to the lid. The first tube delivers pressurized and particle-free air through a
327 bulkhead connection, oriented by plastic tubing (Loc-Line Coolant Hose, 0.64 inch outer
328 diameter) and a flat nozzle. The second tube connects 0.75 inch internal diameter conductive
329 tubing (Simolex Rubber Corp., Plymouth, MI) for aspiration of fungal aerosol, passing it through
330 a bulkhead fitting and into tubing directed toward the WIBS. Aspiration tubing is oriented such
331 that a gentle 90-degree bend brings aerosol up vertically through the top panel.

332 For each experiment, an agar plate with a mature fungal colony was sealed inside the
333 chamber. A thin, wide~~The air delivery~~ nozzle was positioned so that the delivered air stream
334 approximated a blade of air that was allowed to approached the top of the spore colony at a
335 shallow angle in order to eject spores into an approximately-roughly horizontal trajectory. The
336 sample collection tube was positioned immediately past the fungal plate to aspirate aerosolized
337 fungal particles. Filtered room air was delivered by a pump through the aerosolizing flow at

338 approximately 9 – 15 L/min, varied within each experiment to optimize measured spore
339 concentration. Sample flow was 0.3 L/min into the WIBS and excess input flow was balanced by
340 outlet through a particle filter connected through a bulkhead on the top plate.

341 Two additional rubber septa in the top plate allow the user to manipulate two narrow metal
342 rods to move the agar plate once spores were depleted from a given region of the colony. After
343 each spore experiment, the chamber and tubing was evacuated by pumping for 15 minutes, and
344 all interior surfaces were cleaned with isopropanol to avoid contamination between samples.

345 3.2.2 Bacterial growth and aerosolization

346 All bacteria were cultured in nutrient broth (Becton, Dickinson and Company, Sparks, MD)
347 for 18 hours in a shaking incubator at 30°C for *Bacillus atrophaeus* (ATCC 49337, American
348 Type Culture Collection, MD), 37°C for *Escherichia coli* (ATCC 15597), and 26°C
349 *Pseudomonas fluorescens* (ATCC 13525). Bacterial cells were harvested by centrifugation at
350 7000 rpm (6140 g) for 5 min at 4°C (BR4, Jouan Inc., Winchester, VA) and washed 4 times with
351 autoclave-sterilized deionized water (Millipore Corp., Billerica, MA) to remove growth media.
352 The final liquid suspension was diluted with sterile deionized water, transferred to a
353 polycarbonate jar and aerosolized using a three jet Collison nebulizer (BGI Inc., Waltham, MA)
354 operated at 5 L/min (pressure of 12 psi). The polycarbonate jar was used to minimize damage to
355 bacteria during aerosolization (Zhen et al., 2014). The tested airborne cell concentration was
356 about $\sim 10^5$ cells/Liter as determined by an optical particle counter (Model 1.108, Grimm
357 Technologies Inc., Douglasville, GA). Bacterial aerosolization took place in an experimental
358 system containing a flow control system, a particle generation system, and an air-particle mixing
359 system introducing filtered air at 61 L/min as described by Han et al. (2015).

360 3.2.3 Powder aerosolization

361 Dry powders were aerosolized by mechanically agitating material by one of several methods
362 mentioned below and passing filtered air across a vial containing the powder. For each method,
363 approximately 2.5-5.0 g of sample was placed in a 10 mL glass vial. For most samples (method
364 P1), a stir bar was added, and the vial was placed on a magnetic stir plate. Two tubes were
365 connected through the lid of the vial. The first tube connected a filter, allowing particle-free air
366 to enter the vessel. The second tube connected the vial through approximately 33 cm of
367 conductive tubing (0.25 inch inner diam.) to the WIBS for sample collection.

368 The setup was modified (method P2) for a small subset of samples whose solid powder was
369 sufficiently fine to produce high number concentrations of particles (e.g. $> 200 \text{ cm}^{-3}$) and that
370 contained enough submicron aerosol material ~~partieles that could to~~ risk coating the internal
371 flow path and damaging optical components of the instrument. In this case, the same small vial
372 with powder and stir bar was placed in a larger reservoir (~ 0.5 L), but without vial lid. The lid of
373 the larger reservoir was connected to filtered air input and an output connection to the
374 instrument. The additional container volume allowed for greater dilution of aerosol before
375 sampling into the instrument.

376 Some powder samples produced consistent aerosol number concentration even without
377 stirring. For these samples, 2.5 – 5.0 g of material was placed in a small glass vial and set under a

laboratory fume hood (method P3). Conductive tubing was held in place at the opening of the vial using a clamp, and the opposite end was connected to the instrument with a flow rate of 0.3 L/min. The vial was tapped by hand or with a hand tool, physically agitating the material and aerosolizing the powder.

3.2.4 Liquid aerosolization

Disposable, plastic medical nebulizers (Allied Healthcare, St. Louis, MO) were used to aerosolize liquid solutions and suspensions. Each nebulizer contains a reservoir where the solution is held. Pressurized air is delivered through a capillary opening on the side, reducing static pressure and, as a result, drawing fluid into the tube. The fluid is broken up by the air jet into a dispersion of droplets, where most of the droplets are blown onto the internal wall of the reservoir, and droplets remaining aloft are entrained into the sample stream. Output from the medical nebulizer was connected to a dilution chamber (aluminum enclosure, 0.5 L), allowing the droplets to evaporate in the system before particles enter the instrument for detection.

3.2.5 Smoke generation

Wood and cigarette smoke samples were aerosolized through combustion. Each sample was ignited separately using a personal butane lighter while held underneath a laboratory fume hood. Once the flame from the combusting sample was naturally extinguished, the smoldering sample was waved at a height ~5 cm above the WIBS inlet for 3– 5 minutes during sampling.

3.3 Pollen microscopy

Pollen samples were aerosolized using the dry powder vial (P1, P2) and tapping (P3) methods detailed above. Samples were also collected by impaction onto a glass microscope slide for visual analysis using a home-built, single-stage impactor with D_{50} cut $\sim 0.5 \mu\text{m}$ at flow-rate 1.2 L min^{-1} . Pollen were analyzed using an optical microscope (VWR model 89404-886) with a 40x objective lens. Images were collected with an AmScope complementary metal-oxide semiconductor camera (model MU800, 8 megapixels).

4. Results

4.1 Broad separation of particle types

The WIBS is routinely used as an optical particle counter applied to the detection and characterization of fluorescent biological aerosol particles (FBAP). Each interrogated particle provides five discrete pieces of information: fluorescence emission intensity in each of the 3 detection channels (FL1, FL2, and FL3), particle size, and particle asymmetry. Thus, a thorough summary of data from aerosolized particles would require the ability to show statistical distributions in five dimensions. As a simple, first-order representation of the most basic summary of the 69 particle types analyzed, Figure 2 and Table 4-2 show median values for each of the five data parameters plotted in three plot styles (columns of panels in Fig. 2).

For the sake of WIBS analysis, each pollen type was broken into two size categories, because it was observed that most pollen species exhibited two distinct size modes. The largest size mode peaked above $10 \mu\text{m}$ in all cases and often saturated the sizing detector (see also fraction of particles that saturated particle detector for each fluorescence channel in Table 2). This was

417 interpreted to be intact pollen. A broad mode also usually appeared at smaller particle diameters
418 for some pollen species, suggesting that pollen grains had ruptured during dry storage or through
419 the mechanical agitation process. This hypothesis was supported by optical microscopy through
420 which a mixture of intact pollen grains and ruptured fragments were observed (Fig. S2). For the
421 purposes of this investigation, the two modes were separated at the minimum point between
422 modes in order to observe optical properties of the intact pollen and pollen fragments separately.
423 The list number for each pollen (Tables 2, S1) is consistent for the intact and fragmented species,
424 though not all pollen exhibited obvious pollen fragments.

425 The WIBS was developed primarily to discriminate biological from non-biological particles,
426 and the three fluorescence channels broadly facilitate this separation. Biological particles, i.e.
427 pollen, fungal spores, and bacteria (top row of Fig. 2), each show strong median fluorescence
428 signal in at least one of the three channels. In general, all fungal spores sampled (blue dots) show
429 fluorescence in the FL1 channel with lower median emission in FL2 and FL3 channels. Both the
430 fragmented (pink dots) and intact (orange dots) size fractions of pollen particles showed high
431 median fluorescence emission intensity in all channels, varying by species and strongly as a
432 function of particle size. The three bacterial species sampled (green dots) showed intermediate
433 median fluorescence emission in the FL1 channel and very low median intensity in either of the
434 other two channels. To support the understanding of whole biological particles, pure molecular
435 components common to biological material were aerosolized separately and are shown as the
436 second row of Figure 2. Each of the biofluorophores chosen shows relatively high median
437 fluorescence intensity, again varying as a function of size. Key biofluorophores such as NAD,
438 riboflavin, tryptophan, and tyrosine are individually labeled in Figure 2d. Supermicron particles
439 of these pure materials would not be expected in a real-world environment, but are present as
440 dilute components of complex biological material and are useful here for comparison. In general,
441 the spectral properties summarized here match well with fluorescence excitation emission
442 matrices (EEMs) presented by Pöhlker et al. (2012;2013)

443 In contrast to the particles of biological origin, a variety of non-biological particles were
444 aerosolized in order to elucidate important trends and possible interferences. The majority of
445 non-biological particles shown in the bottom row of Figure 2 show little to no median
446 fluorescence in each channel and are therefore difficult to differentiate from one another in the
447 figure. For example, Figure 2g (lower left) shows the median fluorescence intensity of 6 different
448 groups of particle types (33 total dots), but almost all overlap at the same point at the graph
449 origin. The exceptions to this trend include the PAHs (blue dots), **miscellaneous**
450 **particles common household fibers** (green), and several types of combustion soot (black dots).
451 The fluorescent properties of PAHs are well-known in both basic chemical literature and as
452 observed in the atmosphere (Niessner and Krupp, 1991; Finlayson-Pitts and Pitts, November
453 1999; Panne et al., 2000; Slowik et al., 2007). PAHs can be produced by a number of
454 anthropogenic sources and are emitted in the exhaust from vehicles and other combustion
455 sources as well as from biomass burning (Aizawa and Kosaka, 2010, 2008; Abdel-Shafy and
456 Mansour, 2016; Lv et al., 2016). PAHs alone exhibit high fluorescence quantum yields (Pöhlker
457 et al., 2012; Mercier et al., 2013), but as pure materials are not usually present in high
458 concentrations at sizes large enough ($>0.8 \mu\text{m}$) to be detected by the WIBS. Highly fluorescent
459 PAH molecules are also common constituents of other complex particles, including soot particle
460 agglomerates. It has been observed that the fluorescent emission of PAH constituents on soot
461 particles can be weak due to quenching from the bulk material (Panne et al., 2000). Several

462 examples of soot particles shown in Figure 2g are fluorescent in FL1 and indeed should be
463 considered as interfering particle types, as will be discussed. Three **miscellaneous-household**
464 **fiber** particles (laboratory wipes and two colors of cotton t-shirts) were also interrogated by
465 rubbing samples over the WIBS inlet, because of their relevance to indoor aerosol investigation
466 (e.g. Bhangar et al., 2014; Handorean et al., 2015; e.g. Bhangar et al., 2016). These particles (dark
467 blue dots, Fig. 2 bottom row) show varying median intensity in FL1, suggesting that sources
468 such as tissues, cleaning wipes, and cotton clothing could be sources of fluorescent particles
469 within certain built environments.

470 Another interesting point from the observations of median fluorescence intensity is that the
471 three viable bacteria aerosolized in this study each shows moderately fluorescent characteristics
472 in FL1 and low fluorescent characteristics in FL2 and FL3 (Fig. 2a-c). A study by Hernandez et
473 al. (2016) also focused on analysis strategies using the WIBS and shows similar results regarding
474 bacteria. Of the 14 bacteria samples observed in the Hernandez et al. study, 13 were categorized
475 as predominantly A-type particles, thus meaning they exhibited fluorescent properties in FL1 and
476 only a very small fraction of particles showed fluorescence above the applied threshold ($FT + 3\sigma$)
477 in either FL2 or FL3. The FL3 channel in the WIBS-4A has an excitation of 370 nm and
478 emission band of 420-650 nm, similar to that of the UV-APS with an excitation of 355 nm and
479 emission band of 420-575 nm. Previous studies have suggested that viable microorganisms (i.e.
480 bacteria) show fluorescence characteristics in the UV-APS due to the excitation source of 355
481 nm that was originally designed to excite NAD(P)H and riboflavin molecules present in actively
482 metabolizing organisms (Agranovski et al., 2004; Hairston et al., 1997; Ho et al., 1999; Pöhlker et
483 al., 2012). Previous studies with the UV-APS and other UV-LIF instruments using
484 approximately similar excitation wavelengths have shown a strong sensitivity to the detection of
485 “viable” bacteria (Hill et al., 1999b; Pan et al., 1999; Hairston et al., 1997; Brosseau et al., 2000).
486 Because the bacteria here were aerosolized and detected immediately after washing from growth
487 media, we expect that a high fraction of the bacterial signal was a result of living vegetative
488 bacterial cells. The results presented here and from other studies using WIBS instruments, in
489 contrast to reports using other UV-LIF instruments, suggest that the WIBS-4A is highly sensitive
490 to the detection of bacteria using 280 nm excitation (only FL1 emission), but less so using the
491 370 nm excitation (FL3 emission) (e.g. Perring et al., 2015; Hernandez et al., 2016). A study by
492 Agranovski et al. (2003) also demonstrated that the UV-APS was limited in its ability to detect
493 endospores (reproductive bacterial cells from spore-forming species with little or no metabolic
494 activity and thus low NAD(P)H concentration). The lack of FL3 emission observed from
495 bacteria in the WIBS may also suggest a weaker excitation intensity in Xe2 with respect to Xe1,
496 manifesting in lower overall FL3 emission intensity (Könemann et al., In Prep.). Gain voltages
497 applied differently to PMT2 and PMT3 could also impact differences in relative intensity
498 observed. Lastly, it has been proposed that the rapid sequence of Xe1 and Xe2 excitation could
499 lead to quenching of fluorescence from the first excitation flash, leading to overall reduced
500 fluorescence in the FL3 channel (Sivaprakasam et al., 2011). These factors may similarly affect
501 all WIBS instruments and should be kept in mind when comparing results here with other UV-
502 LIF instrument types.

503 **4.2 Fluorescence type varies with particle size**

504 The purpose of Figure 2 is to distill complex distributions of the five data parameters into a
505 single value for each in order to show broad trends that differentiate biological and non-

506 biological particles. By representing the complex data in such a simple way, however, many
507 relationships are averaged away and lost. For example, the histogram of FL1 intensity for fungal
508 spore *Aspergillus niger* (Fig. S3) shows a broad distribution with long tail at high fluorescence
509 intensity, including ca. ~6 % of particles that saturate the FL1 detector (Table S2). If a given
510 distribution were perfectly Gaussian and symmetric, the mean and standard deviation values
511 would be sufficient to fully describe the distribution. However, given that asymmetric
512 distributions often include detector-saturating particles, no single statistical fit characterizes data
513 for all particle types well. Median values were chosen for Figure 2 knowing that the resultant
514 values can reduce the physical meaning in some cases. For example, the same *Aspergillus niger*
515 particles show a broad FL1 peak at ~150 a.u. and another peak at 2047 a.u. (detector saturated),
516 whereas the median FL1 intensity is 543 a.u., at which point there is no specific peak. In this
517 way, the median value only broadly represents the data by weighting both the broad distribution
518 and saturating peak. To complement the median values, however, Table [S2](#) also shows the
519 fraction of particles that were observed to saturate the fluorescence detector in each channel.

520 The representation of median values for each of the five parameters (Fig. 2) shows broad
521 separation between particle classes, but discriminating more finely between particle types with
522 similar properties by this analysis method can be practically challenging. Rather than
523 investigating the intensity of fluorescence emission in each channel, however, a common method
524 of analyzing field data is to apply binary categorization for each particle in each fluorescence
525 channel. For example, by this process, a particle is either fluorescent in a given FL channel
526 (above emission intensity threshold) or non-fluorescent (below threshold). In this way, many of
527 the challenges of separation introduced above are significantly reduced, though others are
528 introduced. Perring et al. (2015) introduced a WIBS classification strategy by organizing
529 particles sampled by the WIBS as either non-fluorescent or into one of seven fluorescence types
530 (e.g. Fig. 1).

531 Complementing the perspective from Figure 2, stacked particle type plots (Fig. 3) show
532 qualitative differences in fluorescence emission by representing different fluorescence types as
533 different colors. The most important observation here is that almost all individual biological
534 particles aerosolized (top two rows of Fig. 3) are fluorescent, meaning that they exhibit
535 fluorescence emission intensity above the standard threshold (FT baseline + 3σ) in at least one
536 fluorescence channel and are depicted with a non-gray color. Figure S4 shows the stacked
537 particle type plots for all 69 materials analyzed in this study as a comprehensive library. In
538 contrast to the biological particles, most particles from non-biological origin were observed not
539 to show fluorescence emission above the threshold in any of the fluorescence channels and are
540 thus colored gray. For example, 11 of the 15 samples of dust aerosolized show <15% of particles
541 to be fluorescent at particle sizes <4 μm . Similarly, 4 of 5 samples of HULIS aerosolized show
542 <7 % of particles to be fluorescent at particle sizes <4 μm . The size cut-point here was chosen
543 arbitrarily to summarize the distributions. Two examples shown in Figure 3 (Dust 10 and HULIS
544 3) are representative of average dust and HULIS types analyzed, respectively, and are relatively
545 non-fluorescent. Of the four dust types that exhibit a higher fraction of fluorescence, two (Dust 3
546 and Dust 4) are relatively similar and show ~75% fluorescent particles <4 μm , with particle type
547 divided nearly equally across the A, B, and AB [particle](#)-types (Fig. S4I). The two others (Dust 2
548 and Dust 6) show very few similarities between one another, where Dust 2 shows size-dependent
549 fluorescence and Dust 6 shows particle type A and B at all particle sizes (Fig. S4I). As seen by
550 the median fluorescence intensity representation (Fig. 2, Table [S2](#)), however, the relative

551 intensity in each channel for all dusts is either below or only marginally above the fluorescence
552 threshold. Thus, the threshold value becomes critically important and can dramatically impact
553 the classification process, as will be discussed in a following section. Similarly, HULIS 5 (Fig.
554 S4K) is the one HULIS type that shows an anomalously high fraction of fluorescence, and is
555 represented by B, C, BC particle types, but at intensity only marginally above the threshold value
556 and at 0% detector saturation in each channel. HULIS 5 is a fulvic acid collected from a
557 eutrophic, saline coastal pond in Antarctica (Brown et al., 2004, McKnight et al., 1994). The
558 collection site lacks the presence of terrestrial vegetation, and therefore all dissolved organic
559 material present originates from microbes. HULIS 5, therefore, is not expected to be
560 representative of soil-derived HULIS present in atmospheric samples in most areas of the world.
561 We present the properties of this material as an example of relatively highly fluorescing, non-
562 biological aerosol types that could theoretically occur, but without comment about its relative
563 importance or abundance.

564 Several types of non-biological particles, specifically brown carbon and combustion soot and
565 smoke, exhibited higher relative fractions of fluorescent particles compared to other non-
566 biological particles. Two of the three types of brown carbon sampled show >50% of particles to
567 be fluorescent at sizes >4 μm (Figs. 3i, l), though their median fluorescence is relatively low and
568 neither shows saturation in any of the three fluorescent channels. Out of six soot samples
569 analyzed, four showed >69% of particles to be fluorescent at sizes >4 μm , most of which are
570 dominated by B particle types. Two samples of combustion soot are notably more highly
571 fluorescent, both in fraction and intensity. Soot 3 (fullerene soot) and Soot 4 (diesel soot) show
572 FL1 intensity of 318 a.u. and 751 a.u., respectively, and are almost completely represented as A
573 particle type. The fullerene soot is not likely a good representative of most atmospherically
574 relevant soot types, however diesel soot is ubiquitous in anthropogenically-influenced areas
575 around the world. The fact that it exhibits high median fluorescence intensity implies that
576 increasing the baseline threshold slightly will not appreciably reduce the fraction of particles
577 categorized as fluorescent, and these particles will thus be counted as fluorescent in many-most
578 instances. The one type of wood smoke analyzed (Soot 6) shows ca. 70% fluorescent at >4 μm ,
579 mostly in the B category, with moderate to low FL2 signal, and-which also presents similarly as
580 cigarette smoke. Additionally, the two smoke samples in this study (Soot 5, cigarette smoke and
581 Soot 6, wood smoke) share similar fluorescent particle type features with two of the brown
582 carbon samples BrC 1 and BrC2. The smoke samples are categorized predominantly as B-type
583 particles, whereas samples more purely comprised of soot exhibit predominantly A-type
584 fluorescence. This distinction between smoke and soot may arise partially because the smoke
585 particles are complex mixtures of amorphous soot with condensed organic liquids, indicating that
586 compounds similar to the brown carbon analyzed here could heavily influence the smoke particle
587 signal.

588 Biological particle types-samples were chosen for Figure 3 to show the most important trends
589 among all particle types analyzed. Two pollen are shown here to highlight two common types of
590 fluorescence properties observed. Pollen 9 (Fig. 3a) shows particle type transitioning between A,
591 AB, and ABC as particle size gets larger. Pollen 9 (*Phleum pratense*) has a physical diameter of
592 $\sim 35 \mu\text{m}$, so the mode seen in Figure 3a is likely-may-be a result of fragmented pollen, and-~~due~~
593 to the upper particle size limit of WIBS detection, intact pollen of this species cannot be detected
594 (Pöhlker et al., 2013). Pollen 8 (Fig. 3d) shows a mode peaking at $\sim 10 \mu\text{m}$ in diameter and
595 comprised of a mixture of B, AB, BC, and ABC particles as well as a larger particle mode

596 comprised of ABC particles. The large particle mode appears almost monodisperse, but this is
597 due to the WIBS ability to sample only the tail of the distribution due to the upper size limit of
598 particle collection (~20 μm as operated). **Particles larger than this limit saturate the sizing**
599 **detector and are binned together into the ~20 μm bin.** It is important to note that excitation pulses
600 from the Xe flash lamps are not likely to penetrate the entirety of large pollen particles, and so
601 emission information is likely limited to outer layers of each pollen grain. Excitation pulses can
602 penetrate a relatively larger fraction of the smaller pollen fragments, however, meaning that the
603 differences in observed fluorescence may arise from differences the layers of material
604 interrogated. Fungi 1 (Fig. 3b) was chosen because it depicts the most commonly observed
605 fluorescence pattern among the fungal spore types analyzed (~3 μm mode mixed with A and AB
606 particles). Fungi 4 (Fig. 3e) represents a second common pattern (particle size peaking at larger
607 diameter, minimal A-type, and dominated by AB, ABC particle types). All three bacteria types
608 analyzed were dominated by A-type fluorescence. One gram-positive (Bacteria 1) and one gram-
609 negative bacteria (Bacteria 3) types are shown in Figure 3c, f, respectively.

610 **4.3 Fluorescence intensity varies strongly with particle size**

611 An extension of observation from the many particle classes analyzed is that particle type (A,
612 AB, ABC, etc.) varies strongly as a function of particle size. This is not surprising, given that it
613 has been frequently observed and reported that particle size significantly impacts fluorescence
614 emission intensity (e.g. Hill et al., 2001; Sivaprakasam et al., 2011). The higher the fluorescent
615 quantum yield of a given fluorophore, the more likely it is to fluoresce. For example, pure
616 biofluorophores (middle row of Fig. 2) and PAHs (bottom row of Fig. 2) have high quantum
617 yields and thus exhibit relatively intense fluorescence emission, even for particles <1 μm . In
618 contrast, more complex particles comprised of a wide mixture of molecular components are
619 typically less fluorescent per volume of material. At small sizes the relative fraction of these
620 particles that fluoresce is small, but as particles increase in size they are more likely to contain
621 enough fluorophores to emit a sufficient number of photons to record an integrated light intensity
622 signal above a given fluorescence threshold. Thus, the observed fluorescence intensity scales
623 approximately between the 2nd and 3rd power of the particle diameter (Sivaprakasam et al.,
624 2011; Taketani et al., 2013; Hill et al., 2015).

625 The general trend of fluorescence dependence on size is less pronounced for FL1 than for
626 FL2 and FL3. This can be seen by the fact that the scatter of points along the FL1 axis in Figure
627 2b is not clearly size-dependent and is strongly influenced by particle type (i.e. composition
628 dependent). In Figure 2c, however, the median points cluster near the vertical (size) axis and
629 both FL2 and FL3 values increase as particle size increases. It is important to note, however, that
630 the method chosen for particle generation in the laboratory strongly impacts the size distribution
631 of aerosolized particles. For example, higher concentrations of an aqueous suspension of particle
632 material generally produce larger particles, and the mechanical force used to agitate powders or
633 aerosolize bacteria can have strong influences on particle viability and physical agglomeration or
634 fragmentation of the aerosol (Mainelis et al., 2005). So, while the absolute size of particles
635 shown here is not a key message, the relative fluorescence at a given size can be informative.

636 As discussed, each individual particle shows increased probability of exhibiting fluorescence
637 emission above a given fluorescence threshold as size increases. Using Pollen 9 (*Phleum*
638 *pratense*, Fig. 3a) as an example, most particles <3 μm show fluorescence in only the FL1

639 channel and are thus classified as A-type particles. For the same pollen, however, particles ca. 2-
640 6 μm in diameter are more likely to be recorded as AB-type particles, indicating that they have
641 retained sufficient FL1 intensity, but have exceeded the FL2 threshold to add B-type
642 fluorescence character. Particles larger still ($>4 \mu\text{m}$) are increasingly likely to exhibit ABC
643 character, meaning that the emission intensity in the FL3 channel has increased to cross the
644 fluorescence threshold. Thus, for a given particle type and a constant threshold as a function of
645 particle size, the relative breakdown of fluorescence type changes significantly as particle size
646 increases. The same general trend can be seen in many other particle types, for example Pollen 8
647 (*Alnus glutinosa*, Fig. 3d), Fungi 1 (*Aspergillus brasiliensis*, Fig. 3b), and to a lesser degree
648 HULIS 3 (Suwannee fulvic acid, Fig. 3j) and Brown Carbon 2 (Fig. 3i). The “pathway” of
649 change, for Pollen 9, starts as A-type at small particle size and adds B and eventually ABC
650 ($A \rightarrow AB \rightarrow ABC$), whereas Pollen 8 starts primarily with B-type at small particle size and
651 separately adds either **AB** or C en route to ABC ($B \rightarrow AB$ or $BC \rightarrow ABC$). In this way, not only is
652 the breakdown of fluorescence type useful in discriminating particle distributions, but the
653 pathway of fluorescence change with particle size can also be instructive.

654 To further highlight the relationship between particle size and fluorescence, four kinds of
655 particles (Dust 2, HULIS 5, Fungi 4, and Pollen 9) were each binned into 4 different size ranges,
656 and the relative number fraction was plotted versus fluorescence intensity signal for each channel
657 (Fig. 4). In each case, the fluorescence intensity distribution shifts to the right (increases) as the
658 particle size bin increases. This trend is strongest in the FL2 and FL3 (middle and right columns
659 of Fig. 4) for most particle types, as discussed above.

660 The fact that particle fluorescence type can change so dramatically with increasing particle
661 size becomes critically important when the Perrings-style particle type classification is utilized for
662 laboratory or field investigation. For example Hernandez et al. (2016) aerosolized a variety of
663 species of pollen, fungal spores, and bacteria in the laboratory and presented the break-down of
664 particle types for each aerosolized species. This first comprehensive overview summarized how
665 different types of biological material (i.e. pollen and bacteria) might be separated based on their
666 fluorescence properties when presented with a population of relatively monodisperse particles.
667 This was an important first step, however, differentiation becomes more challenging when broad
668 size distributions of particles are mixed in an unknown environment. In such a case,
669 understanding how the particle type may change as a function of particle size may become an
670 important aspect of analysis.

671 4.4 Fluorescence threshold defines particle type

672 Particle type analysis is not only critically affected by size, but also by the threshold
673 definition chosen. Figure 5 represents the same matrix of particle types as in Figure 3, but shows
674 the fluorescence intensity distribution in each channel (at a given narrow range of sizes in order
675 to minimize the sizing effect on fluorescence). Figure 5 can help explain the breakdown of
676 particle type (and associated colors) shown in Figure 3. For example, in Figure 5a, the median
677 fluorescence intensity in FL1 for Pollen 9 (2046 a.u., detector saturated) in the size range 3.5-4.0
678 μm far exceeds the 3σ threshold (51 a.u.), and so essentially all particles exhibit FL1 character.
679 Approximately 90% of particles of Pollen 9 are above the 3σ FL2 threshold (25 a.u.), and
680 approximately 63% of particles are above the 3σ FL3 threshold (49 a.u). These three channels of
681 information together describe the distribution of particle type at the same range of sizes: 9% A,

682 26% AB, 63% ABC, and 2% other categories. Since essentially all particles are above the
683 threshold for FL1, particles are thus assigned as A type particles (if < FL2 and FL3 thresholds),
684 AB (if > FL2 threshold and < FL3 threshold), or ABC (if > FL2 and FL3 thresholds). Thus, the
685 distribution of particles at each fluorescence intensity and in relation to a given thresholding
686 strategy defines the fluorescence type breakdown and the pathway of fluorescence change with
687 particle size. It is important to note differences in this pathway for biofluorophores (Figs. S4G
688 and S4H). For example Biofluorophore 1 (riboflavin) follows the pathway $B \text{ or } \rightarrow C \rightarrow BC_2$, while
689 Biofluorophore 11 (tryptophan) follows the pathway $A \rightarrow \underline{ABBC} \rightarrow ABC$.

690 By extension, the choice of threshold bears heavily on how a given particle breakdown
691 appears and thus how a given instrument may be used to discriminate between biological and
692 non-biological particles. A commonly made assumption is that particles exhibiting fluorescence
693 by the WBS (or UV-APS) can be used as a lower limit proxy to the concentration of biological
694 particles, though it is known that interfering particle types confound this simple assumption
695 (Huffman et al., 2010). Increasing the fluorescence threshold can reduce categorizing weakly
696 fluorescent particles as biological, but can also remove weakly fluorescing biological particles of
697 interest (Huffman et al., 2012). Figure 6 provides an analysis of 8 representative particle types (3
698 biological, 5 non-biological) in order to estimate the trade-offs of increasing fluorescence
699 threshold separately in each channel. Once again, the examples chosen here represent general
700 trends and outliers, as discussed previously for Figure 3. Four threshold strategies are presented:
701 three as the instrument fluorescence baseline plus increasing uncertainty on that signal ($FT + 3\sigma$,
702 $FT + 6\sigma$, and $FT + 9\sigma$), as well as the FP3 strategy suggested by Wright et al. (2014). Using Dust
703 4 as an example (Fig. 6d), by increasing the threshold from 3σ (red traces) to 6σ (orange traces),
704 the fraction of dust particles fluorescent in FL1 decreases from approximately 50% to 10%.
705 Increasing the fluorescence threshold even higher to 9σ , reduces the fraction of fluorescence to
706 approximately 1%, thus eliminating nearly all interfering particles of Dust 3. In contrast, for
707 biological particles such as Pollen 9 (Fig. 6b), increasing the threshold from 3σ to 9σ does very
708 little to impact the relative breakdown of fluorescence category or the fraction of particles
709 considered fluorescent in at least one channel. Changing threshold from 3σ to 9σ decreases the
710 FL1 fraction minimally (98.3% to 97.9%), and for FL2 and FL3 the fluorescence fraction
711 decreases from 90% to 50% and from 60% to 42%, respectively. Figure 6 also underscores how
712 increasing particle size affects fluorescence fraction, as several particle types (e.g. Pollen 9 and
713 HULIS 5) show sigmoidal curves that proceed toward the right (lower fraction at a given size) as
714 the threshold applied increases and thus removes more weakly fluorescent particles.

715 To better understand how the different thresholding strategies qualitatively change the
716 distribution of particle fluorescence type, Figure 7 shows stacked fluorescence type distributions
717 for each of the four thresholds analyzed. Looking first at Dust 3 (Fig. 7d), the standard threshold
718 definition of 3σ shows approximately 80% of particles to be fluorescent in at least one channel,
719 resulting in a distribution of predominantly A, B, and AB-type particles. As the threshold is
720 increased, however, the total percentage of fluorescent particles decreases dramatically to 1% at
721 9σ and the particle type of the few remaining particles shifts to A-type particles. A similar trend
722 of fluorescent fraction can also be seen for Soot 6 (wood smoke) and Brown Carbon 2, where
723 almost no particle (10% and 16%, respectively) remain fluorescent using the 9σ threshold. Soot 4
724 (diesel soot), in contrast, exhibits the same fraction and breakdown of fluorescent particles
725 whether using the 3σ or 9σ threshold. Using the FP3 threshold (which employs very high FL1
726 threshold), however, the fluorescent properties of the diesel soot change dramatically to non-

727 fluorescent. As a ‘worst case’ scenario, HULIS 5 shows ca. 60% of particles to be fluorescent
728 using the 3σ threshold, **but this material is unlikely to be representative of commonly observed**
729 **soil HULIS, as discussed above**. In this case, increasing the threshold from 6σ to 9σ only
730 marginally decreases the fraction of fluorescent particles to ca. 35% and 22%, respectively, and
731 the break-down remains relatively constant in B, C, and BC types. Changing the threshold
732 definition to FP3 in this case also does not significantly change the particle type break-down,
733 since the high FP3 threshold applies only to FL1.

734 As stated, the WIBS is most often applied toward the detection and characterization of
735 biological aerosol particles. For the biological particles analyzed (Fig. 7, top rows), increasing
736 the threshold from 3σ to 9σ shows only a marginal decrease in the total fluorescent fraction for
737 Pollen 9, Fungal Spore 1, and Bacteria 1, and only a slight shift in fluorescence type as a
738 function of size. Using the FP3 threshold, however, for each of the three biological species the
739 non-fluorescent fraction increases substantially. Wright et al. (2014) found that the FP3 threshold
740 definition showed a strong correlation with ice nucleating particles and the authors suggested
741 these particles with high FL1 intensity were likely to be fungal spores. This may have been the
742 case, but given the analysis here, the FP3 threshold is also likely to significantly underestimate
743 fungal spore number by missing weakly or marginally fluorescent spores.

744 Based on the threshold analysis results shown in Figure 7, marginally increasing the
745 threshold in each case may help eliminate non-biological, interfering particles without
746 significantly impacting the number of biological particles considered fluorescent. Each threshold
747 strategy brings trade-offs, and individual users must understand these factors to make appropriate
748 decisions for a given scenario. These data suggest that using a threshold definition of FT baseline
749 + 9σ is likely to reduce interferences from most non-biological particles without significantly
750 impacting most biological particles.

751

752 **4.5 Particle asymmetry varies with particle size**

753 As a part of the comprehensive WIBS study, particle asymmetry (AF) was analyzed as a
754 function of particle size for all particles. As described in Section 2.1, AF in the WIBS-4A is
755 determined by comparing the symmetry of the forward elastic scattering response of each
756 particle, measured at the quadrant PMT. Many factors are related to the accuracy of the
757 asymmetry parameter, including the spatial alignment of the collection optics, signal-to-noise
758 and dynamic range of the detector, agglomeration of particles with different refractive indices,
759 and the angle at which a non-symmetrical particle hits the laser (Kaye et al., 2007; Gabey et al.,
760 2010). Figure 8 shows a summary of the relationship between AF and particle size for all
761 material types analyzed in **Table 3**. Soot particles are known to frequently cluster into chains or
762 rings depending on the number of carbon atoms (Von Helden et al., 1993) and, as a result, can
763 have long aspect ratios that would be expected to manifest as large AF values. The bacteria
764 species chosen have rod-like shape features and thus would also exhibit large AF values. These
765 properties were observed by the WIBS, as two types of soot (diesel and fullerene) and all three
766 bacteria showed higher AF values than other particles at approximately the same particle
767 diameter. For an unknown reason, all three brown carbon samples also showed relatively high
768 AF values given that the individual particles of liquid organic aerosol would be expected to be

769 spherical with low AF. Similarly, the intact pollen showed anomalously low AF, because a
770 substantial fraction of each was shown to saturate the WIBS sizing detector, even if the median
771 particle size (shown) is lower than the saturating value. For this reason we postulate that the
772 forward-side-scattering detector may not be able to reliably estimate either particle size or AF
773 when particles are near the sizing limits. Intact pollen, soot samples (diesel and fullerene soot),
774 bacteria and brown carbon samples were excluded from the linear regression fit, because they
775 appeared visually as outliers to the trend. All remaining particle groups of material types (7 in
776 total) are represented by blue in Figure 8. A linear regression R^2 value of 0.87 indicates a high
777 degree of correlation between particle AF and size across the remaining particles. The strong
778 correlation between these two factors across a wide range of particle types, mixed with the
779 confounding anomaly of brown carbon, raises a question about the degree to which the
780 asymmetry factor parameter from the WIBS-4A can be useful or, conversely, to what degree the
781 uncertainty in AF is dominated by instrumental factors, including those listed above.

782 5. Summary and Conclusions

783 UV-LIF instruments, including the WIBS, are common tools for the detection and
784 characterization of biological aerosol particles. The number of commercially available
785 instruments regularly deployed for ambient monitoring of environmental particle properties is
786 rising steeply, yet critical laboratory work has been needed to better understand how the
787 instruments categorize a variety of both biological and non-biological particles. In particular, the
788 differentiation between weakly fluorescent, interfering particles of non-biological origin and
789 weakly fluorescing biological particles is very challenging. Here we have aerosolized a
790 representative list of pollen, fungal spores, and bacteria along with key aerosol types from the
791 groups of fluorescing non-biological materials expected to be most problematic for UV-LIF
792 instrumentation.

793 By analyzing the five WIBS data parameter outputs for each interrogated particle, we have
794 summarized trends within each class of particles and demonstrated the ability of the instrument
795 to broadly differentiate populations of particles. The trend of particle fluorescence intensity and
796 changing particle fluorescence type as a function of particle size was shown in detail. This is
797 critically important for WIBS and other UV-LIF instrumentation users to keep in mind when
798 analyzing populations of unknown, ambient particles. In particular, we show that the pathway of
799 fluorescence particle type change (e.g. $A \rightarrow AB \rightarrow ABC$ or $B \rightarrow BC \rightarrow ABC$) with increasing
800 particle size can be one characteristic feature of unique populations of particles. When
801 comparing the fluorescence break-down of individual aerosol material types, care should be
802 taken to limit comparison within a narrow range of particle sizes in order to reduce complexity
803 due to differing composition or fluorescence intensity effects. Lastly, we looked at the reliability
804 of using the forward scattering to estimate particle shape. Results showed a strong correlation
805 between AF and size for various biological and non-biological particles, indicating the AF
806 parameter may not be reliable for discriminating between different particle types.

807 The fluorescence threshold applied toward binary categorization of fluorescence or non-
808 fluorescent in each channel is absolutely critical to the conceptual strategy that a given user
809 applies to ambient particle analysis. A standard WIBS threshold definition of instrument
810 background (FT baseline) + 3σ is commonly applied to discriminate between particles with or
811 without fluorescence. As has been shown previously, however, any single threshold confounds

812 simple discrimination of biological and non-biological particles by mixing poorly fluorescent
813 biological material into non-fluorescent categories, and highly fluorescent non-biological
814 material into fluorescent categories. Previously introduced thresholding strategies were also used
815 for comparison. The Wright et al. (2014) definition was shown to aid in removing non-biological
816 particles such as soot, but that it can also lead to the dramatic underestimation of the biological
817 fraction. The strategy utilized by Toprak and Schnaiter (2013) was to define fluorescent
818 biological particles as those with fluorescent characteristics in FL1 and FL3, ignoring any
819 particles with fluorescence in FL2. They proposed this because FL1 shows excitation and
820 emission characteristics well suited for the detection of tryptophan, and FL3 for the detection of
821 NAD(P)H and riboflavin. However, the study here, along with studies by Hernandez et al. (2016)
822 and Perring et al. (2015), have shown that FL2 fluorescence characteristics (B, AB, BC, and
823 ABC type) are common for many types of biological particles and so removing particles with
824 FL2 fluorescence is likely to remove many bioparticles from characterization.

825 Any one threshold has associated trade-offs and is likely to create some fraction of both false
826 positive and false negative signals. Here we have shown a systematic analysis of four different
827 fluorescence thresholding strategies, concluding that by raising the threshold to $FT + 9\sigma$, the
828 reduction in biological material counted as fluorescent is likely to be only minimally effected,
829 while the fraction of interfering material is likely to be reduced almost to zero for most particle
830 types. Several materials exhibiting outlier behavior (e.g. HULIS 5, diesel soot) could present as
831 false positive counts using almost any characterization scheme. It is important to note that
832 HULIS 5 was one of a large number of analyzed particle types and in the minority of HULIS
833 types, however, and it is unlikely that this microbe-derived material clear how likely these highly
834 fluorescent materials would be observed are to occur in any given ambient air mass at most
835 locations. More studies may be required to sample dusts, HULIS types, soot and smoke, brown
836 organic carbon materials, and various coatings in different real-world settings and at various
837 stages of aging to better understand how specific aerosol types may contribute to UV-LIF
838 interpretation at a given study location. We also included a comprehensive supplemental
839 document including size distributions for all 69 aerosol materials, stacked by fluorescent particle
840 type and comparing the $FT + 3\sigma$ and $FT + 9\sigma$ threshold strategies. These figures are included as
841 a qualitative reference for other instrument users when comparing against laboratory-generated
842 particles or for use in ambient particle interpretation.

843 It is important here to provide brief atmospheric context to these measurements. Whether 3σ
844 or 9σ thresholds are used, no UV-LIF technology can unambiguously distinguish between all
845 biological and non-biological aerosol types, and so a minority of misidentified particles will
846 always remain. The key aim is not to remove these completely, but to group particles of interest
847 as cleanly as possible with an estimate of the relative magnitude of misidentification. As a simple
848 exercise to estimate this process, consider two scenarios where each sampled air mass contains a
849 total of 10,000 particles, each $3\ \mu\text{m}$ in diameter.

850 • Assume as Scenario 1 that the particle mode is comprised of 10% Dust 10 (taken as a
851 representative, weakly fluorescent dust), 5% Fungi 1 (taken as a representative fungal
852 spore type), and 85% other non-fluorescent material (i.e. sea salt, silicates, non-
853 absorbing organic aerosol). In this scenario, 6.9% of the 485 particles exhibiting some
854 type of fluorescence (FL any) using the 3σ threshold would be misidentified from
855 fluorescing dust and separately 4.4% of the 427 particles using the 9σ threshold.

- Assume as Scenario 2 that a strong dust event is comprised of 90% Dust 10 mixed 10% Fungi 1. Here, 25% of the 1139 fluorescent particles would be misidentified from dust using the 3σ threshold and 17.2% of 985 fluorescent particles using 9σ .

These simple calculations using only dust and fungal spores suggests that a minimum of a few percent of fluorescing particles are expected to arise from non-biological materials, and so the uncertainty in the fraction of fluorescence by these types of analyses are probably limited to no lower than $\pm 5\%$. The uncertainty in assigning the absolute number of fluorescent particles to biological material is somewhat more uncertain, however. For example, if 10,000 dust particles of which only 1% were fluorescent were to be mixed with a small population of 100 biological particles of which 100% were fluorescent, then the number concentration of fluorescent particles would over-count the biological particles by a factor of two. In this way, the number concentration of fluorescent particles is much more susceptible to uncertainties from non-biological particles. The overall uncertainty in discerning between particles will also be strongly dependent on air mass composition. For example, in Scenario 2 hypothesized to simulate a dust storm, the fraction of particle misidentification can be significantly higher when the relative fraction of a weakly fluorescing material is especially high. Air masses that contain non-biological materials that have anomalously high fluorescent fractions would increase the rate of particle misidentification even more dramatically. These scenarios only consider the total fraction of particles to be fluorescent, not taking into account the differing break-down of fluorescent particle type as a function of the 3 different fluorescent channels. Taking these details into account will reduce the fraction of particle misidentification as a function of the similarity between observed biological and non-biological material. As a result, UV-LIF results should be considered uniquely in all situations with appreciation of possible influences from differing aerosol composition on fluorescence results. Additionally, individuals utilizing WIBS instrumentation are cautioned to use the assignment of “biological aerosols” from UV-LIF measurements with great care and are rather encouraged to use “fluorescent aerosol” or some variation more liberally. Ultimately, further analysis methods, including clustering techniques (e.g. Crawford et al., 2015; Crawford et al., 2016; Ruske et al., 2017) will likely need to be employed to further improve discrimination between ambient particles and to reduce the relative rate of misidentification. It should also be noted, however, that a number of ambient studies have compared results of UV-LIF instruments with complementary techniques for bioaerosol detection and have reported favorable comparisons (Healy et al., 2014; Gosselin et al., 2016; Huffman et al., 2012). So while uncertainties remain, increasing anecdotal evidence supports the careful use of UV-LIF technology for bioaerosol detection.

~~It should be noted, however, that~~ the presented assessment is not intended to be exhaustive, but has the potential to guide users of commercial UV-LIF instrumentation through a variety of analysis strategies toward the goal of better detecting and characterizing biological particles. One important ~~note point~~ is that the information presented here is strongly instrument dependent due to fluorescence PMT voltages and gains, specific fluorescence calibrations applied, and other instrument parameters (Robinson et al., 2017). For example, the suggested particle type classification introduced by Perring et al. (2015); will vary somewhat between instruments, though more work will be necessary to determine the magnitude of these changes. Thus, we do not introduce these data primarily as a library to which all other WIBS instrument should be compared rigorously, but rather as general trends that are expected to hold broadly true.

900 Several examples of strongly fluorescing particles of specific importance to the built
901 environment (e.g. cellulose fibers, particles from cotton t-shirts, and laboratory wipes) show that
902 these particle types could be very important sources of fluorescent particles indoors (i.e. Figs.
903 S4S and S4T). This will also require further study, but should be taken seriously by researchers
904 who utilize UV-LIF instrumentation to estimate concentrations and properties of biological
905 material within homes, indoor occupational environments, or hospitals.

906 The study presented here is meant broadly to achieve two aims. The first aim is to present a
907 summary of fluorescent properties of the most important particle types expected in a given
908 sample and to suggest thresholding strategies (i.e. $FT + 9\sigma$) that may be widely useful for
909 improving analysis quality. The second aim is to suggest key analysis and plotting strategies that
910 other UV-LIF, especially WIBS, instrumentation users can utilize to interrogate particles using
911 their own instruments. By proposing several analysis strategies we aim to introduce concepts to
912 the broader atmospheric community in order to promote deeper discussions about how best to
913 continue improving UV-LIF instrumentation and analyses.

914 **6. Acknowledgments**

915 The authors acknowledge the University of Denver for financial support from the faculty start-up
916 fund. Nicole Savage acknowledges financial support from the Phillipson Graduate Fellowship at
917 the University of Denver. Christine Krentz acknowledges financial support from the Summer
918 Undergraduate Research Grant program through the Undergraduate Research Center at the
919 University of Denver. Tobias Könemann and Christopher Pöhlker acknowledge financial support
920 by the Max Planck Society and the Max Planck Graduate Center with the Johannes Gutenberg-
921 Universität Mainz (MPGC). Gediminas Mainelis acknowledges support by the New Jersey
922 Agricultural Experiment Station (NJAES) at Rutgers, The State University of New Jersey. Ulrich
923 Pöschl and Meinrat O. Andreae are acknowledged for useful discussions and support for the
924 authors. Gavin McMeeking from Handix Scientific is acknowledged for the development of the
925 WIBS analysis toolkit. Martin Gallagher, Jonathan Crosier, and the Department of Geology and
926 Earth Science in the School of Earth and Environmental Sciences, University of Manchester
927 provided several samples of raw materials. Marie Gosselin is acknowledged for discussions
928 about WIBS analysis, and Ben Swanson is acknowledged for help with the conceptual design of
929 figures.

930 **7. References**

- 931 Abdel-Shafy, H. I., and Mansour, M. S. M.: A review on polycyclic aromatic hydrocarbons:
932 Source, environmental impact, effect on human health and remediation, *Egyptian Journal of*
933 *Petroleum*, 25, 107-123, <http://dx.doi.org/10.1016/j.ejpe.2015.03.011>, 2016.
- 934 Agranovski, V., Ristovski, Z., Hargreaves, M., Blackall, P. J., and Morawska, L.: Real-time
935 measurement of bacterial aerosols with the UVAPS: performance evaluation, *Journal of Aerosol*
936 *Science*, 34, 301-317, 10.1016/s0021-8502(02)00181-7, 2003.
- 937 Agranovski, V., Ristovski, Z. D., Ayoko, G. A., and Morawska, L.: Performance evaluation of
938 the UVAPS in measuring biological aerosols: Fluorescence spectra from NAD(P)H coenzymes
939 and riboflavin, *Aerosol Sci. Technol.*, 38, 354-364, 10.1080/02786820490437505, 2004.
- 940 Aizawa, T., and Kosaka, H.: Investigation of early soot formation process in a diesel spray flame
941 via excitation-emission matrix using a multi-wavelength laser source, *International Journal of*
942 *Engine Research*, 9, 79-96, 10.1243/14680874jer01407, 2008.
- 943 Aizawa, T., and Kosaka, H.: Effects of Fischer-Tropsch diesel fuel on soot formation processes
944 in a diesel spray flame, *International Journal of Engine Research*, 11, 79-87,
945 10.1243/14680874jer04709, 2010.
- 946 Amann, R. I., Ludwig, W., and Schleifer, K. H.: Phylogenetic identification and in-situ
947 detection of individual microbial-cells without cultivation, *Microbiol. Rev.*, 59, 143-169, 1995.
- 948 Ariya, P. A., Sun, J., Eltouny, N. A., Hudson, E. D., and Hayes, C. T.: Physical and chemical
949 characterization of bioaerosols implications for nucleation processes, *Int. Rev. Phys. Chem.*, 28,
950 1-32, 2009.
- 951 Bhangar, S., Huffman, J. A., and Nazaroff, W. W.: Size-resolved fluorescent biological aerosol
952 particle concentrations and occupant emissions in a university classroom, *Indoor Air*, 24, 604-
953 617, 10.1111/ina.12111, 2014.
- 954 Bhangar, S., Adams, R. I., Pasut, W., Huffman, J. A., Arens, E. A., Taylor, J. W., Bruns, T. D.,
955 and Nazaroff, W. W.: Chamber bioaerosol study: human emissions of size-resolved fluorescent
956 biological aerosol particles, *Indoor Air*, 26, 193-206, 10.1111/ina.12195, 2016.
- 957 Brosseau, L. M., Vesley, D., Rice, N., Goodell, K., Nellis, M., and Hairston, P.: Differences in
958 detected fluorescence among several bacterial species measured with a direct-reading particle
959 sizer and fluorescence detector, *Aerosol Sci. Technol.*, 32, 545-558, 2000.
- 960 Brown, A., McKnight, D., Chin, Y.-P., Roberts, E., and Uhle, M.: Chemical characterization of
961 dissolved organic material in Pony Lake, a saline coastal pond in Antarctica. *Marine Chemistry*,
962 2004.
- 963 Chi, M. C., and Li, C. S.: Fluorochrome in monitoring atmospheric bioaerosols and correlations
964 with meteorological factors and air pollutants, *Aerosol Sci. Tech.*, 41, 672-678, 2007.

- 965 Cox, C. S., and Wathes, C. M.: *Bioaerosols Handbook*, Book, Whole, CRC Press, 1995.
- 966 Crawford, I., Ruske, S., Topping, D. O., and Gallagher, M. W.: Evaluation of hierarchical
967 agglomerative cluster analysis methods for discrimination of primary biological aerosol,
968 *Atmospheric Measurement Techniques*, 8, 4979-4991, 10.5194/amt-8-4979-2015, 2015.
- 969 Crawford, I., Lloyd, G., Herrmann, E., Hoyle, C. R., Bower, K. N., Connolly, P. J., Flynn, M. J.,
970 Kaye, P. H., Choulaton, T. W., and Gallagher, M. W.: Observations of fluorescent aerosol-cloud
971 interactions in the free troposphere at the High-Altitude Research Station Jungfraujoch,
972 *Atmospheric Chemistry and Physics*, 16, 2273-2284, 10.5194/acp-16-2273-2016, 2016.
- 973 DeCarlo, P. F., Slowik, J. G., Worsnop, D. R., Davidovits, P., and Jimenez, J. L.: Particle
974 morphology and density characterization by combined mobility and aerodynamic diameter
975 measurements. Part 1: Theory, *Aerosol Science and Technology*, 38, 1185-1205,
976 10.1080/027868290903907, 2004.
- 977 Delort, A. M., Vaitilingom, M., Amato, P., Sancelme, M., and Parazols, M.: A short overview of
978 the microbial population in clouds: potential roles in atmospheric chemistry and nucleation
979 processes, *Atmos. Res.*, 98, 249-260, 2010.
- 980 Després, V. R., Huffman, J. A., Burrows, S. M., Hoose, C., Safatov, A. S., Buryak, G.,
981 Fröhlich-Nowoisky, J., Elbert, W., Andreae, M. O., Poeschl, U., and Jaenicke, R.: Primary
982 biological aerosol particles in the atmosphere: a review, *Tellus Series B-Chemical and Physical
983 Meteorology*, 64, 15598-15598, 10.3402/tellusb.v64i0.15598, 2012.
- 984 Douwes, J., Thorne, P., Pearce, N., and Heederik, D.: Bioaerosol health effects and exposure
985 assessment: Progress and prospects, *Annals of Occupational Hygiene*, 47, 187-200,
986 10.1093/annhyg/meg032, 2003.
- 987 Finlayson-Pitts, B. J., and Pitts, J., James N.: *Chemistry of the Upper and Lower Atmosphere :
988 Theory, Experiments, and Applications (1)*, Academic Pres, San Diego, USA, 993 pp.,
989 November 1999.
- 990 Fröhlich -Nowoisky, J., Kampf, C. J., Weber, B., Huffman, J. A., Poehlker, C., Andreae, M. O.,
991 Lang-Yona, N., Burrows, S. M., Gunthe, S. S., Elbert, W., Su, H., Hoor, P., Thines, E.,
992 Hoffmann, T., Despres, V. R., and Poeschl, U.: Bioaerosols in the Earth system: Climate, health,
993 and ecosystem interactions, *Atmospheric Research*, 182, 346-376,
994 10.1016/j.atmosres.2016.07.018, 2016.
- 995 Gabey, A. M., Gallagher, M. W., Whitehead, J., Dorsey, J. R., Kaye, P. H., and Stanley, W. R.:
996 Measurements and comparison of primary biological aerosol above and below a tropical forest
997 canopy using a dual channel fluorescence spectrometer, *Atmospheric Chemistry and Physics*, 10,
998 4453-4466, 10.5194/acp-10-4453-2010, 2010.
- 999 Gabey, A. M., Vaitilingom, M., Freney, E., Boulon, J., Sellegri, K., Gallagher, M. W., Crawford,
1000 I. P., Robinson, N. H., Stanley, W. R., and Kaye, P. H.: Observations of fluorescent and
1001 biological aerosol at a high-altitude site in central France, *Atmospheric Chemistry and Physics*,
1002 13, 7415-7428, 10.5194/acp-13-7415-2013, 2013.

- 1003 Gosselin, M. I., Rathnayake, C. M., Crawford, I., Pohlker, C., Frohlich-Nowoisky, J., Schmer,
1004 B., Despres, V. R., Engling, G., Gallagher, M., Stone, E., Poschl, U., and Huffman, J. A.:
1005 Fluorescent bioaerosol particle, molecular tracer, and fungal spore concentrations during dry and
1006 rainy periods in a semi-arid forest, *Atmospheric Chemistry and Physics*, 16, 15165-15184,
1007 10.5194/acp-16-15165-2016, 2016.
- 1008 Griffiths, W. D., and Decosemo, G. A. L.: THE ASSESSMENT OF BIOAEROSOLS - A
1009 CRITICAL-REVIEW, *Journal of Aerosol Science*, 25, 1425-1458, 10.1016/0021-
1010 8502(94)90218-6, 1994.
- 1011 Hairston, P. P., Ho, J., and Quant, F. R.: Design of an instrument for real-time detection of
1012 bioaerosols using simultaneous measurement of particle aerodynamic size and intrinsic
1013 fluorescence, *Journal of Aerosol Science*, 28, 471-482, 1997.
- 1014 Han, T., Zhen, H. J., Fennell, D. E., and Mainelis, G.: Design and Evaluation of the Field-
1015 Deployable Electrostatic Precipitator with Superhydrophobic Surface (FDEPSS) with High
1016 Concentration Rate, *Aerosol and Air Quality Research*, 15, 2397-2408,
1017 10.4209/aaqr.2015.04.0206, 2015.
- 1018 Handorean, A., Robertson, C. E., Harris, J. K., Frank, D., Hull, N., Kotter, C., Stevens, M. J.,
1019 Baumgardner, D., Pace, N. R., and Hernandez, M.: Microbial aerosol liberation from soiled
1020 textiles isolated during routine residuals handling in a modern health care setting, *Microbiome*, 3,
1021 72-72, 10.1186/s40168-015-0132-3, 2015.
- 1022 Healy, D. A., O'Connor, D. J., Burke, A. M., and Sodeau, J. R.: A laboratory assessment of the
1023 Waveband Integrated Bioaerosol Sensor (WIBS-4) using individual samples of pollen and fungal
1024 spore material, *Atmospheric Environment*, 60, 534-543, 10.1016/j.atmosenv.2012.06.052, 2012.
- 1025 Healy, D. A., Huffman, J. A., O'Connor, D. J., Pohlker, C., Poschl, U., and Sodeau, J. R.:
1026 Ambient measurements of biological aerosol particles near Killarney, Ireland: a comparison
1027 between real-time fluorescence and microscopy techniques, *Atmospheric Chemistry and Physics*,
1028 14, 8055-8069, 10.5194/acp-14-8055-2014, 2014.
- 1029 Heidelberg, J. F., Shahamat, M., Levin, M., Rahman, I., Stelma, G., Grim, C., and and Colwell,
1030 R. R.: Effect of aerosolization on culturability and viability of gram-negative bacteria, *Appl.*
1031 *Environ.*, 63, 3585-3588, 1997.
- 1032 Hernandez, M., Perring, A. E., McCabe, K., Kok, G., Granger, G., and Baumgardner, D.:
1033 Chamber catalogues of optical and fluorescent signatures distinguish bioaerosol classes,
1034 *Atmospheric Measurement Techniques*, 9, 3283-3292, 10.5194/amt-9-3283-2016, 2016.
- 1035 Hill, S. C., Pinnick, R. G., Niles, S., Pan, Y. L., Holler, S., Chang, R. K., Bottiger, J., Chen, B.
1036 T., Orr, C. S., and and Feather, G.: Real-time measurement of fluorescence spectra from single
1037 airborne biological particles, *Field Anal. Chem. Technol.*, 3, 221-239, 1999a.
- 1038 Hill, S. C., Pinnick, R. G., Niles, S., Pan, Y. L., Holler, S., Chang, R. K., Bottiger, J., Chen, B.
1039 T., Orr, C. S., and Feather, G.: Real-time measurement of fluorescence spectra from single
1040 airborne biological particles, *Field Anal. Chem. Technol.*, 3, 221-239, 1999b.

- 1041 Hill, S. C., Pinnick, R. G., Niles, S., Fell, N. F., Pan, Y. L., Bottiger, J., Bronk, B. V., Holler, S.,
1042 and Chang, R. K.: Fluorescence from Airborne Microparticles: Dependence on Size,
1043 Concentration of Fluorophores, and Illumination Intensity, *Appl. Optics*, 40, 3005-3013, 2001.
- 1044 Hill, S. C., Williamson, C. C., Doughty, D. C., Pan, Y. L., Santarpia, J. L., and Hill, H. H.: Size-
1045 dependent fluorescence of bioaerosols: Mathematical model using fluorescing and absorbing
1046 molecules in bacteria, *Journal of Quantitative Spectroscopy & Radiative Transfer*, 157, 54-70,
1047 10.1016/j.jqsrt.2015.01.011, 2015.
- 1048 Ho, J., Spence, M., and Hairston, P.: Measurement of Biological Aerosol with a Fluorescent
1049 Aerodynamic Particle Sizer (FLAPS): Correlation of Optical Data with Biological Data.
1050 *Aerobiologia*, 1999.
- 1051 Ho, J.: Future of biological aerosol detection, *Advances in Biodetection*, 457, 125-148,
1052 [http://dx.doi.org/10.1016/S0003-2670\(01\)01592-6](http://dx.doi.org/10.1016/S0003-2670(01)01592-6), 2002.
- 1053 Huffman, J. A., Treutlein, B., and Poeschl, U.: Fluorescent biological aerosol particle
1054 concentrations and size distributions measured with an Ultraviolet Aerodynamic Particle Sizer
1055 (UV-APS) in Central Europe, *Atmospheric Chemistry and Physics*, 10, 3215-3233, 2010.
- 1056 Huffman, J. A., Sinha, B., Garland, R. M., Snee-Pollmann, A., Gunthe, S. S., Artaxo, P., Martin,
1057 S. T., Andreae, M. O., and Poeschl, U.: Size distributions and temporal variations of biological
1058 aerosol particles in the Amazon rainforest characterized by microscopy and real-time UV-APS
1059 fluorescence techniques during AMAZE-08, *Atmospheric Chemistry and Physics*, 12, 11997-
1060 12019, 10.5194/acp-12-11997-2012, 2012.
- 1061 Huffman, J. A., Prenni, A. J., DeMott, P. J., Pohlker, C., Mason, R. H., Robinson, N. H.,
1062 Frohlich-Nowoisky, J., Tobo, Y., Despres, V. R., Garcia, E., Gochis, D. J., Harris, E., Mueller-
1063 Germann, I., Ruzene, C., Schmer, B., Sinha, B., Day, D. A., Andreae, M. O., Jimenez, J. L.,
1064 Gallagher, M., Kreidenweis, S. M., Bertram, A. K., and Poeschl, U.: High concentrations of
1065 biological aerosol particles and ice nuclei during and after rain, *Atmospheric Chemistry and
1066 Physics*, 13, 6151-6164, 10.5194/acp-13-6151-2013, 2013.
- 1067 Huffman, J. A., and Santarpia, J. L.: Online techniques for quantification and characterization of
1068 biological aerosol, in: *Microbiology of Aerosols*, edited by: Delort, A. M., and Amato, P., Wiley
1069 (In Press), Hoboken, NJ, Chapter 4, 2017.
- 1070 Jaenicke, R.: Abundance of cellular material and proteins in the atmosphere, *Science*, 308, 73,
1071 2005.
- 1072 Kanaani, H., Hargreaves, M., Ristovski, Z., and Morawska, L.: Performance assessment of
1073 UVAPS: Influence of fungal spore age and air exposure, *Journal of Aerosol Science*, 38, 83-96,
1074 10.1016/j.jaerosci.2006.10.003, 2007.
- 1075 Kanaani, H., Hargreaves, M., Smith, J., Ristovski, Z., Agranovski, V., and Morawska, L.:
1076 Performance of UVAPS with respect to detection of airborne fungi, *Journal of Aerosol Science*,
1077 39, 175-189, 10.1016/j.jaerosci.2007.10.007, 2008.

- 1078 Kanaani, H., Hargreaves, M., Ristovski, Z., and Morawska, L.: Fungal spore fragmentation as a
1079 function of airflow rates and fungal generation methods, *Atmospheric Environment*, 43, 3725-
1080 3735, 10.1016/j.atmosenv.2009.04.043, 2009.
- 1081 Kaye, P., Aptowicz, K., Chang, R., Foot, V., and Videen, G.: Optics of Biological Particles. In:
1082 Angularly Resolved Elastic Scattering from Airborne Particles, 2007.
- 1083 Kaye, P. H., Eyles, N. A., Ludlow, I. K., and Clark, J. M.: AN INSTRUMENT FOR THE
1084 CLASSIFICATION OF AIRBORNE PARTICLES ON THE BASIS OF SIZE, SHAPE, AND
1085 COUNT FREQUENCY, *Atmospheric Environment Part a-General Topics*, 25, 645-654,
1086 10.1016/0960-1686(91)90062-c, 1991.
- 1087 Kaye, P. H., Stanley, W. R., Hirst, E., Foot, E. V., Baxter, K. L., and Barrington, S. J.: Single
1088 particle multichannel bio-aerosol fluorescence sensor, *Optics Express*, 13, 3583-3593,
1089 10.1364/opex.13.003583, 2005.
- 1090 Könemann, T., Savage, N., McMeeking, G., Su, H., Huffman, J. A., Pöhlker, C., and Pöschl, U.:
1091 Spectral Intensity Bioaerosol Sensor (SIBS): Technical Description and Laboratory Assessment
1092 of a Novel Instrument for Single Particle Detection. In Prep.
- 1093 Lavoie, J., Marchand, G. E., Cloutier, Y., Halle, S., Nadeau, S., Duchaine, C., and Pichette, G.:
1094 Evaluation of bioaerosol exposures during hospital bronchoscopy examinations, *Environmental
1095 Science-Processes & Impacts*, 17, 288-299, 10.1039/c4em00359d, 2015.
- 1096 Li, J., Zhou, L., Zhang, X., Xu, C., Dong, L., and Yao, M.: Bioaerosol emissions and detection of
1097 airborne antibiotic resistance genes from a wastewater treatment plant, *Atmospheric
1098 Environment*, 124, 404-412, 10.1016/j.atmosenv.2015.06.030, 2016.
- 1099 Lv, Y., Li, X., Xu, T. T., Cheng, T. T., Yang, X., Chen, J. M., Iinuma, Y., and Herrmann, H.:
1100 Size distributions of polycyclic aromatic hydrocarbons in urban atmosphere: sorption mechanism
1101 and source contributions to respiratory deposition, *Atmospheric Chemistry and Physics*, 16,
1102 2971-2983, 10.5194/acp-16-2971-2016, 2016.
- 1103 Mainelis, G., Berry, D., An, H. R., Yao, M. S., DeVoe, K., Fennell, D. E., and Jaeger, R.: Design
1104 and performance of a single-pass bubbling bioaerosol generator, *Atmospheric Environment*, 39,
1105 3521-3533, 10.1016/j.atmosenv.2005.02.043, 2005.
- 1106 Mason, R. H., Si, M., Li, J., Chou, C., Dickie, R., Toom-Sauntry, D., Poehlker, C., Yakobi-
1107 Hancock, J. D., Ladino, L. A., Jones, K., Leitch, W. R., Schiller, C. L., Abbatt, J. P. D.,
1108 Huffman, J. A., and Bertram, A. K.: Ice nucleating particles at a coastal marine boundary layer
1109 site: correlations with aerosol type and meteorological conditions, *Atmospheric Chemistry and
1110 Physics*, 15, 12547-12566, 10.5194/acp-15-12547-2015, 2015.
- 1111 McKnight, D. M., Andrews, E. D., Spaulding, S. A., and Aiken, G. R.: AQUATIC FULVIC-
1112 ACIDS IN ALGAL-RICH ANTARCTIC PONDS, *Limnology and Oceanography*, 39, 1972-
1113 1979, 1994.

- 1114 Mercier, X., Faccinnetto, A., and Desgroux, P.: Cleaner Combustion: Developing Detailed
1115 Chemical Kinetic Models, Green Energy and Technology, Springer, London, 2013.
- 1116 Morris, C. E., Georgakopoulos, D. G., and Sands, D. C.: Ice nucleation active bacteria and their
1117 potential role in precipitation, Journal de Physique IV, 121, 87-103, 10.1051/jp4:2004121004,
1118 2004.
- 1119 Möhler, O., DeMott, P. J., Vali, G., and Levin, Z.: Microbiology and atmospheric processes: the
1120 role of biological particles in cloud physics, Biogeosciences, 4, 1059-1071, 2007.
- 1121 Niessner, R., and Krupp, A.: DETECTION AND CHEMICAL CHARACTERIZATION OF
1122 POLYCYCLIC AROMATIC HYDROCARBON AEROSOLS BY MEANS OF LASER-
1123 INDUCED FLUORESCENCE, Particle & Particle Systems Characterization, 8, 23-28,
1124 10.1002/ppsc.19910080106, 1991.
- 1125 O'Connor, D. J., Daly, S. M., and Sodeau, J. R.: On-line monitoring of airborne bioaerosols
1126 released from a composting/green waste site, Waste Management, 42, 23-30,
1127 10.1016/j.wasman.2015.04.015, 2015a.
- 1128 O'Connor, D. J., Healy, D. A., and Sodeau, J. R.: A 1-month online monitoring campaign of
1129 ambient fungal spore concentrations in the harbour region of Cork, Ireland, Aerobiologia, 31,
1130 295-314, 10.1007/s10453-015-9365-7, 2015b.
- 1131 Pan, Y. L., Holler, S., Chang, R. K., Hill, S. C., Pinnick, R. G., Niles, S., Bottiger, J. R., and
1132 Bronk, B. V.: Real-time detection and characterization of individual flowing airborne biological
1133 particles: fluorescence spectra and elastic scattering measurements, P. Soc. Photo-Opt. Ins.,
1134 3855, 117-125, 1999.
- 1135 Panne, U., Knoller, A., Kotzick, R., and Niessner, R.: On-line and in-situ detection of polycyclic
1136 aromatic hydrocarbons (PAH) on aerosols via thermodesorption and laser-induced fluorescence
1137 spectroscopy, Fresenius J. Anal. Chem., 366, 408-414, 2000.
- 1138 Penner, J. E.: Carbonaceous Aerosols Influencing Atmospheric Radiation: Black and Organic
1139 Carbon, 35, 1994.
- 1140 Perring, A. E., Schwarz, J. P., Baumgardner, D., Hernandez, M. T., Spracklen, D. V., Heald, C.
1141 L., Gao, R. S., Kok, G., McMeeking, G. R., McQuaid, J. B., and Fahey, D. W.: Airborne
1142 observations of regional variation in fluorescent aerosol across the United States, Journal of
1143 Geophysical Research-Atmospheres, 120, 1153-1170, 10.1002/2014JD022495, 2015.
- 1144 Pinnick, R. G., Hill, S. C., Nachman, P., Pendleton, J. D., Fernandez, G. L., Mayo, M. W., and
1145 Bruno, J. G.: Fluorescence Particle Counter for Detecting Airborne Bacteria and Other
1146 Biological Particles, Aerosol Sci. Technol., 23, 653-664, 1995.
- 1147 Powelson, M. H., Espelien, B. M., Hawkins, L. N., Galloway, M. M., and De Haan, D. O.:
1148 Brown Carbon Formation by Aqueous-Phase Carbonyl Compound Reactions with Amines and
1149 Ammonium Sulfate, Environmental Science & Technology, 48, 985-993, 10.1021/es4038325,
1150 2014.

- 1151 Primmerman, C.: Detection of biological agents. *Lincoln Laboratory Journal*, 2000.
- 1152 Pöhlker, C., Huffman, J. A., and Poeschl, U.: Autofluorescence of atmospheric bioaerosols -
1153 fluorescent biomolecules and potential interferences, *Atmospheric Measurement Techniques*, 5,
1154 37-71, 10.5194/amt-5-37-2012, 2012.
- 1155 Pöhlker, C., Huffman, J. A., Foerster, J. D., and Poeschl, U.: Autofluorescence of atmospheric
1156 bioaerosols: spectral fingerprints and taxonomic trends of pollen, *Atmospheric Measurement
1157 Techniques*, 6, 3369-3392, 10.5194/amt-6-3369-2013, 2013.
- 1158 Pöschl, U.: Atmospheric aerosols: Composition, transformation, climate and health effects,
1159 *Angewandte Chemie-International Edition*, 44, 7520-7540, 10.1002/anie.200501122, 2005.
- 1160 Pöschl, U., Martin, S. T., Sinha, B., Chen, Q., Gunthe, S. S., Huffman, J. A., Borrmann, S.,
1161 Farmer, D. K., Garland, R. M., Helas, G., Jimenez, J. L., King, S. M., Manzi, A., Mikhailov, E.,
1162 Pauliquevis, T., Petters, M. D., Prenni, A. J., Roldin, P., Rose, D., Schneider, J., Su, H., Zorn, S.
1163 R., Artaxo, P., and Andreae, M. O.: Rainforest Aerosols as Biogenic Nuclei of Clouds and
1164 Precipitation in the Amazon, *Science*, 329, 1513-1516, 10.1126/science.1191056, 2010.
- 1165 Robinson, E., Gao, R.-S., Schwarz, J., Fahey, D., and Perring, A.: Fluorescence Calibration
1166 Method for Single Particle Aerosol Fluorescence Instruments. 2017.
- 1167 Ruske, S., Topping, D. O., Foot, V. E., Kaye, P. H., Stanley, W. R., Crawford, I., Morse, A. P.,
1168 and Gallagher, M. W.: Evaluation of machine learning algorithms for classification of primary
1169 biological aerosol using a new UV-LIF spectrometer, *Atmospheric Measurement Techniques*,
1170 10, 695-708, 10.5194/amt-10-695-2017, 2017.
- 1171 Saari, S., Mensah-Attipoe, J., Reponen, T., Veijalainen, A. M., Salmela, A., Pasanen, P., and
1172 Keskinen, J.: Effects of fungal species, cultivation time, growth substrate, and air exposure
1173 velocity on the fluorescence properties of airborne fungal spores, *Indoor Air*, 25, 653-661,
1174 10.1111/ina.12166, 2015a.
- 1175 Saari, S., Niemi, J. V., Ronkko, T., Kuuluvainen, H., Jarvinen, A., Pirjola, L., Aurela, M.,
1176 Hillamo, R., and Keskinen, J.: Seasonal and Diurnal Variations of Fluorescent Bioaerosol
1177 Concentration and Size Distribution in the Urban Environment, *Aerosol and Air Quality
1178 Research*, 15, 572-581, 10.4209/aaqr.2014.10.0258, 2015b.
- 1179 Sivaprakasam, V., Lin, H. B., Huston, A. L., and Eversole, J. D.: Spectral characterization of
1180 biological aerosol particles using two-wavelength excited laser-induced fluorescence and elastic
1181 scattering measurements, *Optics Express*, 19, 6191-6208, 10.1364/oe.19.006191, 2011.
- 1182 Slowik, J. G., Cross, E. S., Han, J. H., Kolucki, J., Davidovits, P., Williams, L. R., Onasch, T. B.,
1183 Jayne, J. T., Kolb, C. E., and Worsnop, D. R.: Measurements of morphology changes of fractal
1184 soot particles using coating and denuding experiments: Implications for optical absorption and
1185 atmospheric lifetime, *Aerosol Science and Technology*, 41, 734-750,
1186 10.1080/02786820701432632, 2007.

- 1187 Sodeau, J. R., and O'Connor, D. J.: Chapter 16 - Bioaerosol Monitoring of the Atmosphere for
1188 Occupational and Environmental Purposes, in: *Comprehensive Analytical Chemistry, The*
1189 *Quality of Air*, Elsevier, 391-420, 2016.
- 1190 Taketani, F., Kanaya, Y., Nakamura, T., Koizumi, K., Moteki, N., and Takegawa, N.:
1191 Measurement of fluorescence spectra from atmospheric single submicron particle using laser-
1192 induced fluorescence technique, *Journal of Aerosol Science*, 58, 1-8,
1193 10.1016/j.jaerosci.2012.12.002, 2013.
- 1194 Toprak, E., and Schnaiter, M.: Fluorescent biological aerosol particles measured with the
1195 Waveband Integrated Bioaerosol Sensor WIBS-4: laboratory tests combined with a one year
1196 field study, *Atmospheric Chemistry and Physics*, 13, 225-243, 10.5194/acp-13-225-2013, 2013.
- 1197 Twohy, C. H., McMeeking, G. R., DeMott, P. J., McCluskey, C. S., Hill, T. C. J., Burrows, S.
1198 M., Kulkarni, G. R., Tanarhte, M., Kafle, D. N., and Toohey, D. W.: Abundance of fluorescent
1199 biological aerosol particles at temperatures conducive to the formation of mixed-phase and cirrus
1200 clouds, *Atmospheric Chemistry and Physics*, 16, 8205-8225, 10.5194/acp-16-8205-2016, 2016.
- 1201 Valsan, A. E., Ravikrishna, R., Biju, C. V., Poehlker, C., Despres, V. R., Huffman, J. A.,
1202 Poeschl, U., and Gunthe, S. S.: Fluorescent biological aerosol particle measurements at a tropical
1203 high-altitude site in southern India during the southwest monsoon season, *Atmospheric*
1204 *Chemistry and Physics*, 16, 9805-9830, 10.5194/acp-16-9805-2016, 2016.
- 1205 Von Helden, G., Hsu, M. T., Gotts, N., and Bowers, M. T.: CARBON CLUSTER CATIONS
1206 WITH UP TO 84 ATOMS - STRUCTURES, FORMATION MECHANISM, AND
1207 REACTIVITY, *Journal of Physical Chemistry*, 97, 8182-8192, 10.1021/j100133a011, 1993.
- 1208 Whitehead, J. D., Gallagher, M. W., Dorsey, J. R., Robinson, N., Gabey, A. M., Coe, H.,
1209 McFiggans, G., Flynn, M. J., Ryder, J., Nemitz, E., and Davies, F.: Aerosol fluxes and dynamics
1210 within and above a tropical rainforest in South-East Asia, *Atmospheric Chemistry and Physics*,
1211 10, 9369-9382, 10.5194/acp-10-9369-2010, 2010.
- 1212 Whitehead, J. D., Darbyshire, E., Brito, J., Barbosa, H. M. J., Crawford, I., Stern, R., Gallagher,
1213 M. W., Kaye, P. H., Allan, J. D., Coe, H., Artaxo, P., and McFiggans, G.: Biogenic cloud nuclei
1214 in the central Amazon during the transition from wet to dry season, *Atmospheric Chemistry and*
1215 *Physics*, 16, 9727-9743, 10.5194/acp-16-9727-2016, 2016.
- 1216 Wright, T. P., Hader, J. D., McMeeking, G. R., and Petters, M. D.: High Relative Humidity as a
1217 Trigger for Widespread Release of Ice Nuclei, *Aerosol Science and Technology*, 48, 5,
1218 10.1080/02786826.2014.968244, 2014.
- 1219 Wu, Y., Chen, A. L., Luhung, I., Gall, E. T., Cao, Q. L., Chang, V. W. C., and Nazaroff, W. W.:
1220 Bioaerosol deposition on an air-conditioning cooling coil, *Atmospheric Environment*, 144, 257-
1221 265, 10.1016/j.atmosenv.2016.09.004, 2016.
- 1222 Xie, Y. Y., Fajardo, O. A., Yan, W. Z., Zhao, B., and Jiang, J. K.: Six-day measurement of size-
1223 resolved indoor fluorescent bioaerosols of outdoor origin in an office, *Particuology*, 31, 161-169,
1224 10.1016/j.partic.2016.09.004, 2017.

- 1225 Yu, X. W., Wang, Z. B., Zhang, M. H., Kuhn, U., Xie, Z. Q., Cheng, Y. F., Poschl, U., and Su,
1226 H.: Ambient measurement of fluorescent aerosol particles with a WIBS in the Yangtze River
1227 Delta of China: potential impacts of combustion-related aerosol particles, *Atmospheric*
1228 *Chemistry and Physics*, 16, 11337-11348, 10.5194/acp-16-11337-2016, 2016.
- 1229 Zelenyuk, A., Cai, Y., and Imre, D.: From agglomerates of spheres to irregularly shaped
1230 particles: Determination of dynamic shape factors from measurements of mobility and vacuum
1231 aerodynamic diameters, *Aerosol Science and Technology*, 40, 197-217,
1232 10.1080/02786820500529406, 2006.
- 1233 Zhen, H., Han, T., Fennell, D., and Mainelis, G.: A systematic comparison of four bioaerosol
1234 generators: Effect on culturability and membrane integrity when aerosolizing *E. coli* bacteria. A
1235 systematic comparison of four bioaerosol generators: Effect on culturability and membrane
1236 integrity when aerosolizing *E. coli* bacteria., *Journal of Aerosol Science*, 2014
- 1237 Ziemba, L. D., Beyersdorf, A. J., Chen, G., Corr, C. A., Crumeyrolle, S. N., Diskin, G., Hudgins,
1238 C., Martin, R., Mikoviny, T., Moore, R., Shook, M., Thornhill, K. L., Winstead, E. L., Wisthaler,
1239 A., and Anderson, B. E.: Airborne observations of bioaerosol over the Southeast United States
1240 using a Wideband Integrated Bioaerosol Sensor, *Journal of Geophysical Research-Atmospheres*,
1241 121, 8506-8524, 10.1002/2015JD024669, 2016.
- 1242
- 1243

1244 **8. Tables**

1245 Table 1. Fluorescence and asymmetry factor values of standard PSLs, determined as the peak
1246 (mean) of a Gaussian fit applied to a histogram of the fluorescence signal in each channel.
1247 Uncertainties are one standard deviation from the Gaussian mean.

	FL1	FL2	FL3	AF
2 μm Green	69 ± 49	1115 ± 57	214 ± 29	6 ± 2
2 μm Red	44 ± 30	160 ± 18	28 ± 13	5 ± 2
2.1 μm Blue	724 ± 111	1904 ± 123	2045 ± 6	5 ± 2

1248

1249 **Table 2.** Median values for each of the five data parameters, along with percent of particles that
 1250 saturate fluorescence detector in each fluorescence channel. Uncertainty (as one standard
 1251 deviation, σ) listed for particle size and asymmetry factor (AF). Only a sub-selection of pollen
 1252 are characterized as fragmented pollen because not all pollen presented the smaller size fraction
 1253 or fluorescence characteristics that represent fragments.

Materials	FL1	FL1 Sat %	FL2	FL2 Sat %	FL3	FL3 Sat %	Size (μm)	AF	Aerosolization method	
BIOLOGICAL MATERIALS										
Pollen										
Intact Pollen										
1	<i>Urtica dioica</i> (Stinging Nettle)	2047.0	99.2	2047.0	99.4	1072.0	9.9	16.9 \pm 2.2	18.5 \pm 8.3	Powder (P1)
2	<i>Artemisia vulgaris</i> (Common Mugwort)	1980.0	48.3	2047.0	99.7	2047.0	90.3	19.7 \pm 1.0	14.2 \pm 7.6	Powder (P1)
3	<i>Castanea sativa</i> (European Chestnut)	830.0	19.3	258.0	2.9	269.0	0.8	15.3 \pm 1.7	17.0 \pm 9.5	Powder (P1)
4	<i>Corylus avellana</i> (Hazel)	1371.0	44.4	532.0	5.6	99.0	2.8	16.6 \pm 2.1	24.2 \pm 12.6	Powder (P1)
5	<i>Taxus baccata</i> (Common Yew)	525.0	0.4	561.0	0.2	615.0	0.0	16.0 \pm 1.3	22.2 \pm 10.0	Powder (P1)
6	<i>Rumex acetosella</i> (Sheep Sorrel)	2047.0	73.5	2047.0	55.1	693.0	2.7	16.2 \pm 2.0	21.7 \pm 10.8	Powder (P1)
7	<i>Olea europaea</i> (European Olive Tree)	131.0	1.1	395.0	0.4	119.0	0.0	19.7 \pm 1.2	17.7 \pm 7.6	Powder (P1)
8	<i>Alnus glutinosa</i> (Black Alder)	109.0	3.3	432.0	1.2	102.0	0.9	18.6 \pm 1.7	15.8 \pm 8.5	Powder (P1)
9	<i>Phleum pratense</i> (Timothy Grass)	2047.0	100.0	2012.0	49.8	651.0	1.9	15.1 \pm 1.7	24.1 \pm 12.2	Powder (P1)
10	<i>Populus alba</i> (White Poplar)	2047.0	95.9	2047.0	92.2	1723.0	39.2	18.7 \pm 1.9	21.2 \pm 10.4	Powder (P1)
11	<i>Taraxacum officinale</i> (Common Dandelion)	2047.0	99.1	1309.0	21.8	1767.0	44.2	15.4 \pm 1.8	22.2 \pm 11.9	Powder (P1)
12	<i>Amaranthus retroflexus</i> (Redroot Amaranth)	980.0	36.7	1553.0	36.7	1061.0	18.0	17.7 \pm 2.2	19.4 \pm 12.1	Powder (P1)
13	<i>Aesculus hippocastanum</i> (Horse-chestnut)	762.0	23.5	876.0	23.5	776.0	23.5	16.2 \pm 2.0	22.2 \pm 13.4	Powder (P1)
14	<i>Lycopodium</i> (Clubmoss)	40.0	0.1	32.0	0.0	27.0	0.0	3.9 \pm 1.86	24.5 \pm 15.9	Powder (P1)
Fragment Pollen										
3	<i>Castanea sativa</i> (European Chestnut)	74.0	11.0	113.0	0.4	84.0	0.1	7.0 \pm 3.1	24.6 \pm 13.7	Powder (P1)
4	<i>Corylus avellana</i> (Hazel)	263.0	28.8	119.0	0.5	46.0	0.2	6.1 \pm 3.7	20.4 \pm 13.7	Powder (P1)
5	<i>Taxus baccata</i> (Common Yew)	40.0	0.2	28.0	0.1	34.0	0.0	2.6 \pm 2.2	16.0 \pm 12.2	Powder (P1)
6	<i>Rumex acetosella</i> (Sheep Sorrel)	417.0	87.1	88.0	0.4	71.0	0.1	6.0 \pm 2.5	24.4 \pm 12.4	Powder (P1)
7	<i>Olea europaea</i> (European Olive Tree)	40.0	1.9	22.0	0.1	33.0	0.0	2.6 \pm 1.6	10.4 \pm 9.3	Powder (P1)
8	<i>Alnus glutinosa</i> (Black Alder)	46.0	4.6	46.0	0.3	44.0	0.2	6.1 \pm 3.2	25.2 \pm 14.6	Powder (P1)
9	<i>Phleum pratense</i> (Timothy Grass)	2047.0	85.5	129.0	1.2	63.0	0.1	6.0 \pm 3.2	23.1 \pm 13.4	Powder (P1)
10	<i>Populus alba</i> (White Poplar)	642.0	35.2	237.0	8.6	103.0	0.5	7.4 \pm 4.0	24.7 \pm 14.2	Powder (P1)
11	<i>Taraxacum officinale</i> (Common Dandelion)	2047.0	71.9	195.0	0.4	88.0	0.8	6.1 \pm 3.1	23.7 \pm 13.5	Powder (P1)

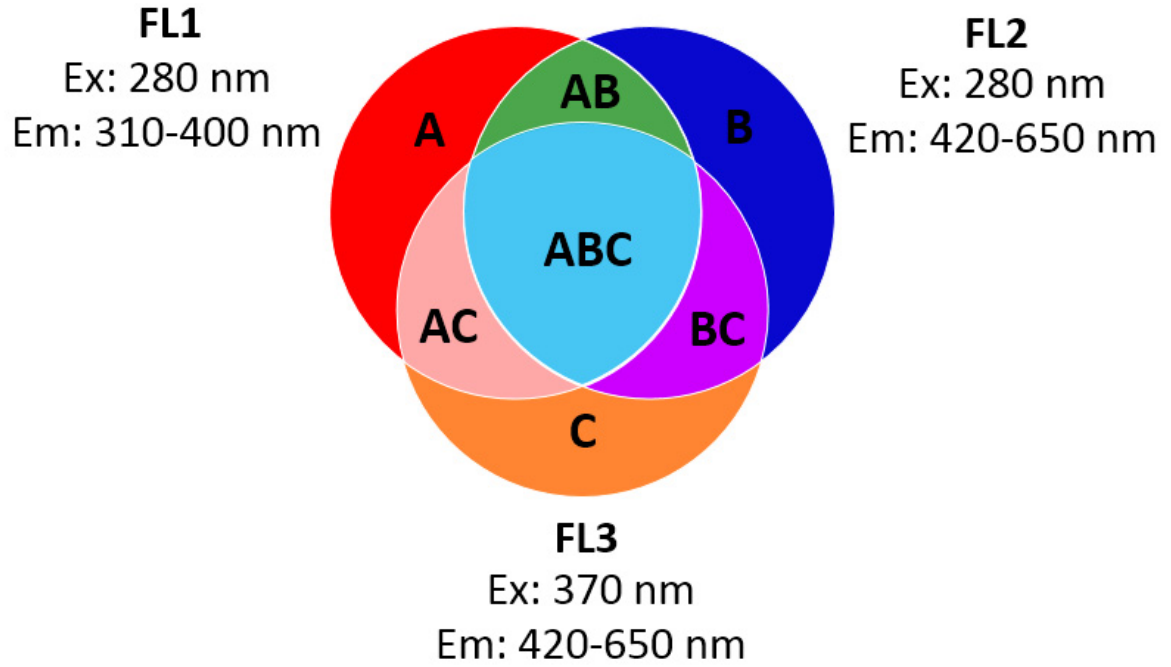
12	<i>Amaranthus retroflexus</i> (Redroot Amaranth)	104.0	15.6	138.0	5.6	101.0	3.4	7.3 ± 2.8	27.7 ± 14.6	Powder (P1)
13	<i>Aesculus hippocastanum</i> (Horse-chestnut)	43.0	6.0	106.0	0.2	42.0	0.2	4.3 ± 3.1	19.7 ± 13.4	Powder (P1)
Fungal spores										
1	<i>Aspergillus brasiliensis</i>	1279.0	38.5	22.0	0.0	33.0	0.0	3.6 ± 1.8	20.8 ± 10.3	Fungal
2	<i>Aspergillus niger</i> ; WB 326	543.0	6.2	18.0	0.0	29.0	0.0	2.7 ± 0.9	17.1 ± 10.7	Fungal
3	<i>Rhizopus stolonifera</i> (Black Bread Mold); UNB-1	78.0	11.2	20.0	0.1	34.0	0.1	4.4 ± 2.3	21.4 ± 14.4	Fungal
4	<i>Saccharomyces cerevisiae</i> (Brewer's Yeast)	2047.0	96.6	97.0	0.3	41.0	0.1	7.2 ± 3.7	28.7 ± 16.8	Fungal
5	<i>Aspergillus versicolor</i> ; NRRL 238	2047.0	78.2	55.0	0.0	40.0	0.0	4.5 ± 2.5	24.5 ± 16.9	Fungal
Bacteria										
1	<i>Bacillus atrophaeus</i>	443.0	1.0	10.0	0.0	36.0	0.0	2.2 ± 0.4	17.4 ± 4.1	Bacterial
2	<i>Escherichia coli</i>	454.0	1.4	12.0	0.0	33.0	0.0	1.2 ± 0.3	19.3 ± 2.8	Bacterial
3	<i>Pseudomonas Stutzeri</i>	675.0	0.4	16.0	0.0	36.0	0.0	1.1 ± 0.3	19.2 ± 2.8	Bacterial
Biofluorophores										
1	Riboflavin	41.0	0.0	190.0	2.5	119.0	1.3	2.5 ± 2.5	13.2 ± 12.2	Powder (P1)
2	Chitin	116.5	6.2	61.0	0.1	40.0	0.0	2.7 ± 2.1	16.1 ± 13.5	Powder (P1)
3	NAD	49.0	0.2	962.0	26.7	515.0	15.0	2.1 ± 2.2	12.2 ± 10.1	Powder (P1)
4	Folic Acid	41.0	0.0	34.0	0.1	28.0	0.1	3.7 ± 3.4	18.6 ± 13.6	Powder (P1)
5	Cellulose, fibrous medium	54.0	0.2	37.0	0.1	27.0	0.0	3.7 ± 2.5	20.4 ± 15.7	Powder (P1)
6	Ergosterol	2047.0	81.8	457.0	2.6	355.0	11.6	6.8 ± 4.0	22.6 ± 12.9	Powder (P1)
7	Pyridoxine	661.0	0.0	39.0	0.0	28.0	0.0	1.0 ± 0.2	20.0 ± 13.0	Powder (P1)
8	Pyridoxamine	706.0	10.7	40.0	0.0	28.0	0.0	5.2 ± 2.5	20.2 ± 12.7	Powder (P1)
9	Tyrosine	2047.0	59.7	42.0	0.0	29.0	0.0	2.9 ± 3.4	15.4 ± 11.6	Powder (P1)
10	Phenylalanine	53.0	0.0	29.0	0.0	24.0	0.0	3.2 ± 2.0	21.1 ± 15.4	Powder (P1)
11	Tryptophan	2047.0	78.0	357.0	9.0	30.0	0.0	3.5 ± 2.9	20.9 ± 17.0	Powder (P1)
12	Histidine	59.0	0.2	29.0	0.0	25.0	0.0	2.0 ± 1.7	11.6 ± 10.0	Powder (P1)
NON-BIOLOGICAL MATERIALS										
Dust										
1	Arabic Sand	48.0	0.1	37.0	0.0	29.0	0.0	3.1 ± 2.2	16.1 ± 15.7	Powder (P3)
2	California Sand	66.0	1.1	42.0	0.0	31.0	0.0	4.0 ± 1.9	18.8 ± 14.6	Powder (P2)
3	Africa Sand	88.0	0.0	48.0	0.0	26.0	0.0	2.2 ± 1.4	15.3 ± 11.0	Powder (P2)
4	Murkee-Murkee Australian Sand	88.0	0.7	47.0	0.0	26.0	0.0	1.9 ± 1.1	10.9 ± 9.2	Powder (P2)

5	Manua Key Summit Hawaii Sand	54.0	0.1	33.0	0.0	25.0	0.0	1.5 ± 0.7	10.8 ± 13.4	Powder (P2)
6	Quartz	66.0	0.0	38.0	0.0	24.0	0.0	1.7 ± 0.8	11.2 ± 12.7	Powder (P2)
7	Kakadu Dust	58.0	0.0	35.0	0.0	25.0	0.0	2.7 ± 1.4	15.0 ± 12.0	Powder (P2)
8	Feldspar	60.0	0.0	36.0	0.0	25.0	0.0	1.2 ± 0.6	10.2 ± 10.6	Powder (P2)
9	Hematite	51.0	0.0	32.0	0.0	25.0	0.0	1.8 ± 1.0	10.8 ± 11.9	Powder (P2)
10	Gypsum	49.0	0.0	30.0	0.0	26.0	0.0	4.1 ± 3.0	19.3 ± 12.2	Powder (P2)
11	Bani AMMA	48.0	0.2	31.0	0.0	26.0	0.0	3.1 ± 2.1	15.8 ± 13.7	Powder (P2)
12	Arizona Test Dest	46.0	0.0	29.0	0.0	25.0	0.0	1.4 ± 0.7	10.5 ± 10.5	Powder (P2)
13	Kaolinite	46.0	0.0	29.0	0.0	25.0	0.0	1.5 ± 0.8	9.9 ± 10.3	Powder (P2)
HULIS										
1	Waskish Peat Humic Acid Reference	46.0	0.0	29.0	0.0	25.0	0.0	1.7 ± 0.8	10.9 ± 9.8	Powder (P1)
2	Suwannee River Humic Acid Standard II	46.0	0.0	30.0	0.0	26.0	0.0	2.0 ± 1.2	13.2 ± 16.5	Powder (P2)
3	Suwannee River Fulvic Acid Standard I	46.0	0.0	34.0	0.0	28.0	0.0	1.7 ± 1.0	12.0 ± 10.1	Powder (P2)
4	Elliott Soil Humic Acid Standard	47.0	0.0	29.0	0.0	25.0	0.0	1.2 ± 0.6	10.5 ± 10.2	Powder (P1)
5	Pony Lake (Antarctica) Fulvic Acid Reference	46.0	0.0	49.0	0.0	37.0	0.0	2.4 ± 1.8	14.0 ± 13.3	Powder (P2)
6	Nordic Aquatic Fulvic Acid Reference	48.0	0.1	32.0	0.0	27.0	0.0	1.8 ± 1.4	11.6 ± 9.6	Powder (P2)
Polycyclic Hydrocarbons										
1	Pyrene	490.0	7.4	2047.0	91.5	2047.0	81.8	5.0 ± 3.5	17.4 ± 12.6	Powder (P1)
2	Phenanthrene	2047.0	81.9	2047.0	66.3	360.0	22.4	3.9 ± 3.5	14.5 ± 13.6	Powder (P1)
3	Naphthalene	886.0	11.6	45.0	2.1	30.0	0.7	1.1 ± 1.0	10.6 ± 9.5	Powder (P1)
Combustion Soot and Smoke										
1	Aquadag	22.0	0.0	14.0	0.0	29.0	0.0	1.2 ± 0.6	10.5 ± 6.6	Liquid
2	Ash	48.0	0.2	31.0	0.0	23.0	0.0	1.7 ± 1.3	12.6 ± 11.9	Powder (P1)
3	Fullerene Soot	318.0	0.0	30.0	0.0	26.0	0.0	1.1 ± 0.5	17.0 ± 10.6	Powder (P2)
4	Diesel Soot	750.5	0.2	30.0	0.0	26.0	0.0	1.1 ± 0.4	21.2 ± 10.1	Powder (P1)
5	Cigarette Smoke	28.0	0.6	30.0	0.1	36.0	0.0	1.0 ± 0.8	9.5 ± 4.5	Smoke
6	Wood Smoke (<i>Pinus Nigra</i> , <i>Black Pine</i>)	32.0	0.1	30.0	0.0	36.0	0.0	1.0 ± 0.7	9.5 ± 4.3	Smoke
7	Fire Ash	42.0	0.2	33.0	0.0	28.0	0.0	1.8 ± 1.2	14.0 ± 16.7	Powder (P1)
Brown Carbon										
1	Methylglyoxal + Glycine	17.0	0.0	53.0	0.0	88.0	0.0	1.2 ± 0.4	18.4 ± 3.1	Liquid
2	Glycolaldehyde + Methylamine	15.0	0.0	19.0	0.0	47.0	0.0	1.2 ± 0.4	17.9 ± 2.4	Liquid
3	Glyoxal + Ammonium Sulfate	30.0	0.0	9.0	0.0	35.0	0.0	1.3 ± 0.6	14.1 ± 3.5	Liquid

Miscellaneous non-biological/Common household fibers										
1	Laboratory wipes	112.0	30.6	54.0	15.2	47.0	15.4	3.6v5.7	16.4 ± 14.4	Rubbed material over inlet
2	Cotton t-shirt (white)	567.0	34.9	145.0	16.1	139.0	16.4	4.9 ± 4.7	23.5 ± 16.2	
3	Cotton t-shirt (black)	56.0	13.5	22.0	1.7	34.0	1.5	2.7 ± 4.0	17.6 ± 14.8	

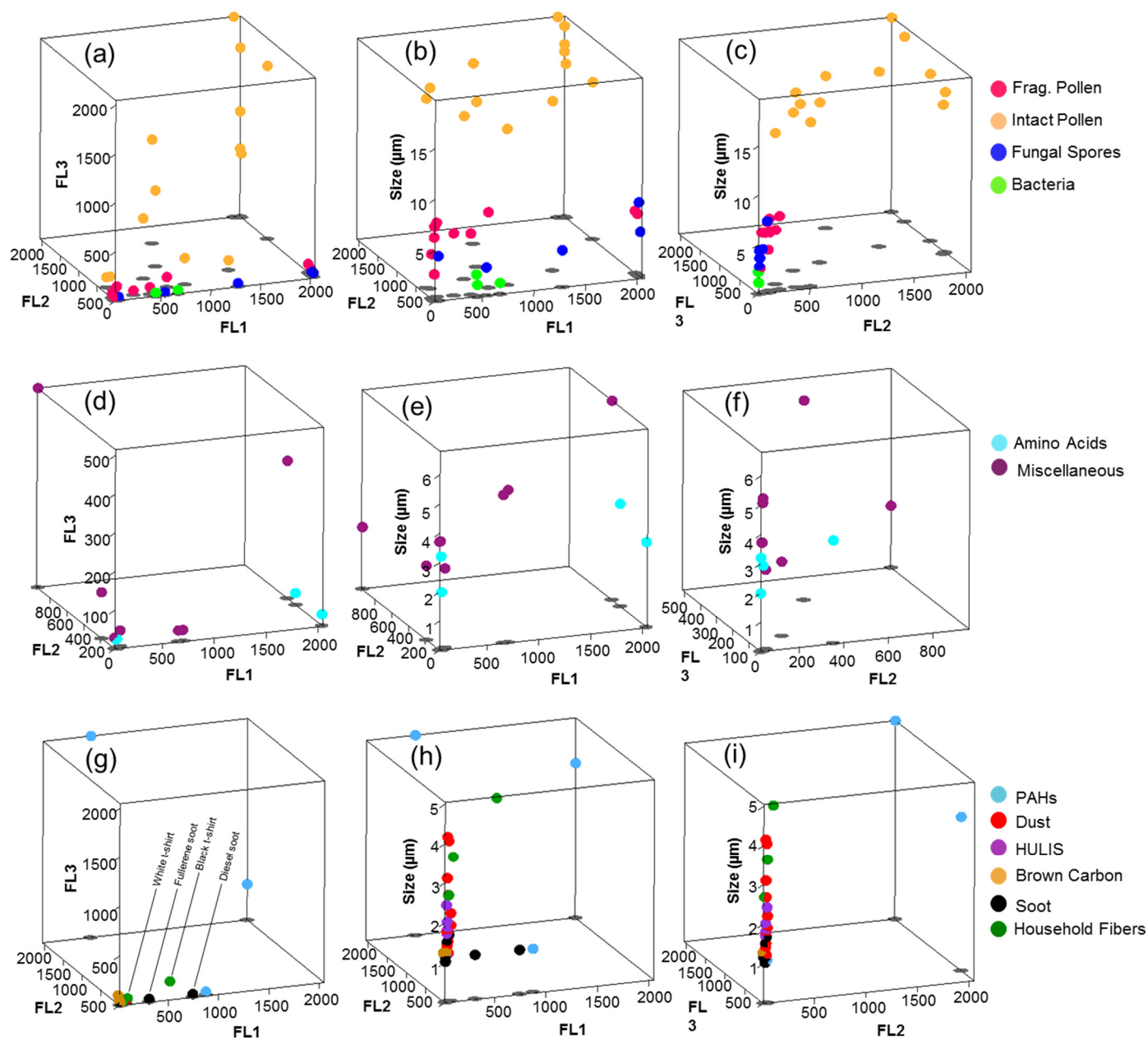
1254

1255 9. Figures



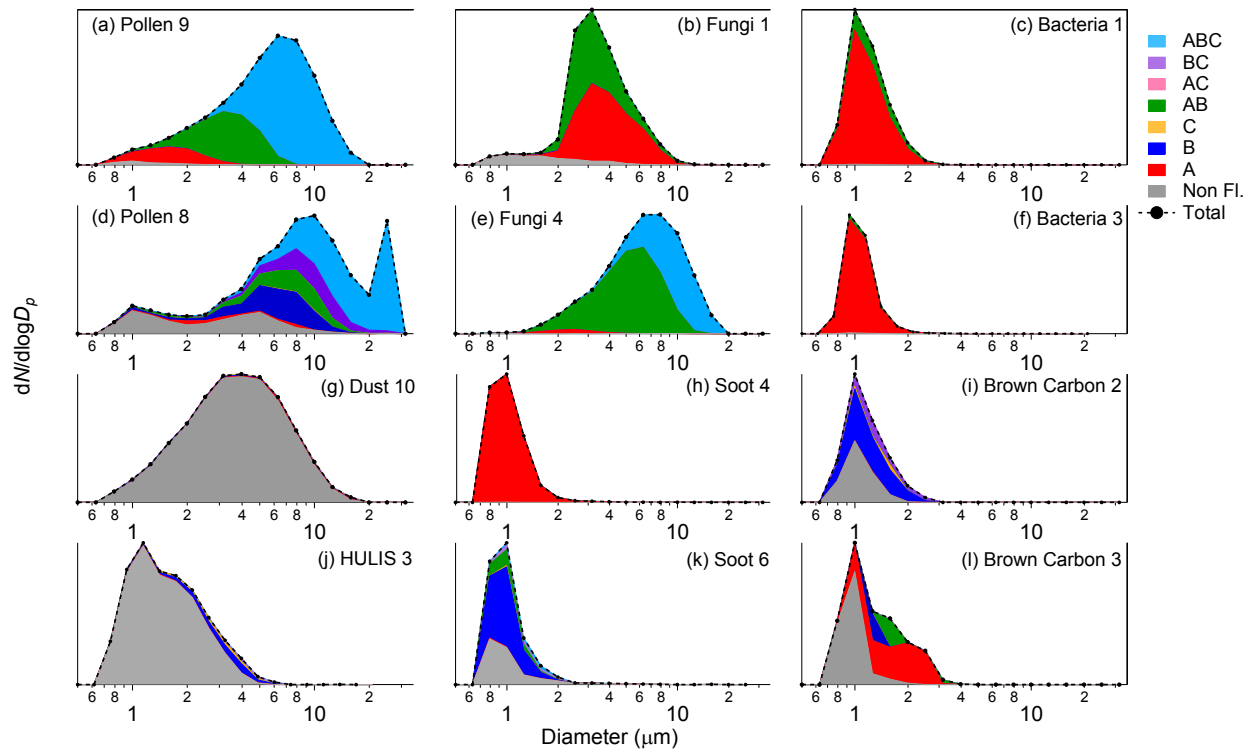
1256

1257 Figure 1. Particle type classification, as introduced by introduced by Perring et al. (2015). Large
1258 circles each represent one fluorescence channel (FL1, FL2, FL3). Colored zones represent
1259 particle types that each exhibit fluorescence in one, two, or three channels.



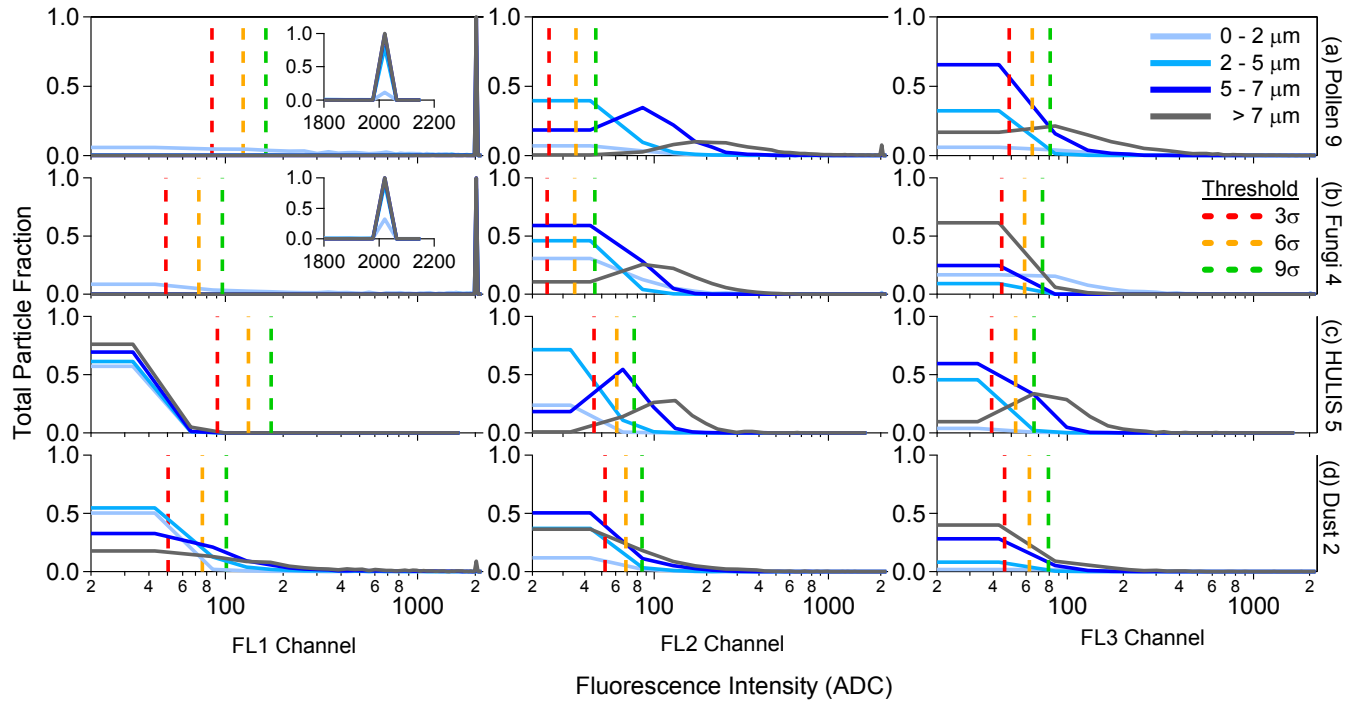
1260

1261 Figure 2. Representations including 4 of the 5 parameters recorded by the WIBS: FL1, FL2, FL3,
 1262 and particle size. Biological material types (a-c), bio-fluorophores (d-f), and non-biological
 1263 particle types (g-i). Data points represent median values. Gray ovals are shadows (cast directly
 1264 downward onto the bottom plane) included to help reader with 3-D representation. Tags in (d)
 1265 and (g) used to differentiate particles of specific importance within text.



1266

1267 Figure 3. Stacked particle type size distributions including particle type classification, as
 1268 introduced by introduced by Perring et al. (2015) using FT + 3 σ threshold definition. Examples
 1269 of each material type were selected to show general trends from larger pool of samples. Soot 4
 1270 (h) as an example of combustion soot and Soot 6 (wood smoke) as an example of smoke aerosol.

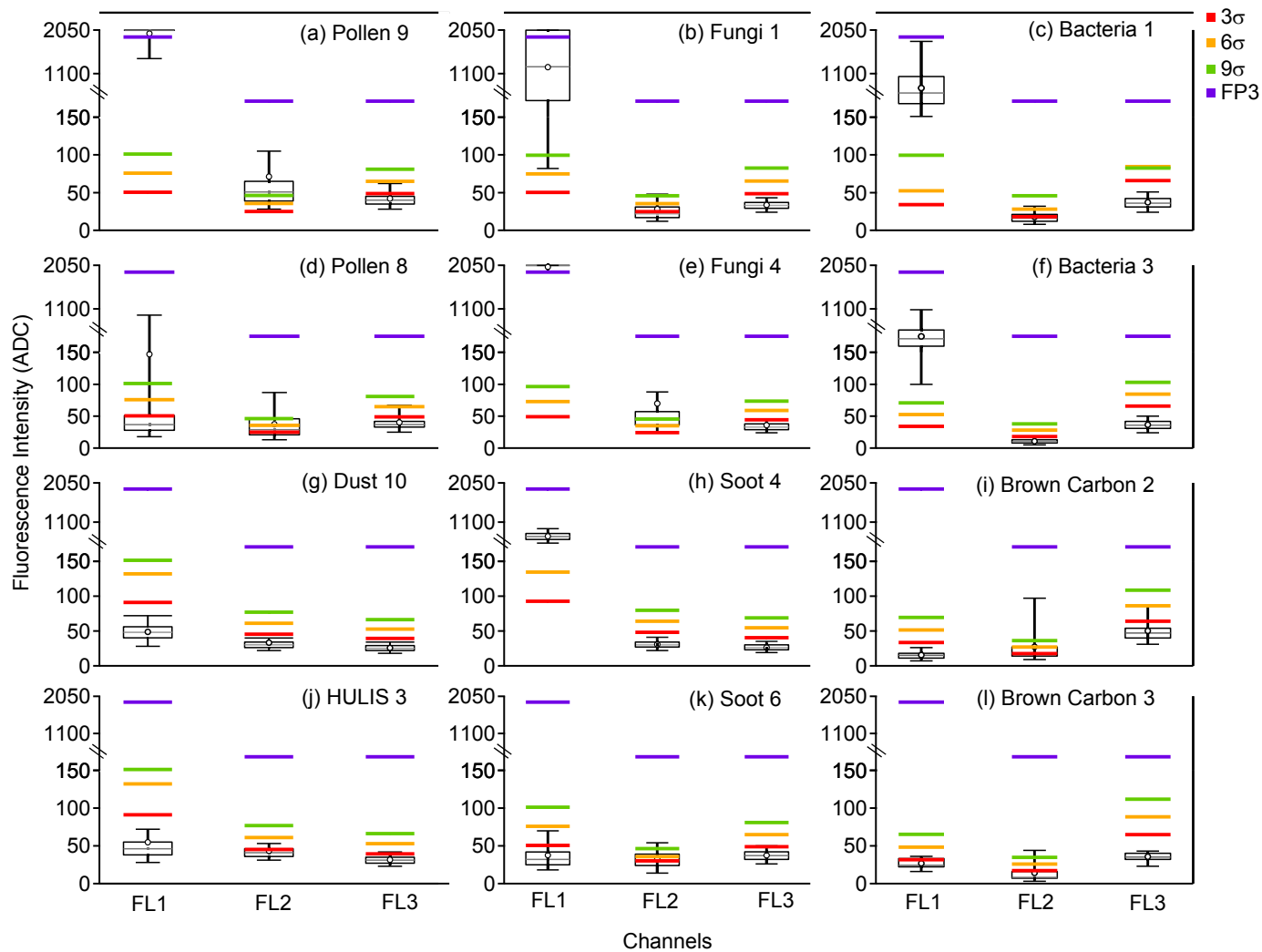


1271

1272

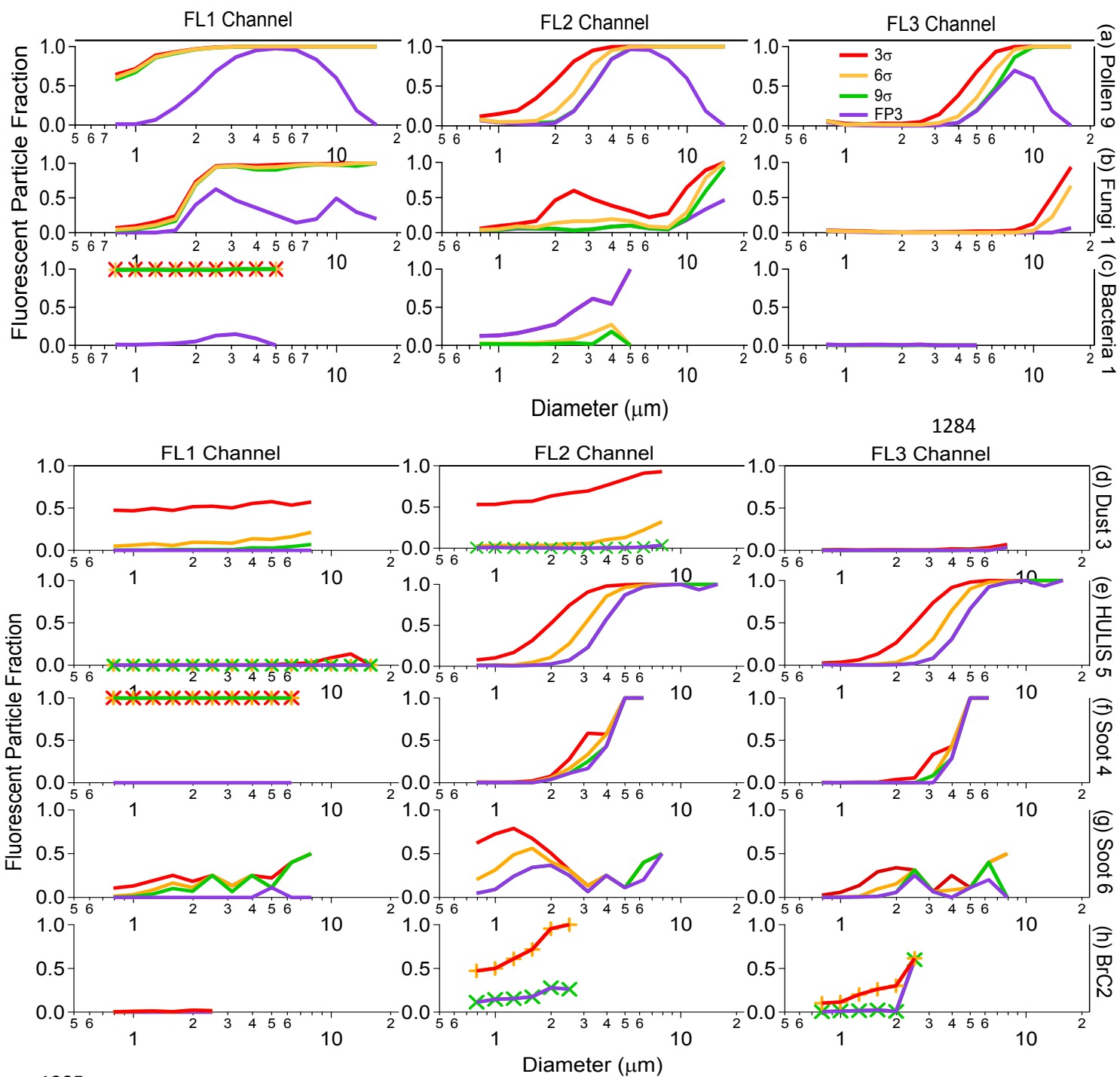
1273 Figure 4. Relative fraction of fluorescent particles versus fluorescence intensity in analog-to-
 1274 digital counts (ADC) for each channel. Particles are binned into 4 different size ranges (trace
 1275 colors). Vertical lines indicate three thresholding definitions. Insets shown for particles that
 1276 exhibit fluorescence saturation characteristics.

1277



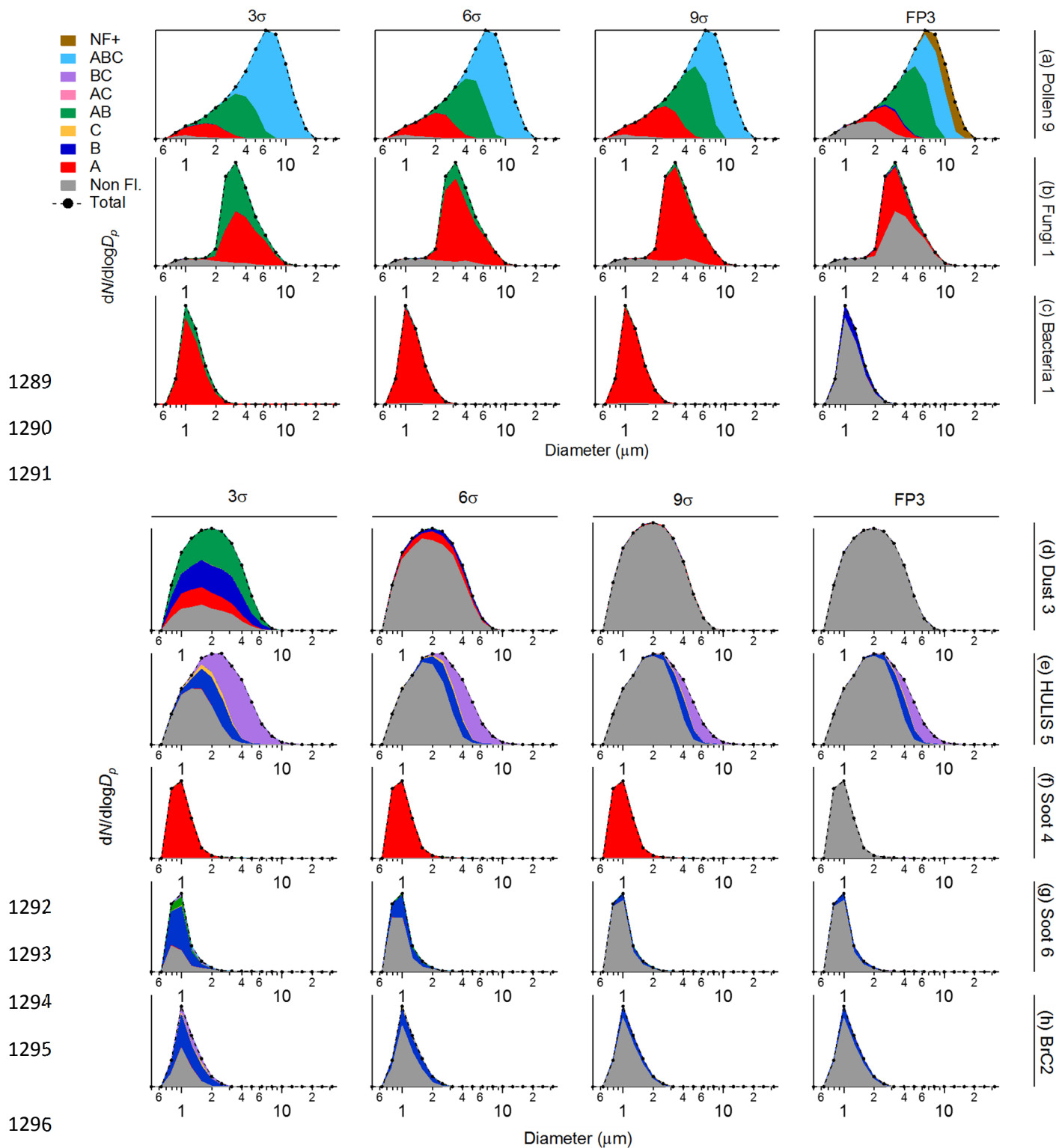
1278

1279 **Figure 5.** Box whisker plots showing statistical distributions of fluorescence intensity in analog-
 1280 to-digital counts (ADC) in each channel. Averages are limited to particles in the size range 3.5-
 1281 4.0 μm for pollen, fungal spore, HULIS, and dust samples and in the range 1.0-1.5 μm for
 1282 bacteria, brown carbon, and soot samples. Horizontal bars associated with each box-whisker
 1283 show four separate threshold levels.

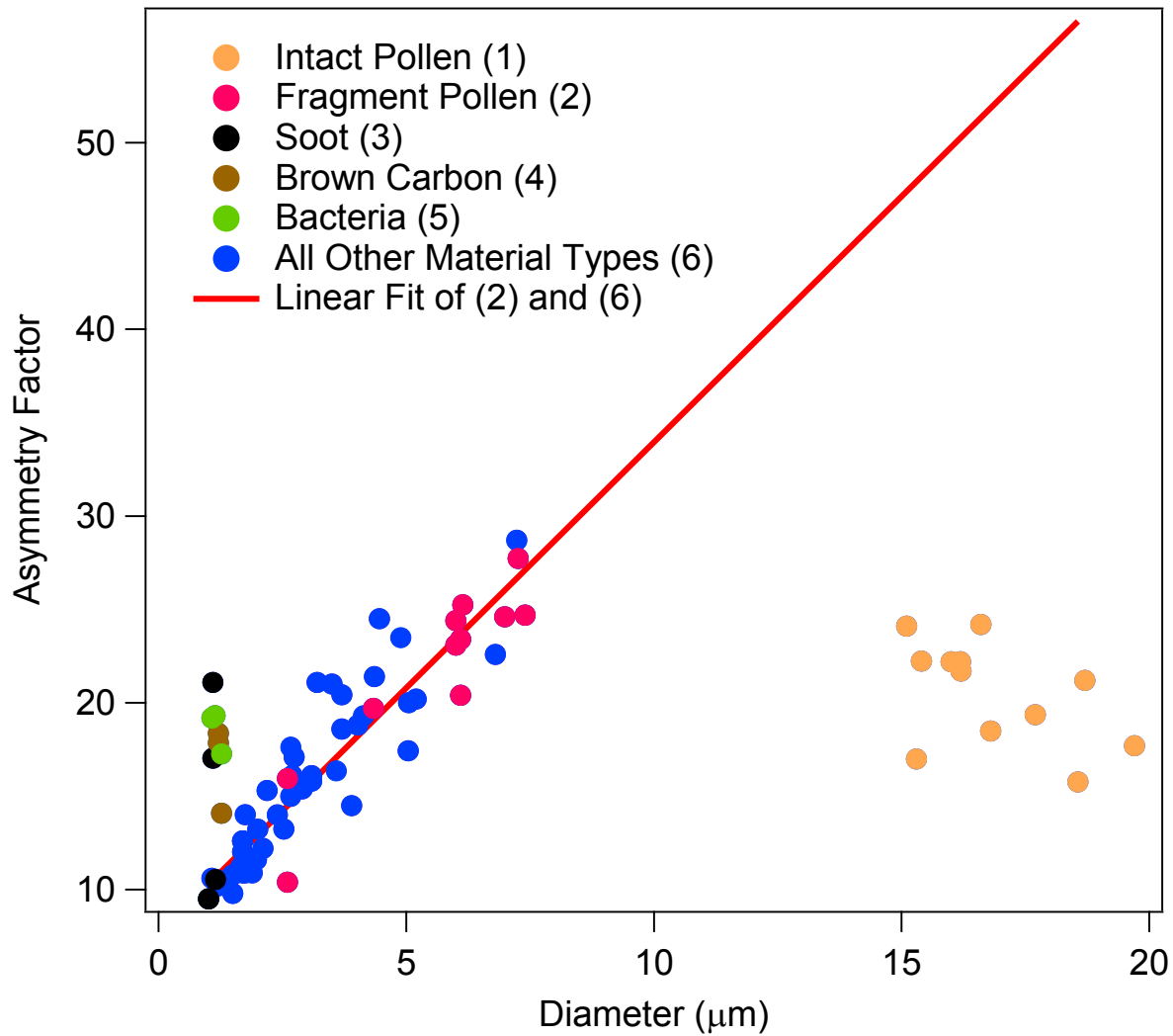


1285

1286 Figure 6. Fraction of particle number exhibiting fluorescent in a given channel versus particle
 1287 diameter for various material types for four different thresholds definitions. Data markers shown
 1288 only when disambiguation of traces is necessary. Brown carbon sample denoted by BrC.



1297 **Figure 7.** Stacked particle type size distributions for representative particle classes shown using
 1298 four separate thresholding strategies. NF+ particle type (right-most column) represents particles
 1299 that exceed the FL2 and/or FL3 upper bound of the Wright et al. (2014) FP3 definition and that
 1300 are therefore considered as one set of “non-fluorescent” particles by that definition. Legend
 1301 above top rows indicate threshold definition used.



1302

1303 Figure 8. Median values of particle asymmetry factor versus particle size for all particle types
 1304 analyzed. Fitted linear regression shown, with equation $y = 2.63x + 7.64$ and $R^2 = 0.87$. Linear
 1305 regression analysis was done for samples pooled from the categories of Fragmented Pollen (2)
 1306 and All Other Material Types (6).

1 Supplemental Information for:

2 Systematic Characterization and Fluorescence Threshold Strategies for the Wideband Integrated
3 Bioaerosol Sensor (WIBS) Using Size-Resolved Biological and Interfering Particles

4 NICOLE SAVAGE¹, Christine Krentz¹, Tobias Könnemann², Taewon T. Han³, Gediminas
5 Mainelis³, Christopher Pöhlker², J. Alex Huffman¹

6 ¹ *University of Denver, Department of Chemistry and Biochemistry, Denver, USA*

7 ² *Max Planck Institute for Chemistry, Multiphase Chemistry and Biogeochemistry Departments,*
8 *Mainz, Germany*

9 ³ *Rutgers, The State University of New Jersey, Department of Environmental Science, New*
10 *Jersey, USA*

11 Table S1. Material types analyzed, including biological and non-biological. Table includes
 12 threshold values for FT + 3 σ and FT +9 σ .

Materials		Provider	Part Number	Aerosolization Method	3 σ FL1	3 σ FL2	3 σ FL3	9 σ FL1	9 σ FL2	9 σ FL3
BIOLOGICAL MATERIALS										
Pollen										
1	<i>Urtica dioica</i> (Stinging Nettle)	BONAPOL	-	Powder (P1)	49.0	24.3	44.4	96.5	45.6	73.5
2	<i>Artemisia vulgaris</i> (Common Mugwort)	BONAPOL	-	Powder (P1)	49.0	24.3	44.4	96.5	45.6	73.5
3	<i>Castanea sativa</i> (European Chestnut)	BONAPOL	-	Powder (P1)	48.2	24.1	46.1	95.2	45.2	77.6
4	<i>Corylus avellana</i> (Hazel)	BONAPOL	-	Powder (P1)	48.2	24.1	46.1	95.2	45.2	77.6
5	<i>Taxus baccata</i> (Common Yew)	BONAPOL	-	Powder (P1)	48.2	24.1	46.1	95.2	45.2	77.6
6	<i>Rumex acetosella</i> (Sheep Sorrel)	BONAPOL	-	Powder (P1)	48.2	24.1	46.1	95.2	45.2	77.6
7	<i>Olea europaea</i> (European Olive Tree)	BONAPOL	-	Powder (P1)	48.2	24.1	46.1	95.2	45.2	77.6
8	<i>Alnus glutinosa</i> (Black Alder)	BONAPOL	-	Powder (P1)	50.5	24.9	48.8	101.2	46.3	80.9
9	<i>Phleum pratense</i> (Timothy Grass)	BONAPOL	-	Powder (P1)	50.5	24.9	48.8	101.2	46.3	80.9
10	<i>Populus alba</i> (White Poplar)	BONAPOL	-	Powder (P1)	47.7	23.9	46.2	95.6	44.8	77.8
11	<i>Taraxacum officinale</i> (Common Dandelion)	BONAPOL	-	Powder (P1)	47.7	23.9	46.2	95.6	44.8	77.8
12	<i>Amaranthus retroflexus</i> (Redroot Amaranth)	BONAPOL	-	Powder (P1)	45.6	24.4	46.6	89.5	45.7	78.9
13	<i>Aesculus hippocastanum</i> (Horse-chestnut)	BONAPOL	-	Powder (P1)	45.6	24.4	46.6	89.5	45.7	78.9
14	<i>Lycopodium</i> (Clubmoss)	Polysci., Inc.	16867	Powder (P1)	85.1	52.3	46.1	162.5	85.2	79.2
Fungal spores										
1	<i>Aspergillus brasiliensis</i>	ATCC*	-	Fungal	50.3	24.7	48.5	99.5	45.9	82.4
2	<i>Aspergillus niger</i> ; WB 326	ATCC	16888	Fungal	50.3	24.7	48.5	99.5	45.9	82.4
3	<i>Rhizopus stolonifera</i> (Black Bread Mold); UNB-1	ATCC	14037	Fungal	50.3	24.7	48.5	99.5	45.9	82.4
4	<i>Saccharomyces cerevisiae</i> (Brewer's Yeast)	ATCC	-	Fungal	49.0	24.3	44.5	96.5	45.6	73.5
5	<i>Aspergillus versicolor</i> ; NRRL 238	ATCC	10106	Fungal	49.0	24.3	44.5	96.5	45.6	73.5

Bacteria										
1	<i>Bacillus atrophaeus</i>	ATCC	49337	Bacterial	34.1	18.1	65.8	70.8	38.1	103.0
2	<i>Escherichia coli</i>	ATCC	15597	Bacterial	34.1	18.1	65.8	70.8	38.1	103.0
3	<i>Pseudomonas stutzeri</i>	ATCC	13525	Bacterial	34.1	18.1	65.8	70.8	38.1	103.0
Biofluorophores										
1	Riboflavin	Sigma	R7649	Powder (P1)	87.3	56.2	49.1	166.8	92.4	84.3
2	Chitin	Sigma	C9752	Powder (P1)	87.3	56.2	49.1	166.8	92.4	84.3
3	NAD	Sigma	N8129	Powder (P1)	87.3	56.2	49.1	166.8	92.4	84.3
4	Folic Acid	Sigma	F7876	Powder (P1)	87.3	56.2	49.1	166.8	92.4	84.3
5	Cellulose, fibrous medium	Sigma	4352396	Powder (P1)	85.3	54.5	48.5	159.7	88.6	82.1
6	Ergosterol	Sigma	45480	Powder (P1)	92.8	48.0	40.5	176.1	79.7	68.8
7	Pyridoxine	Sigma	P5669	Powder (P1)	96.7	46.1	40.6	186.5	77.7	69.0
8	Pyridoxamine	Sigma	P9380	Powder (P1)	92.8	48.0	40.5	176.1	79.7	68.8
9	Tyrosine	Sigma	855456	Powder (P1)	87.1	52.3	44.8	166.4	86.8	75.8
10	Phenylalanine	Sigma	78019	Powder (P1)	85.3	54.5	48.5	159.7	88.6	82.1
11	Tryptophan	Sigma	93659	Powder (P1)	85.3	54.5	48.5	159.7	88.6	82.1
12	Histidine	Sigma	H8000	Powder (P1)	90.9	45.2	39.3	173.0	76.8	66.3
NON-BIOLOGICAL MATERIALS										
Dust										
1	Arabic Sand	UM-SEES **	-	Powder (P3)	85.1	52.3	46.1	162.5	85.2	79.2
2	California Sand	UM-SEES	-	Powder (P2)	85.1	52.3	46.1	162.5	85.2	79.2
3	Africa Sand	UM-SEES	-	Powder (P2)	87.9	45.7	39.4	166.4	77.8	66.8
4	Murkee-Murkee Australian Sand	UM-SEES	-	Powder (P2)	87.9	45.7	39.4	166.4	77.8	66.8
5	Manua Key Summit Hawaii Sand	UM-SEES	-	Powder (P2)	87.9	45.7	39.4	166.4	77.8	66.8
6	Quartz	UM-SEES	-	Powder (P2)	87.9	45.7	39.4	166.4	77.8	66.8
7	Kakadu Dust	UM-SEES	-	Powder (P2)	87.9	45.7	39.4	166.4	77.8	66.8

8	Feldspar	UM-SEES	-	Powder (P2)	87.9	45.7	39.4	166.4	77.8	66.8
9	Hematite	UM-SEES	-	Powder (P2)	87.9	45.7	39.4	166.4	77.8	66.8
10	Gypsum	UM-SEES	-	Powder (P2)	90.9	45.2	39.3	173.0	76.8	66.3
11	Bani AMMA	UM-SEES	-	Powder (P2)	90.9	45.2	39.3	173.0	76.8	66.3
12	Arizona Test Dest	UM-SEES	-	Powder (P2)	90.9	45.2	39.3	173.0	76.8	66.3
13	Kaolinite	Sigma		Powder (P2)	90.9	45.2	39.3	173.0	76.8	66.3

HULIS

1	Waskish Peat Humic Acid Reference	IHSS***	1R107H	Powder (P1)	90.9	45.2	39.3	173.0	76.8	66.3
2	Suwannee River Humic Acid Standard II	IHSS	2S101H	Powder (P2)	90.9	45.2	39.3	173.0	76.8	66.3
3	Suwannee River Fulvic Acid Standard I	IHSS	1S101F	Powder (P2)	90.9	45.2	39.3	173.0	76.8	66.3
4	Elliott Soil Humic Acid Standard	IHSS	1S102H	Powder (P1)	90.9	45.2	39.3	173.0	76.8	66.3
5	Pony Lake (Antarctica) Fulvic Acid Reference	IHSS	1R109F	Powder (P2)	90.9	45.2	39.3	173.0	76.8	66.3
6	Nordic Aquatic Fulvic Acid Reference	IHSS	1R105F	Powder (P2)	90.9	45.2	39.3	173.0	76.8	66.3

Polycyclic Hydrocarbons

1	Pyrene	Sigma	82648	Powder (P1)	92.8	48.0	40.5	176.1	79.7	68.8
2	Phenanthrene	Sigma	695114	Powder (P1)	92.8	48.0	40.5	176.1	79.7	68.8
3	Naphthalene	Sigma	84679	Powder (P1)	92.8	48.0	40.5	176.1	79.7	68.8

Combustion Soot and Smoke

1	Aquadag	Synthesized in lab	-	Liquid	45.6	24.4	46.6	89.5	45.7	78.9
2	Ash	MPIC	-	Powder (P1)	96.7	46.1	40.6	186.5	77.7	69.0
3	Fullerene Soot	Alfa Aesar	40971	Powder (P2)	92.8	48.0	40.5	176.1	79.7	68.8
4	Diesel Soot	NIST	2975	Powder (P1)	92.8	48.0	40.5	176.1	79.7	68.8
5	Cigarette Smoke	Marlboro 83s	-	Smoke	50.5	24.9	48.8	101.2	46.3	80.9
6	Wood Smoke (<i>Pinus Nigra</i> , <i>Black Pine</i>)	Local Sample	-	Smoke	50.5	24.9	48.8	101.2	46.3	80.9

7	Fire Ash	UM-SEES	-	Powder (P1)	85.1	52.3	46.1	162.5	85.2	79.2
Brown Carbon										
1	Methylglyoxal + Glycine	Synthesized in lab	-	Liquid	30.9	16.8	60.8	63.8	35.1	101.2
2	Glycolaldehyde + Methylamine	Synthesized	-	Liquid	33.5	17.6	64.0	69.4	36.1	108.5
3	Glyoxal + Ammonium Sulfate	Synthesized	-	Liquid	31.5	17.2	64.9	65.2	34.7	111.7
Common Household Fibers										
1	Laboratory wipes	Kimberly Clark	-		46.4	23.7	43.9	92.7	44.5	73.9
2	Cotton t-shirt (white)	Hanes	-		46.4	23.7	43.9	92.7	44.5	73.9
3	Cotton t-shirt (black)	Hanes	-		46.4	23.7	43.9	92.7	44.5	73.9
4	2 µm Green	Thermo-Sci.	G0200	Liquid	-	-	-	-	-	-
5	2 µm Red	Thermo-Sci.	R0200	Liquid	-	-	-	-	-	-
6	2.1 µm Blue	Thermo-Sci.	B0200	Liquid	-	-	-	-	-	-

13 *ATCC: American Type Culture Collection

14 ** University of Manchester – School of Earth and Environmental Sciences

15 *** International Humic Substance Society

16
17
18
19
20
21
22
23
24
25
26

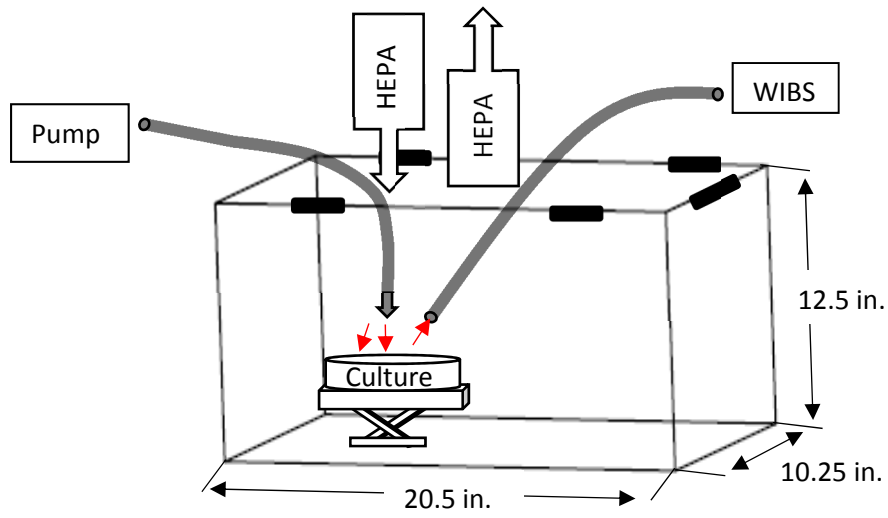
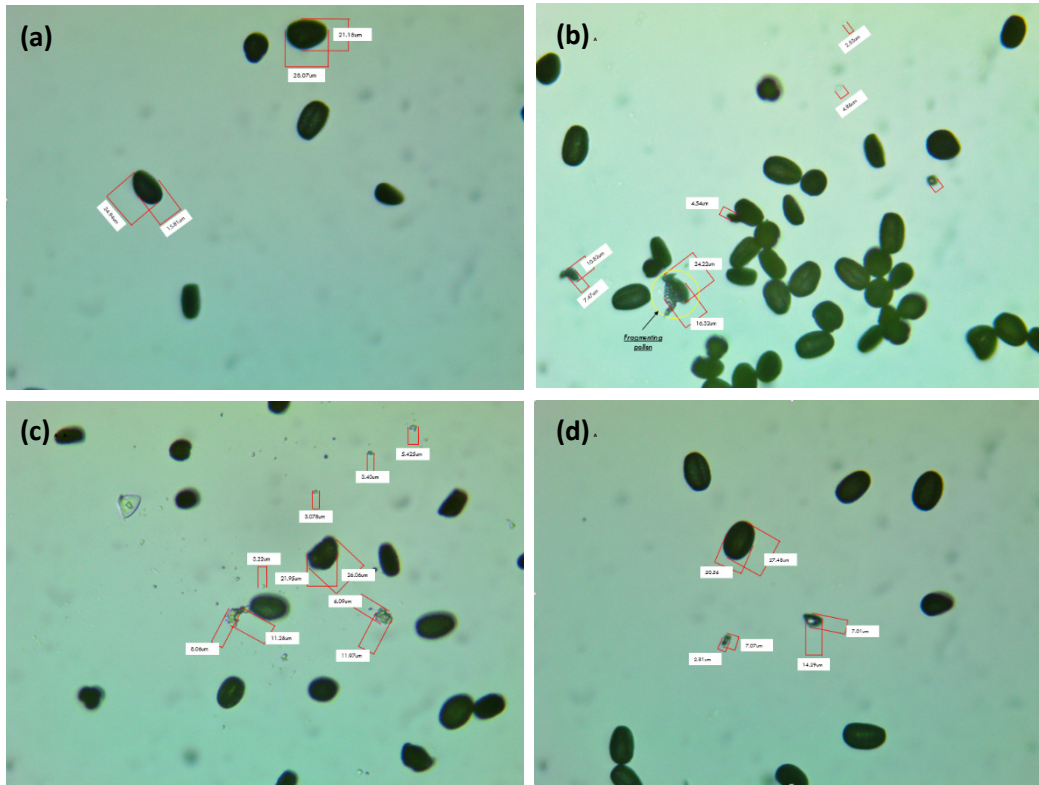
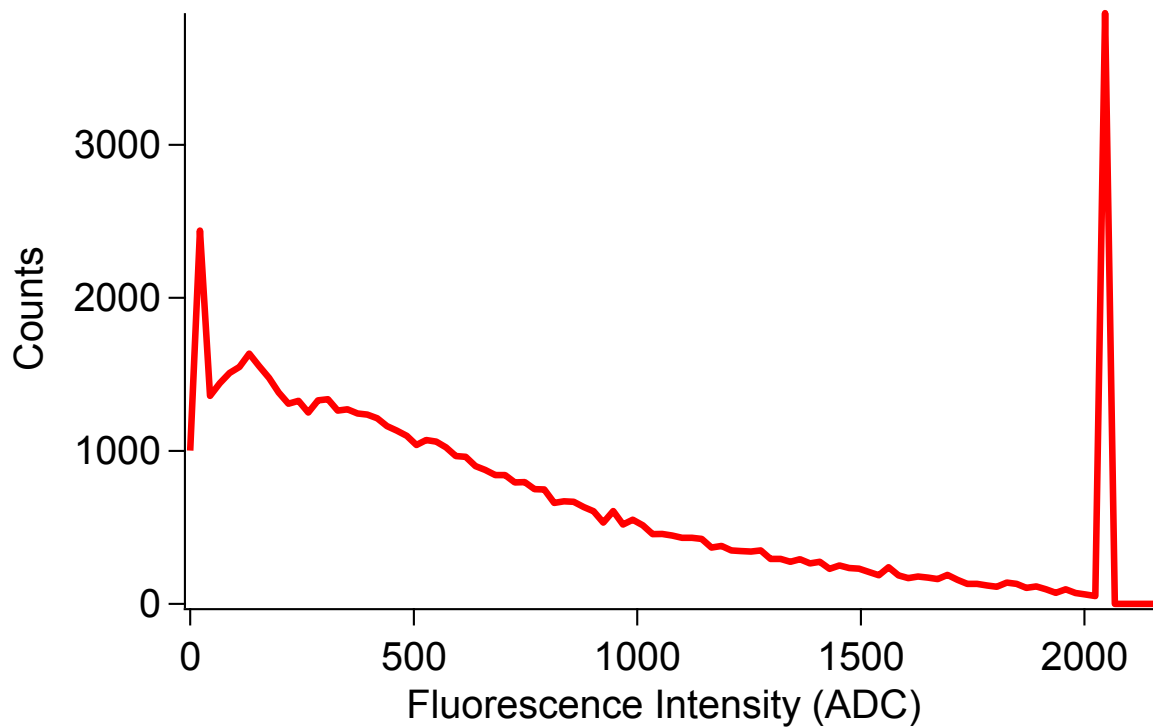


Figure S1. Schematic diagram of home-built chamber for the aerosolization of fungal spores.

27
28
29
30
31
32
33
34
35
36
37
38
39
40
41
42



43 Figure S2. Impacted pollen (*Olea europaea*) images collected with an AmScope camera
44 (MU800, AmScope) with an objective lens with 40x magnification. (a) Not stirred (b-d) Stirred.



45

46 Figure S3. Fluorescence intensity histogram of FL1 for *Aspergillus niger* (Fungi 2). One broad
47 mode extending from 0-2000 analog-to-digital counts (ADC) and a second mode showing
48 detector saturation at ~2047 ADC.

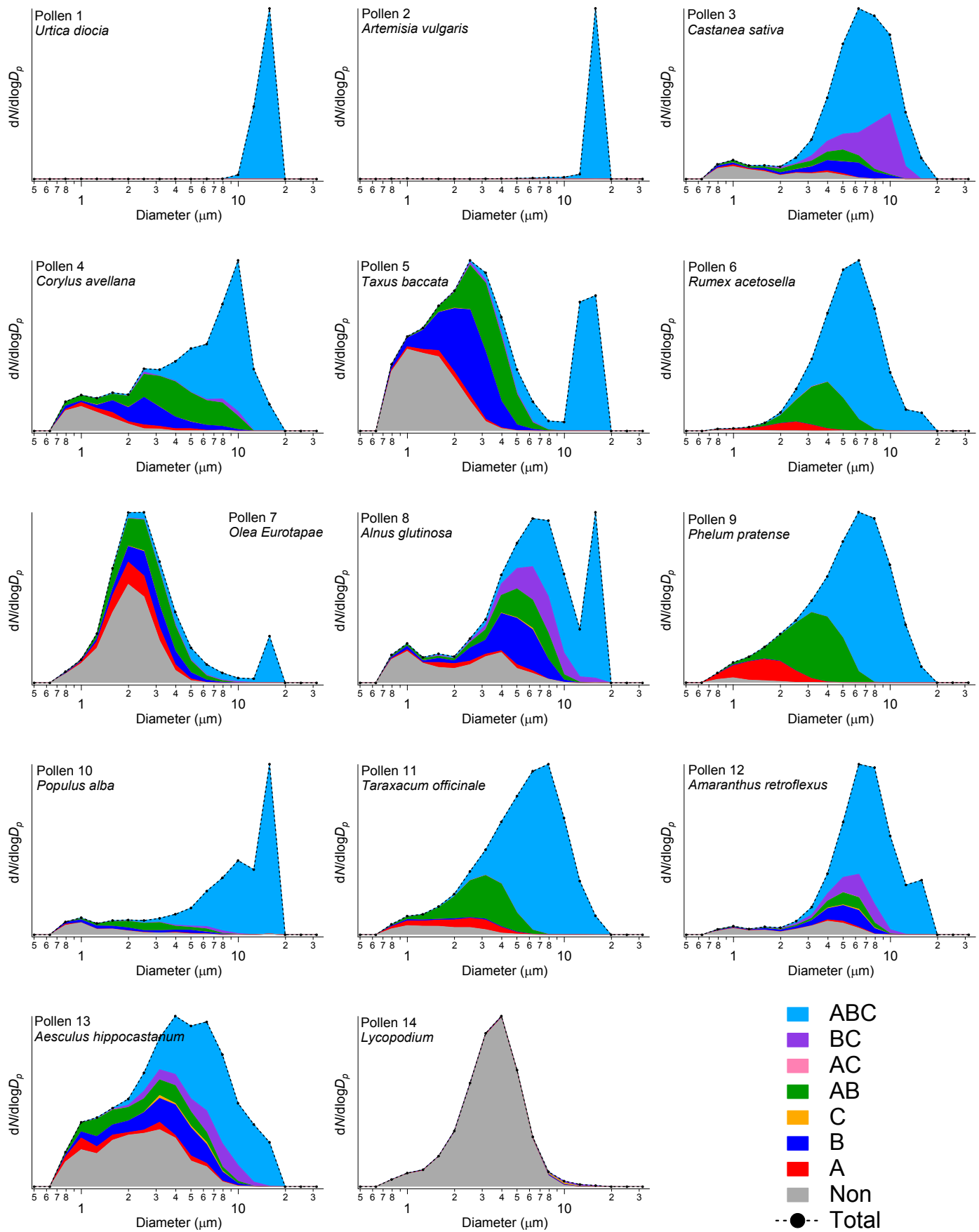


Figure S4A. Stacked particle type size distributions of pollen using FT + 3σ threshold

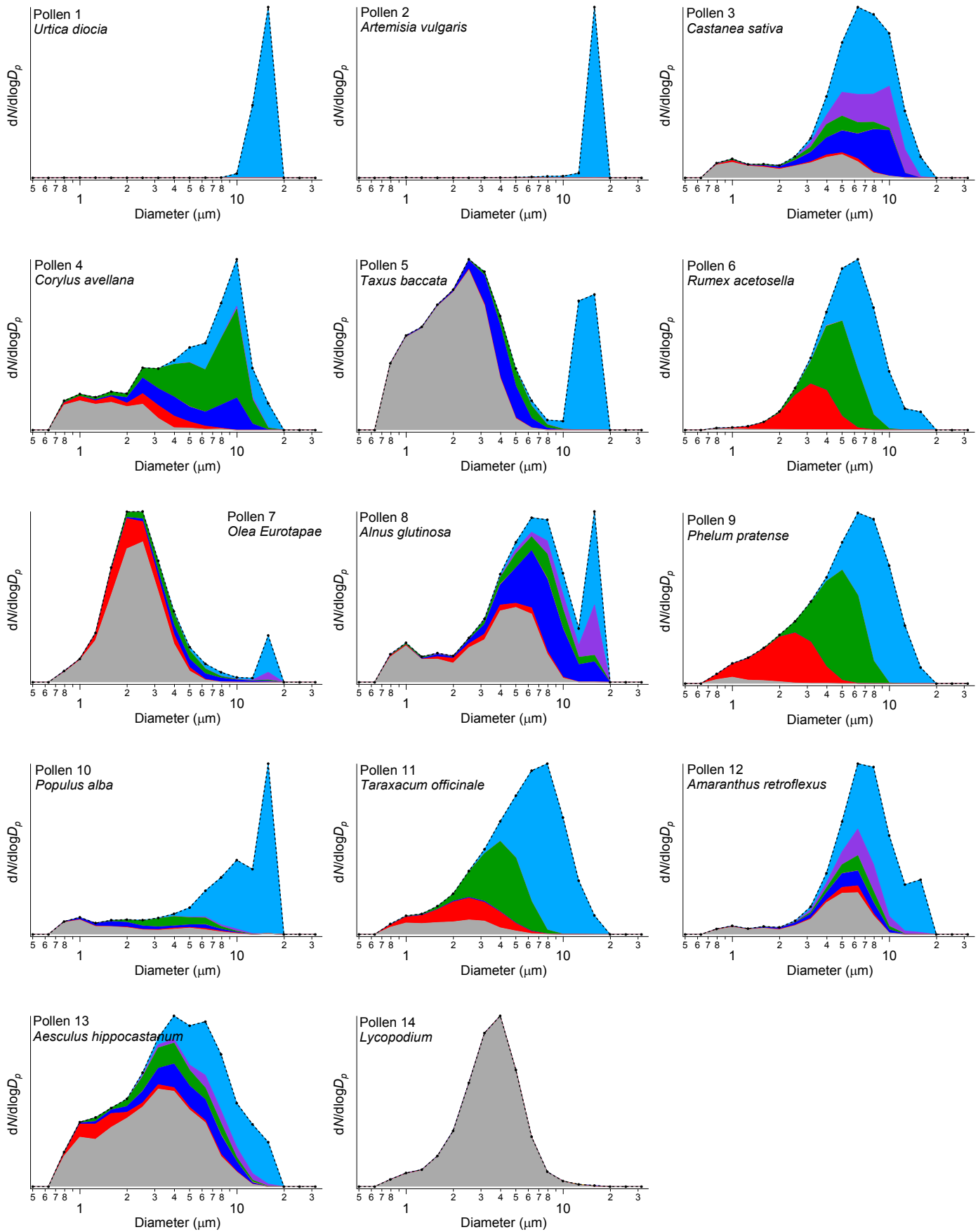


Figure S4B. Stacked particle type size distributions of pollen using FT + 9σ threshold

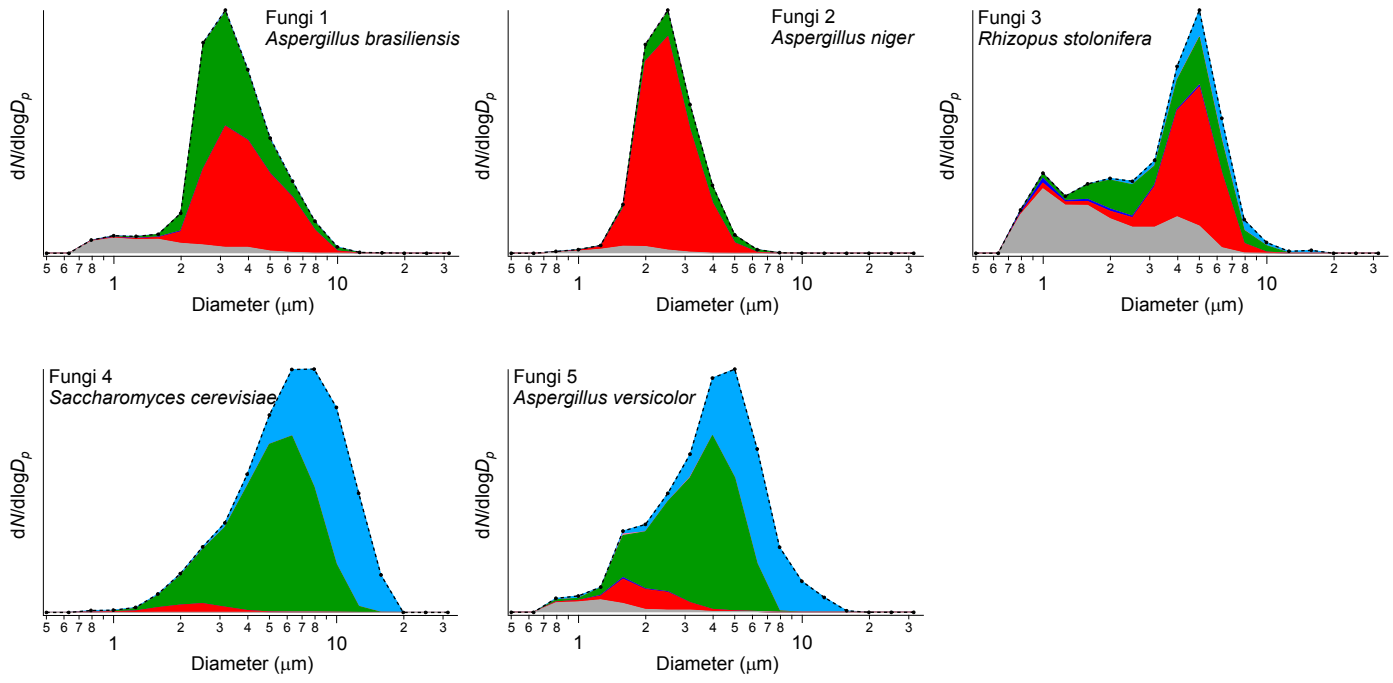


Figure S4C. Stacked particle type size distributions of fungal spores using $FT + 3\sigma$ threshold

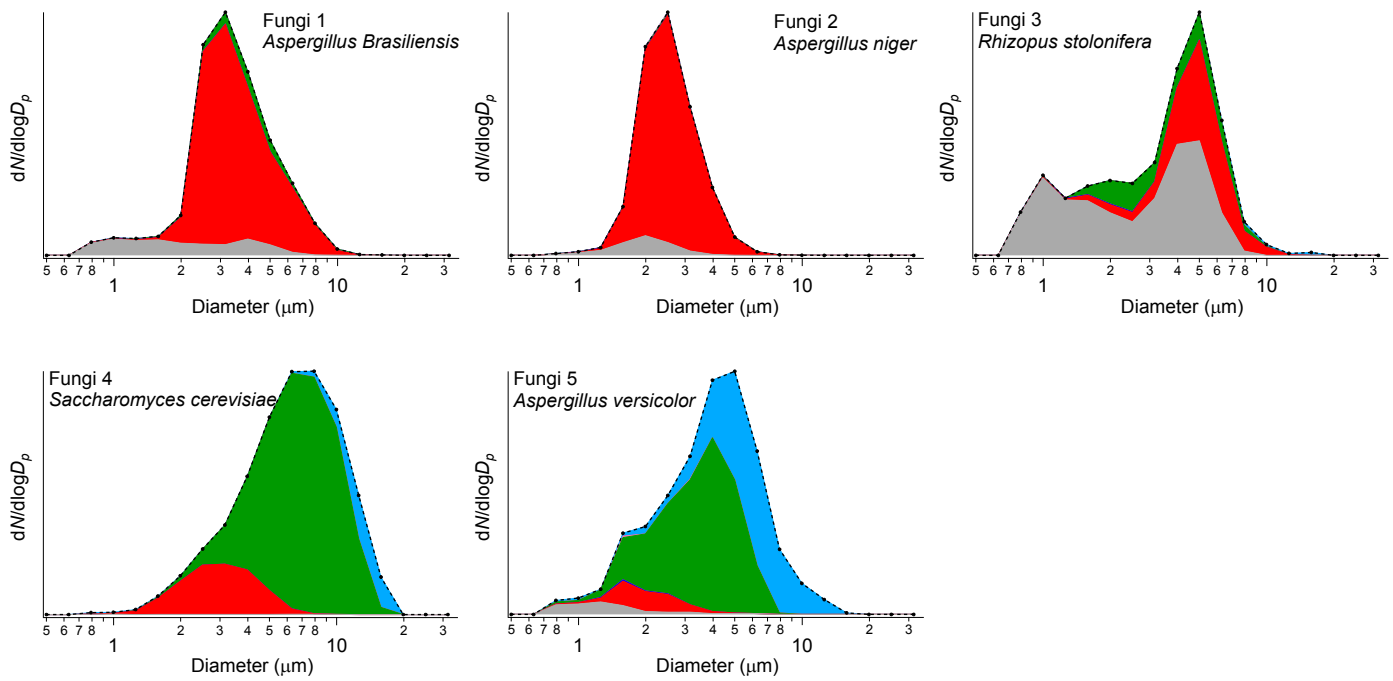


Figure S4D. Stacked particle type size distributions of fungal spores using $FT + 9\sigma$ threshold

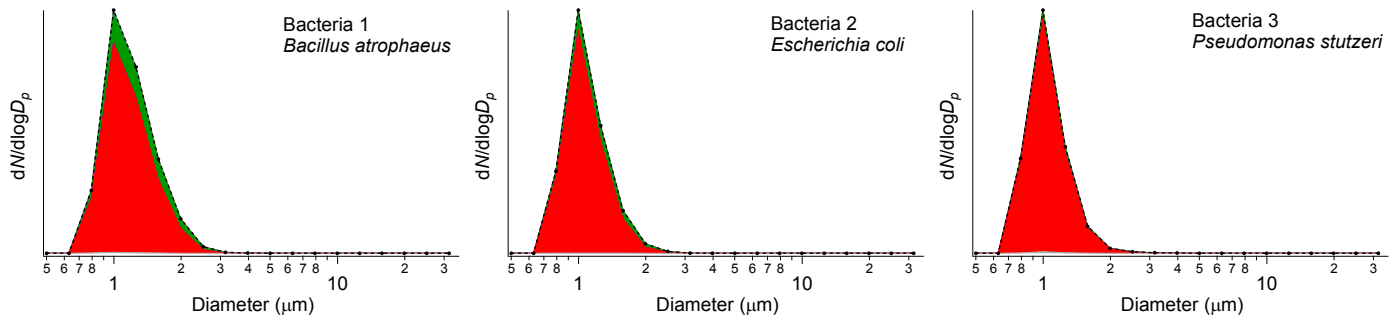


Figure S4E. Stacked particle type size distributions of bacteria using $FT + 3\sigma$ threshold

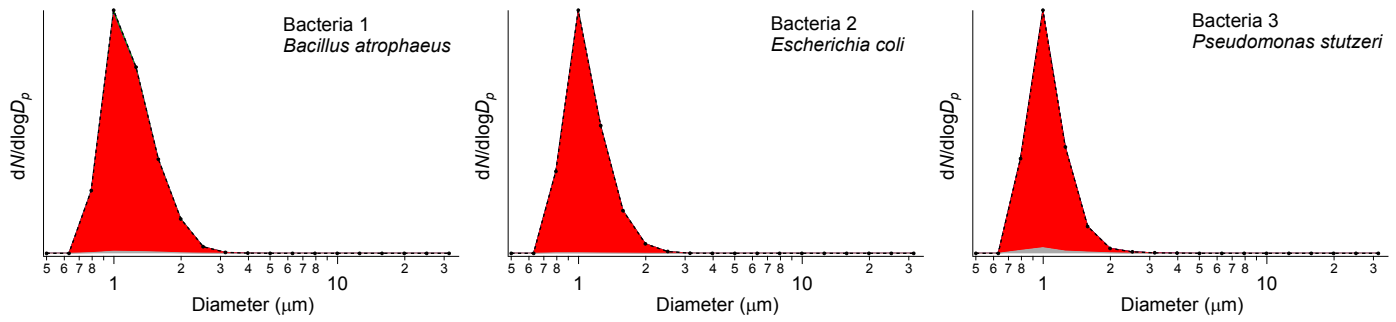


Figure S4F. Stacked particle type size distributions of bacteria using $FT + 9\sigma$ threshold

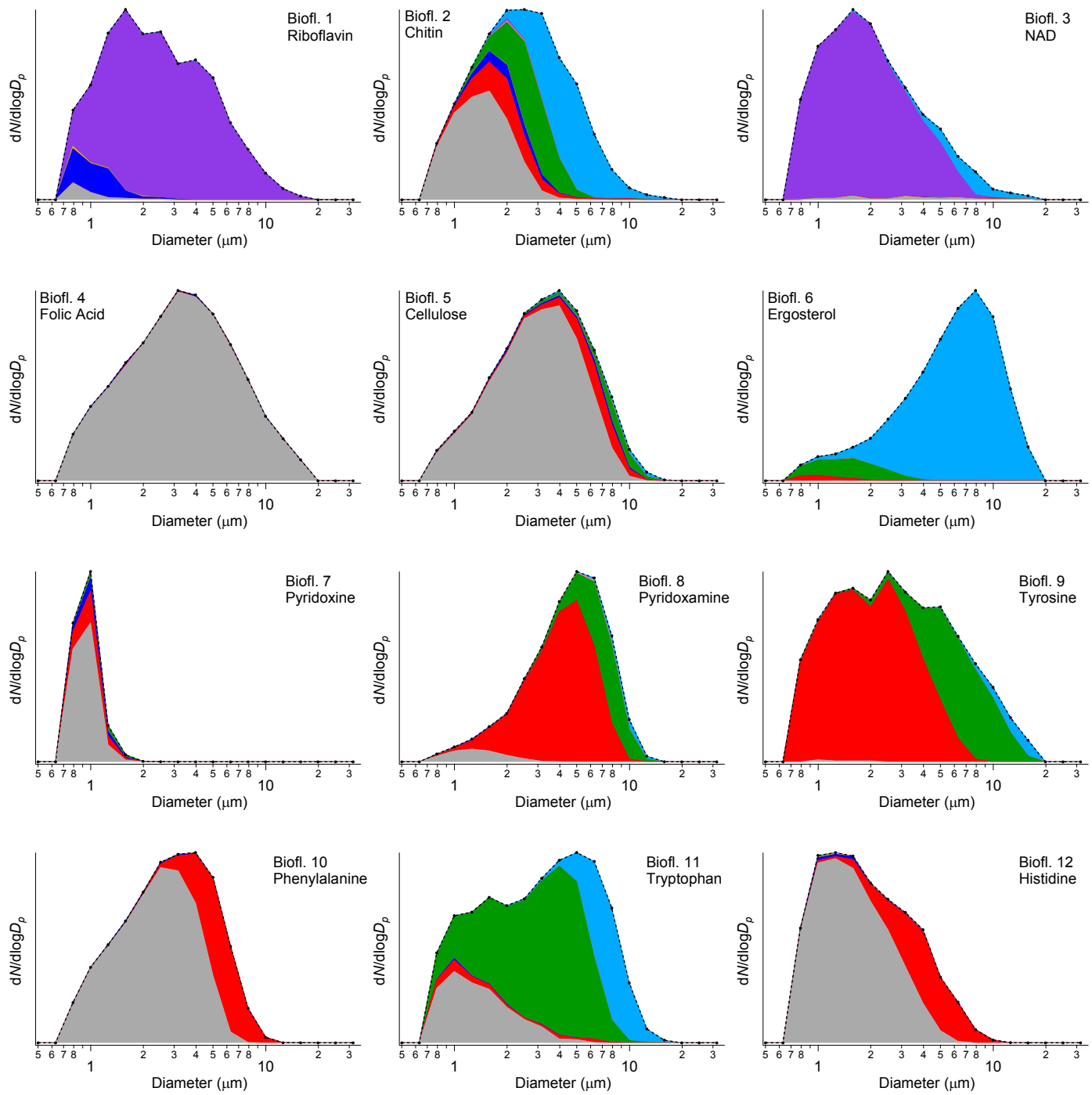


Figure S4G. Stacked particle type size distributions of biofluorophores using FT + 3σ threshold

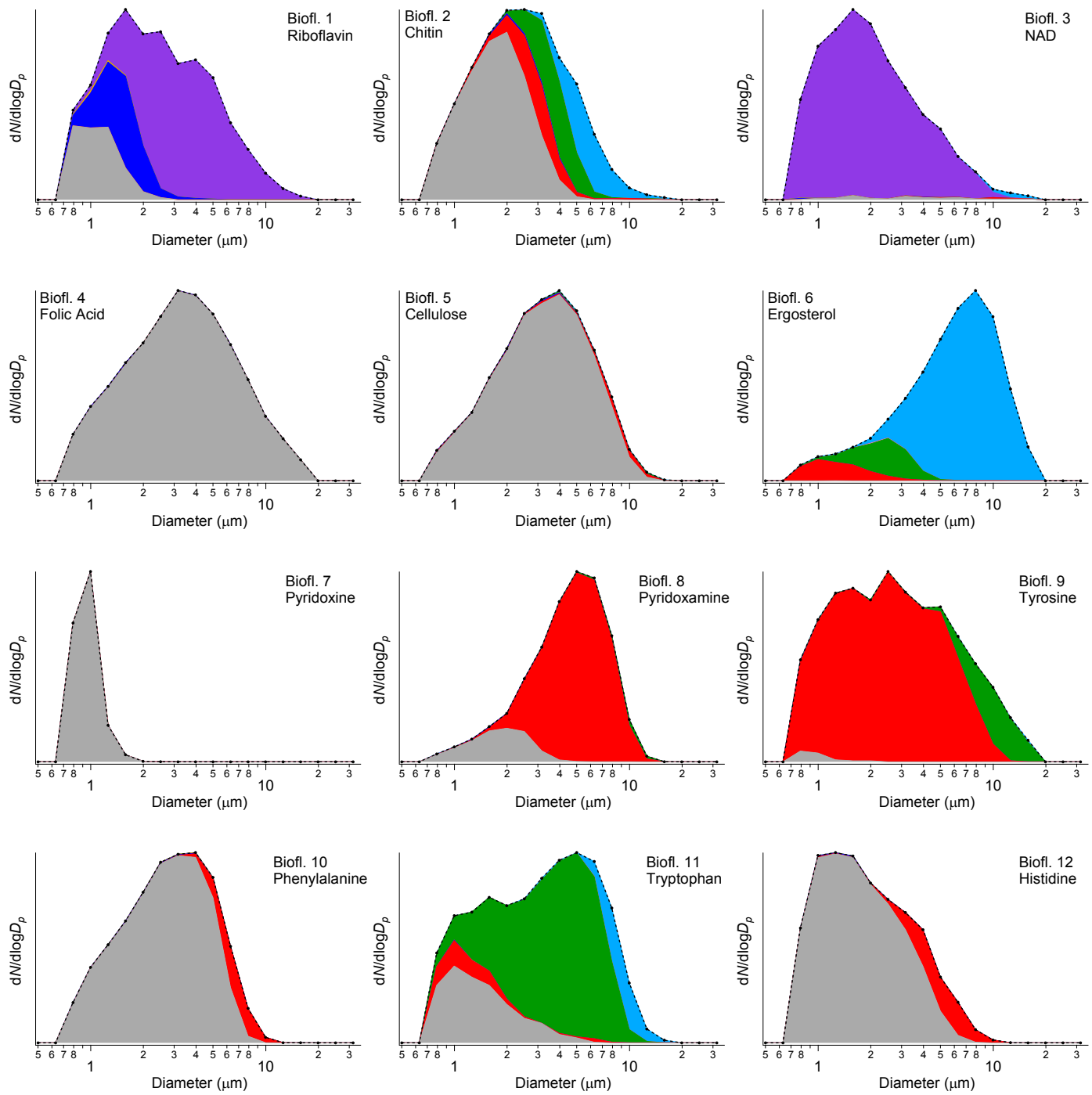


Figure S4H. Stacked particle type size distributions of biofluorophores using FT + 9σ threshold

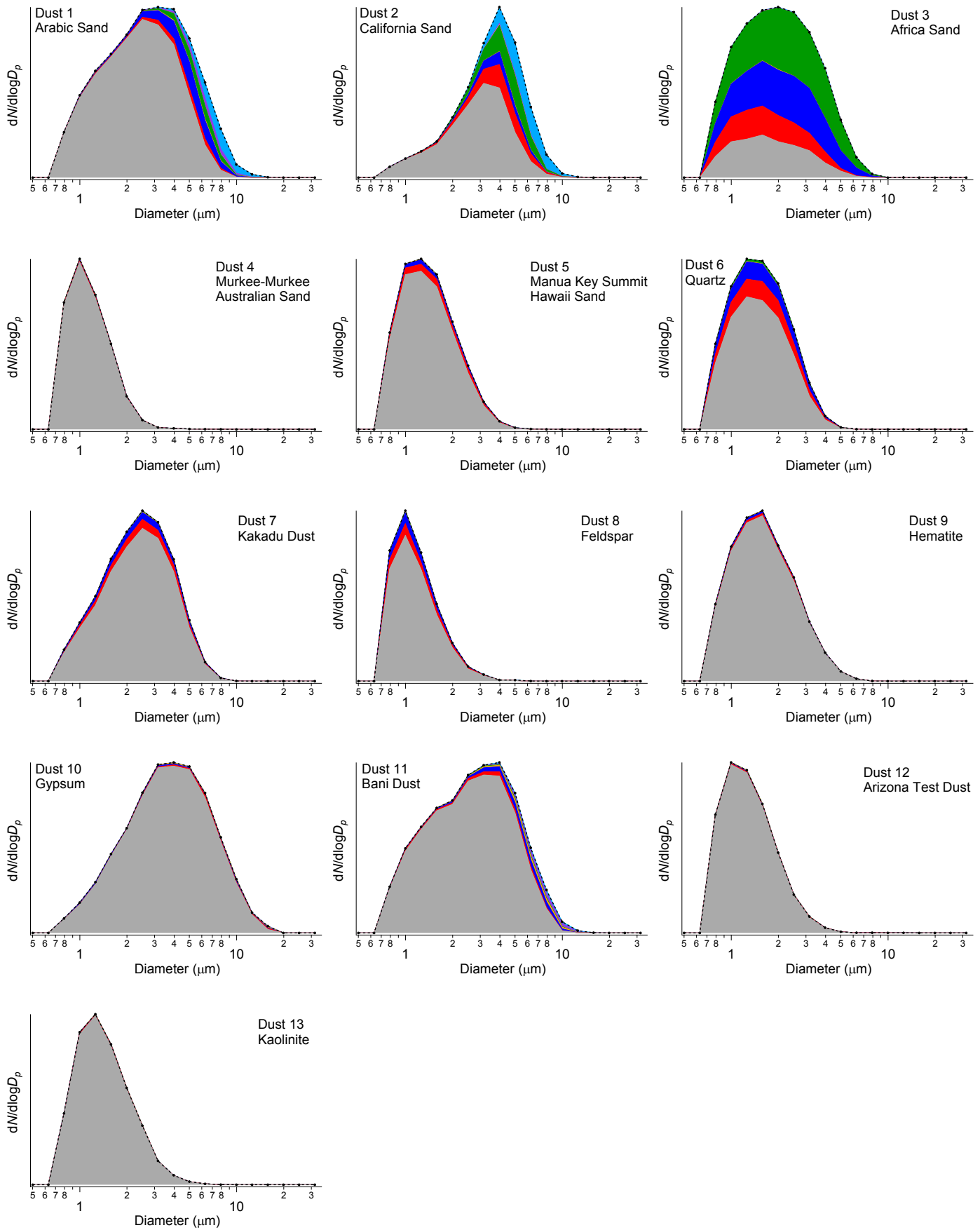


Figure S4I. Stacked particle type size distributions of dust using $FT + 3\sigma$ threshold

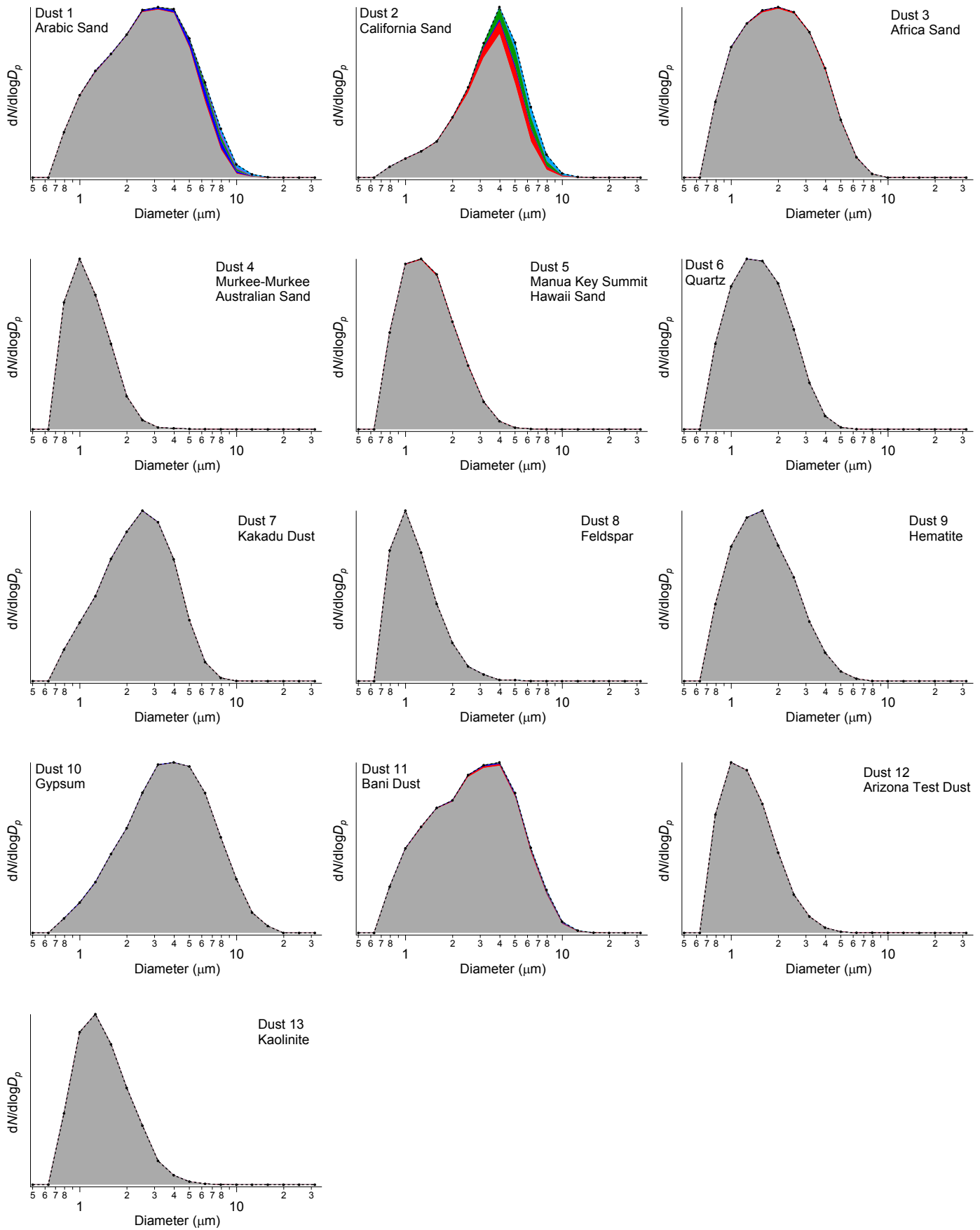


Figure S4J. Stacked particle type size distributions of dust using FT + 9σ threshold

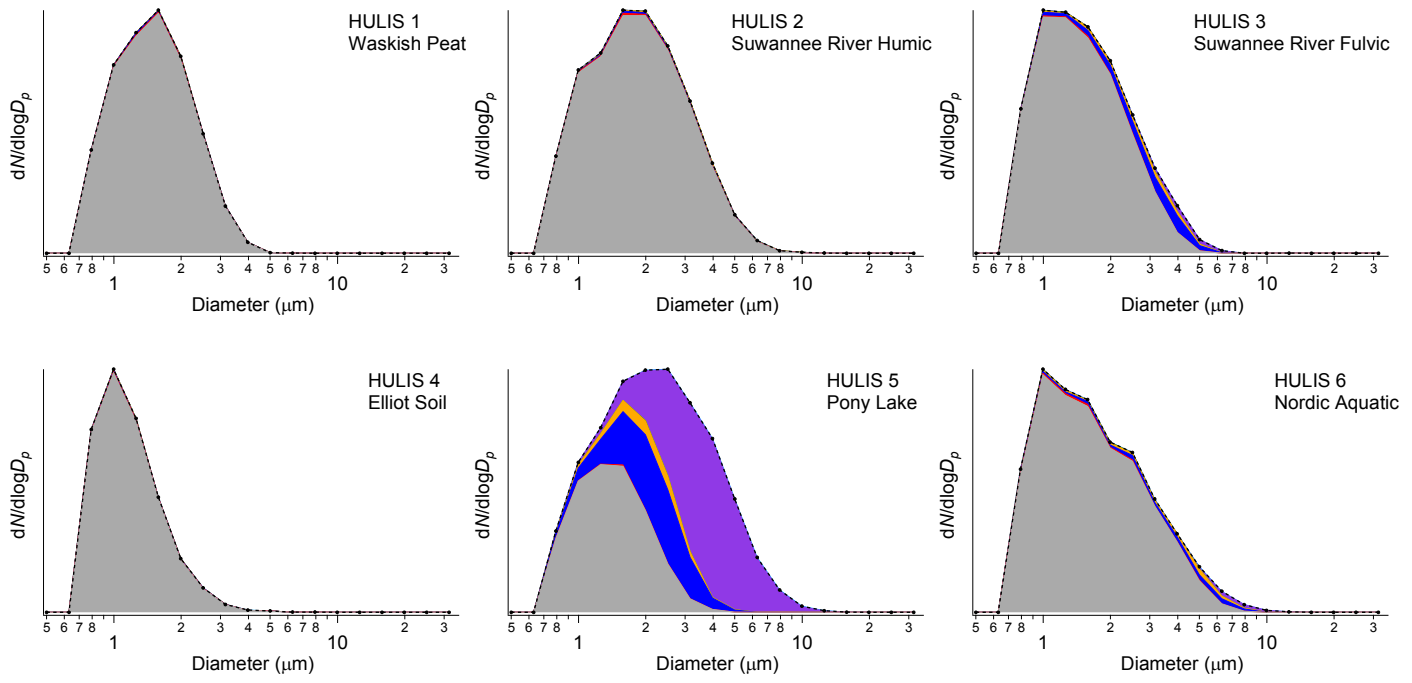


Figure S4K. Stacked particle type size distributions of HULIS using FT + 3 σ threshold

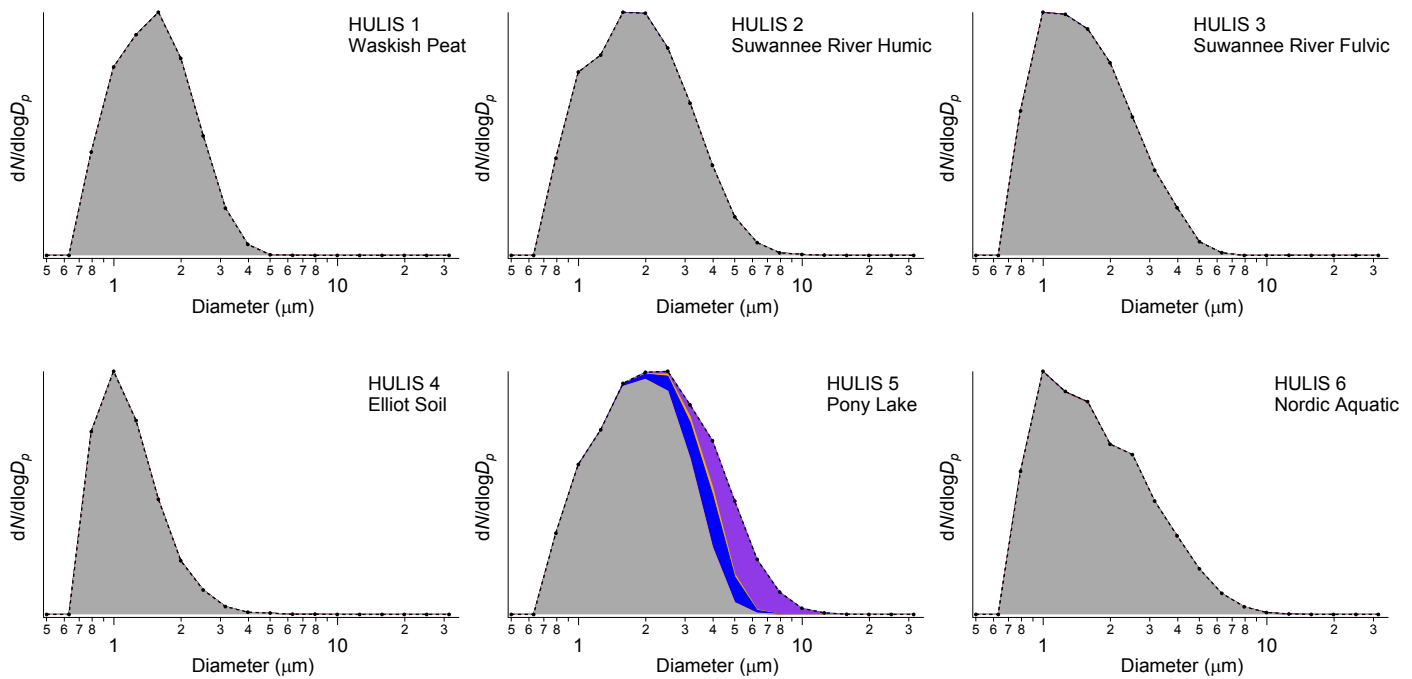


Figure S4L. Stacked particle type size distributions of HULIS using FT + 9 σ threshold

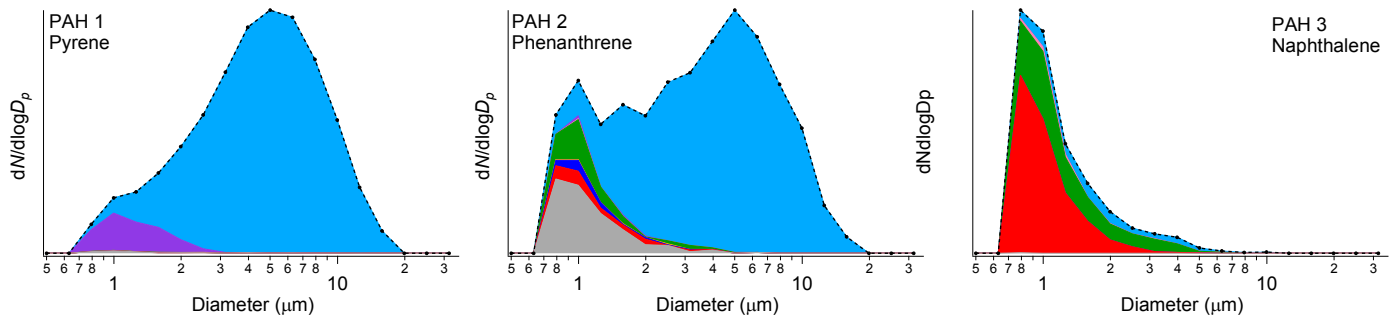


Figure S4M. Stacked particle type size distributions of PAHs using FT + 3σ threshold

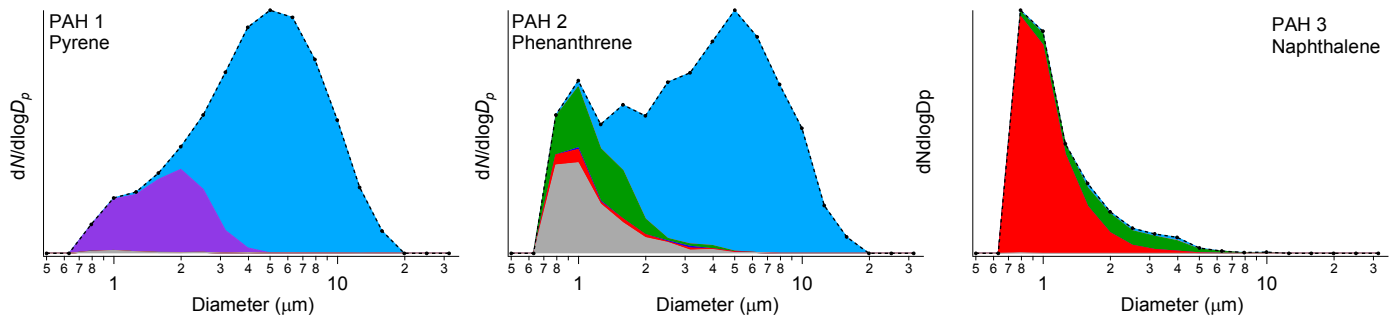


Figure S4N. Stacked particle type size distributions of PAHs using FT + 9σ threshold

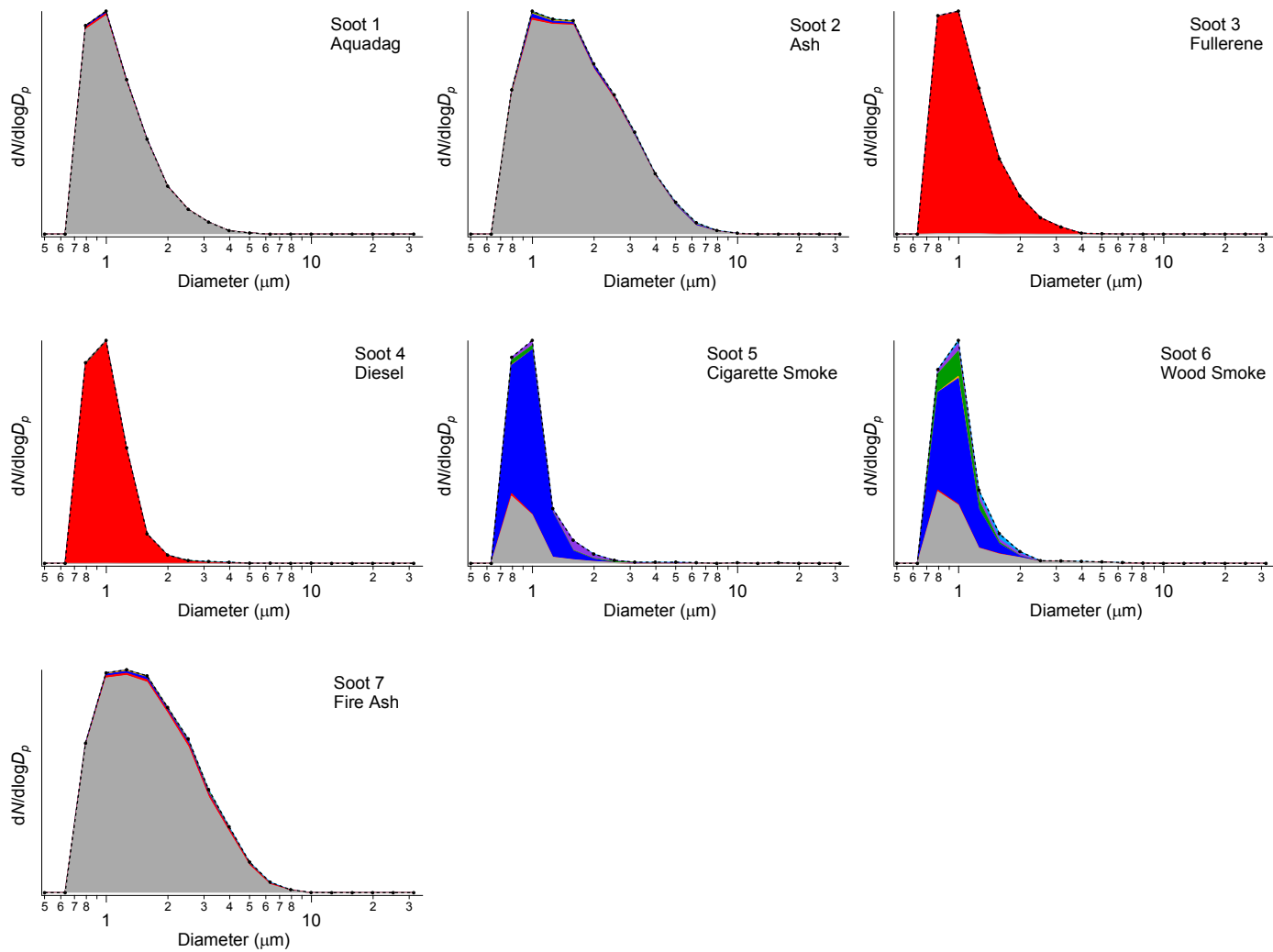


Figure S40. Stacked particle type size distributions of soot using FT + 3σ threshold

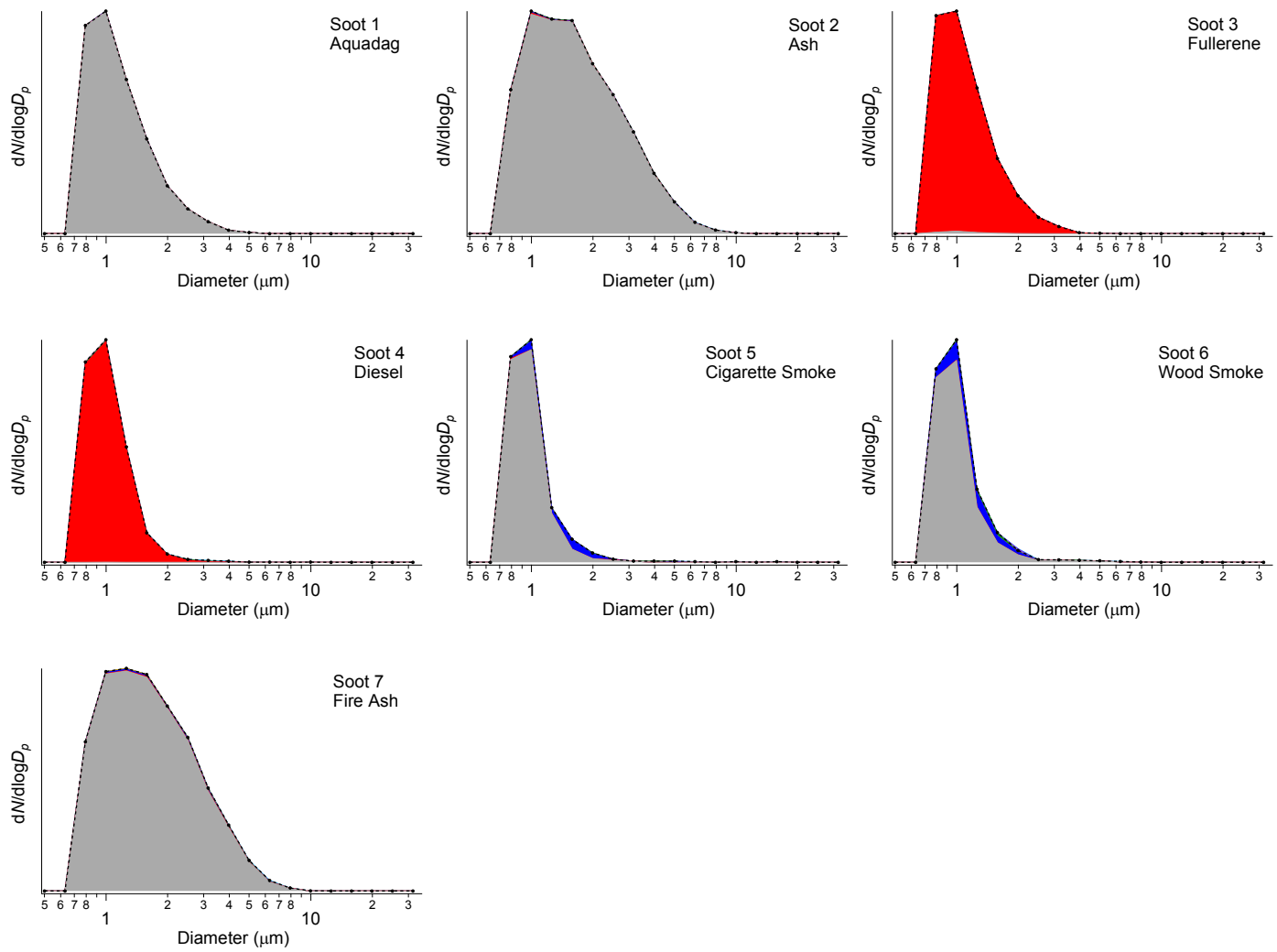


Figure S4P. Stacked particle type size distributions of soot using $FT + 9\sigma$ threshold

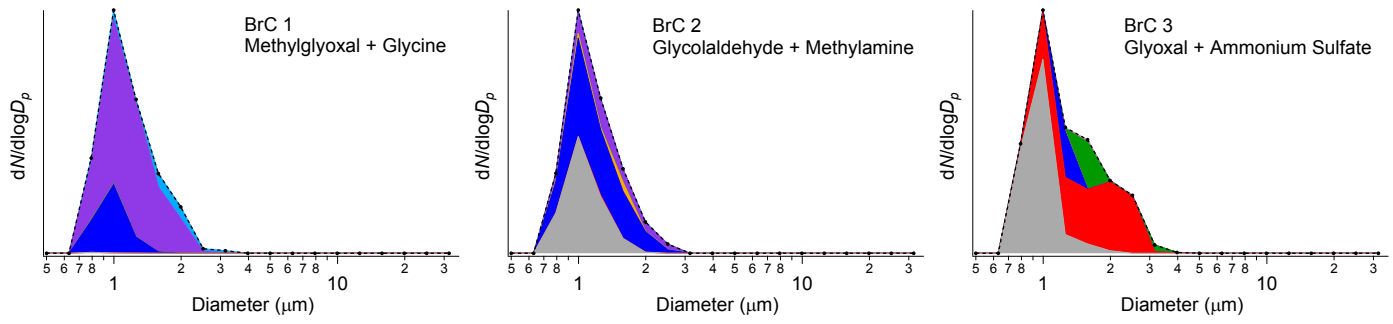


Figure S4Q. Stacked particle type size distributions of brown carbon (BrC) using $FT + 3\sigma$ threshold

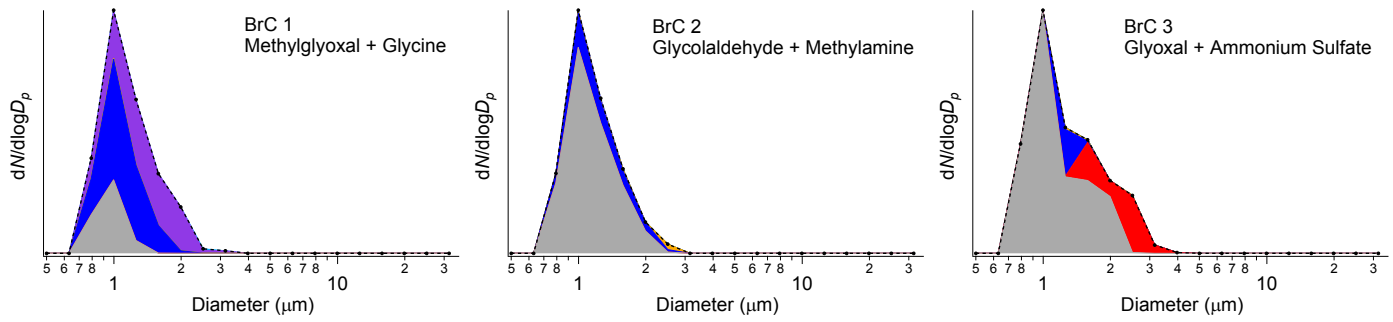


Figure S4R. Stacked particle type size distributions of brown carbon (BrC) using $FT + 9\sigma$ threshold

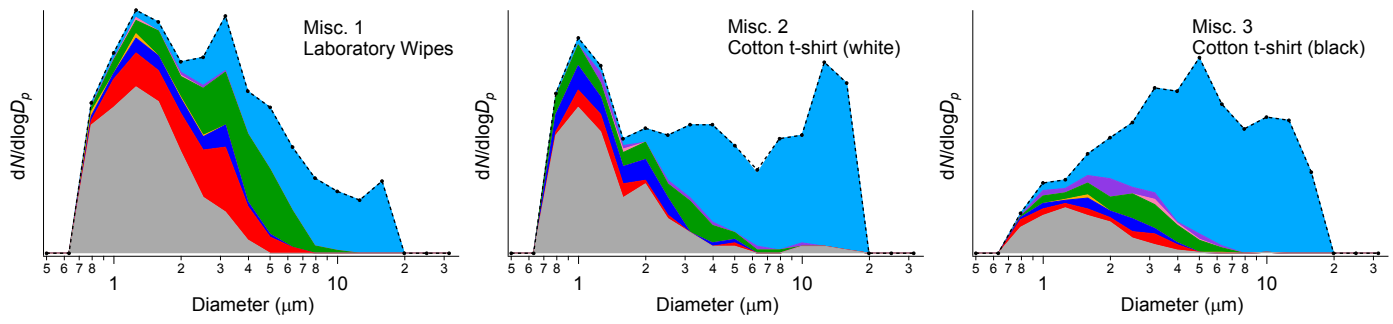


Figure S4S. Stacked particle type size distributions of miscellaneous samples using $FT + 3\sigma$ threshold

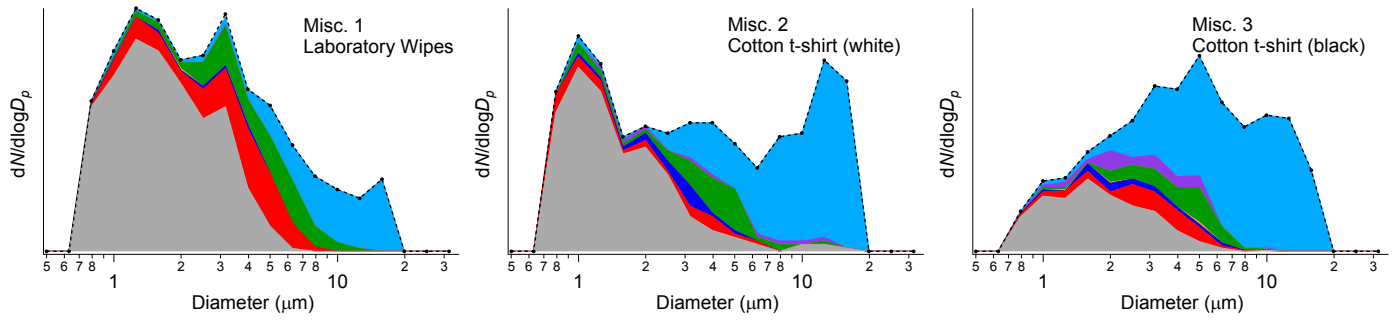


Figure S4T. Stacked particle type size distributions of miscellaneous samples using $FT + 9\sigma$ threshold